# Spread Spectrum Multi-$h$ Modulation

A THESIS

Presented to

The Faculty of the Division of Graduate Studies

By

William D. Lane



In Partial Fulfillment

of the Requirements for the Degree of

Doctor of Philosophy in Electrical Engineering

Georgia Institute of Technology

July, 1988

# Spread Spectrum Multi-$h$ Modulation

Approved:

Dr. Aubrey M. Bush, Chairman

Dr. Gordon L. Stüber

Dr. Stephen B. Wicker

Date approved by Chairman



per ltr

This dissertation is dedicated to

my mother,

Bettye R. Lane

and

to the memory of

my father,

Charles F. Lane,

whose life is my paragon

and whose passing is my inspiration.

# Acknowledgments

It is my pleasure to acknowledge and express my sincere gratitude and appreciation to my thesis advisor, Dr. Aubrey M. Bush. His patience, dedication, wisdom, and commitment have been the hallmarks of my tutelage. For these I am deeply grateful.

I wish to also extend my sincere thanks to Dr. G. Stüber for his interest and knowledge in spread spectrum systems that were the stimulation and inspiration for this research.

I am grateful to Drs. S. Wicker, L. Callahan, and L. Pickering for their stimulating comments and suggestions concerning this research.

I am pleased to acknowledge the support of the United States Army that provided the opportunity for advanced schooling.

Finally and most importantly, I wish to acknowledge the commitment, dedication, sacrifice, and support of my wife, [redacted] and children, [redacted] This thesis is as much theirs as it is mine.

# Contents

# List of Figures

# List of Tables

# Glossary of Symbols

| | |
|---|---|
| $\alpha_i$ | Information bit during interval, $i$ |
| $\hat{\alpha}_i$ | Estimate of information bit during interval, $i$ |
| $\underline{\alpha}$ | Binary digital information sequence |
| $\underline{c}$ | Digital $\pm 1$ spreading sequence |
| $c(t)$ | Spreading function as function of time |
| $c_{ij}$ | Dibit value over chip interval $j$ in bit interval $i$ |
| $\underline{C}$ | Multi-variant Gaussian covariance matrix |
| $C_a$ | Multiplicative constant in autocorrelation functions |
| $D$ | Distance operator in transition matrices |
| $\underline{D}$ | Linear transformation matrix |
| $d_{12}$ | Euclidean distance between signals one and two |
| $d_f$ | Minimum free distance of error events |
| $E$ | Error operator in transition matrices |
| $E_b$ | Bit signal energy |
| $E_c$ | Chip level signal energy |
| $\mathrm{erfc}(\cdot)$ | Complementary error function |
| $\mathcal{F}$ | Fourier transform operator |
| $f$ | Frequency variable |
| $f_n$ | Normalized frequency variable |
| $f_0$ | Radio frequency carrier frequency |
| $g(t)$ | Frequency pulse shaping function |
| $G(f)$ | Fourier transform of lowpass signal |
| $H$ | Number of modulation indices or period of the cyclical change in modulation indices |

| | |
|---|---|
| $H0$ | Hypothesis of noise only reception |
| $H1$ | Hypothesis of signal plus noise reception |
| $\underline{h}$ | Sequence of cyclical modulation indices or frequency deviation ratios |
| $h_i$ | Modulation index over a bit interval |
| $h_{i,j}$ | Modulation index over a chip interval $j$ of bit interval $i$ |
| $h_{(i+j) \bmod H}$ | Specific value of modulation index in chip $j$ of bit $i$ |
| $\Im$ | Imaginary operator function |
| $\underline{I}$ | Identity matrix |
| $I_1$ | Inphase quadrature term for positive information bit |
| $I_2$ | Inphase quadrature term for negative information bit |
| $IC$ | Inphase cosinusoidal term for quadrature expansion |
| $IS$ | Inphase sinusoidal term for quadrature expansion |
| $I(t)$ | Inphase term in quadrature expansion of signaling terms |
| $\mathcal{L}$ | Maximum likelihood decision variable |
| $L$ | Bit duration of frequency pulse shaping function |
| $L_{cj}$ | Inphase quadrature decision statistic |
| $L_{sj}$ | Quadrature decision statistic |
| LPF | Low pass filter |
| $l$ | Log-likelihood decision variable |
| $M$ | Information symbol alphabet |
| $N$ | Length of arbitrary bit sequence |
| $N(\cdot,\cdot)$ | Normal random variable distribution |
| $N_c$ | Number of chips per information bit interval |
| $N_D$ | Bit delay in Viterbi Algorithm processor |
| $N_0$ | Single-sided noise energy |
| $N1C$ | Cosinusoidal noise term in inphase quadrature expression of correlation filter output for positive information bit |
| $N2C$ | Cosinusoidal noise term in inphase quadrature expression of correlation filter output for negative information bit |

$N1S$ Sinusoidal noise term in quadrature expression of correlation filter output for positive information bit

$N2S$ Sinusoidal noise term in quadrature expression of correlation filter output for negative information bit

$n_i$ Numerator of individual modulation index

$n(t)$ Additive white Gaussian noise function

$P(\cdot)$ Probability distribution function

$P_b$ Probability of bit error

$P_e$ Probability of error event

$P_D$ Probability of detection

$P_F$ Probability of false alarm

$p$ Fixed integer denominator of set of modulation indices

$p(\cdot)$ Probability density function

$q(t)$ Phase shaping function

$Q(x)$ Exponential error function

$Q_1$ Quadrature term for positive information bit

$Q_2$ Quadrature term for negative information bit

$QC$ Quadrature cosinusoidal term for quadrature expansion

$QS$ Quadrature sinusoidal term for quadrature expansion

$Q(t)$ Quadrature term in quadrature expansion of signaling terms

$r(t_1, t_2)$ Lowpass autocorrelation function

$r(t)$ Received signal at input to receiver

$R(\tau)$ Lowpass autocorrelation value for time difference, $\tau = t_1 - t_2$

$\acute{\alpha}$ Autocorrelation variable time difference in the interval, 0 to $HT_c$

$S1C$ Cosinusoidal signal term in inphase quadrature expression of correlation filter output for positive information bit

$S2C$ Cosinusoidal signal term in inphase quadrature expression of correlation filter output for negative information bit

| | |
|---|---|
| $S1S$ | Sinusoidal signal term in quadrature expression of correlation filter output for positive information bit |
| $S2S$ | Sinusoidal signal term in quadrature expression of correlation filter output for negative information bit |
| $S(f)$ | Power spectral density |
| $s(t)$ | Spread spectrum multi-$h$ signal |
| $t$ | Time variable |
| $T$ | Split difference state gain transition expression |
| $T_A$ | Split difference state gain transition expression for a given modulation indexing code |
| $T_B$ | Split difference state gain transition expression for a given modulation indexing code |
| $T_b$ | Information bit duration or interval |
| $T_c$ | Chip duration or interval |
| $T_p$ | Repetitive period of spread spectrum multi-$h$ trellis structure |
| $T_s$ | Information symbol duration or interval |
| $u(t)$ | Complex envelope signal |
| $\underline{U}$ | Eigenvector matrix of covariance matrix |
| $x(t)$ | General signal expression |
| $\underline{Z}$ | Matrix of inverse square roots of eigenvalues |
| $\mathcal{E}$ | Expected value operator |
| $\delta$ | Kronecker delta function |
| $\Delta$ | Differnece change operator |
| $\gamma_i$ | Difference of information bit values in interval, $i$ |
| $\gamma_{ij}$ | Difference of bit and chip products in bit interval $i$ and chip interval $j$ |
| $\eta$ | Decision threshold |
| $\Lambda$ | Generalized likelihood decision statistic |
| $\lambda_i$ | Bit decision metric |
| $\lambda_j$ | Chip decision metric |

$\mu$ Mean value of sum of Gaussian log-likelihood decision statistics

$\mu_g$ Mean value of sum of Gaussian log-likelihood decision statistics under no signal hypothesis

$\mu_{H0}$ Mean value of sum of Gaussian log-likelihood decision statistics under no signal hypothesis

$\mu_{H1}$ Mean value of sum of Gaussian log-likelihood decision statistics under signal present hypothesis

$\mu_{gj}$ Mean value of individual Gaussian log-likelihood decision statistics under no signal hypothesis

$\mu_j$ Mean value of individual Gaussian log-likelihood decision statistics

$\mu_i$ Number of information bit errors in error event of length, $d_i$

$\mu_s$ Mean value of sum of Gaussian log-likelihood decision statistics under signal present hypothesis

$\mu_{sj}$ Mean value of individual Gaussian log-likelihood decision statistics under signal present hypothesis

$\nu_i$ Weighting function for chip/bit values over error event of length, $d_i$

$\omega_0$ Radian frequency variable

$\phi$ Information modulated signal phase

$\Psi$ Autocorrelation integral expression over finite duration

$\psi_{ij}$ Initial phase of received signal at start of a chip interval

$\sigma^2$ Variance of sum of Gaussian log-likelihood decision statistics

$\sigma^2_{H0}$ Variance of sum of Gaussian log-likelihood decision statistics under no signal hypothesis

$\sigma^2_{H1}$ Variance of sum of Gaussian log-likelihood decision statistics under signal present hypothesis

$\sigma^2_j$ Variance of individual Gaussian log-likelihood decision statistics

$\sigma^2_{gj}$ Variance of individual Gaussian log-likelihood decision statistics under no signal hypothesis

$\sigma^2_{sj}$ Variance of individual Gaussian log-likelihood decision statistics under signal present hypothesis

$\Re$ Real value operator

$\theta_0$ Arbitrary initial phase

$\theta_{ln}$ Previous phase state value in Markov state structure

$\theta_{ij}$ Previous phase state value during chip interval $j$ of bit interval $i$

$v_{ii}$ Eigenvalues of covariance matrix

# Summary

The possibility of communicating reliably by electromagnetic radiation, with only an intended party receiving the message, has long challenged engineers to devise techniques, such as spread spectrum modulation, to combat unintended detection. Coincidently, the constraints of the electromagnetic spectrum have led to the use of bandwidth and power efficient modulation schemes such as continuous phase modulation and multi-$h$ modulation.

The analysis contained herein is the first theoretical and numerical characterization of the combination of direct sequence spread spectrum techniques with multi-$h$ continuous phase modulation; thereby yielding a new class of signals collectively referred to as *spread spectrum multi-h* (SSMH) modulated signals. By applying a pseudorandom direct spreading sequence to a digital information sequence prior to multi-$h$ modulation, a unique communication scheme is created whereby control over the transmitted spectrum is afforded so as to have a signal with a low probability of intercept by an unintended receiver.

In the process of defining and characterizing the signaling structure, it is shown for the first time that the cyclic modulation indices can be applied on either a chip or on a bit interval basis with distinct signal structure and performance differences. It is also shown for the first time that there is a close resemblance between the power spectral densities of the two techniques. These results provide a unique design flexibility for the system engineer.

By spreading a known bandwidth efficient modulation scheme, the power density spectrum is controlled so that the transmitted spectrum will have a wide flat mainlobe and rapid sidelobe rolloff. The spectra for SSMH signals are analytically derived using new applications of autocorrelation and cyclostationary techniques. Numerical analysis reveals the novel determination that the spectra for both techniques are similar and resemble the spread replicas of their parent multi-$h$ schemes.

Coincident with the spectral control, the power efficient modulation allows transmission at lower signal-to-noise ratios when the receiver knows *a priori* the spreading sequence and the modulation index sequence. Optimal coherent receiver structures are analytically derived and upper bounds to the bit error rate performance are determined. Analysis reveals the new and significant result that performance is dependent on the spreading sequence and on the allowable phase states. It is shown that the Viterbi Algorithm can be successfully used to sequentially detect information sequences based on bit metrics derived from the sum of individual chip metrics.

The optimal receiver structure is numerically evaluated in an additive white Gaussian noise environment. For the first time for this type of signal, realistic evaluation is performed by adding correlated noise samples to the outputs of noise free correlation filter detectors. It is shown that the receiver performance is dependent on the selected modulation indices and on the spreading rate; and can exceed Direct Sequence Binary Phase Shift Keying by one to two decibels at bit error rates of $10^{-5}$.

The performance of the modulation scheme as a low probability of intercept technique is investigated from a detectability standpoint. Composite likelihood ratio analysis reveals a novel reduction by 50-70 percent in the detectability of a completely known (except information and spreading sequences) SSMH signal as compared to DS/BPSK signals at bit error rates of $10^{-4}$.

Tentative conclusions from this study indicate that spread spectrum multi-$h$ modulation is a viable technique for low probability of intercept applications. New methods for the application of continuous phase modulation indices have been derived and the impact of the spreading sequence on performance has been revealed. Realistic numerical evaluations with correlated noise samples indicate enhanced performance and reduced probability of detection when compared to DS/BPSK. Spectral control is obtained along with power efficiency to allow detection at lower signal-to-noise ratios.

# CHAPTER 1

# Introduction

The possibility of transferring information, that is, communicating, from one location, or person, to another with only the intended party receiving the message, has long intrigued and challenged engineers and military commanders alike. At the beginning of this century when radio transmissions were first making an appearance, an anonymous observer noted [29], '...the homing-pigeon service should be discontinued as soon as some system of wireless telegraphy is adopted.' Today, the insecurity and unreliability of the pigeon service no longer exists; instead engineers continue to grapple with the challenges of providing reliable and secure wireless systems.

The rapidly increasing demand for utilization of the frequency spectrum has led to expanded research in efficient methods of transmission to enhance the transfer of digital information. This is especially true on nonlinear links where constant envelope signals are affected the least by nonlinearities in the transmission process. This has led to extensive research and development of bandwidth efficient techniques such as continuous phase modulation (CPM), where the information is carried in the instantaneous carrier phase or frequency, while the envelope of the signal remains constant. Multi-$h$ modulation is a form of constant envelope CPM that is both power and bandwidth efficient.

Coincident with the development of CPM, extensive development has taken place in communications techniques that are immune to intercept and jamming. Spread spectrum techniques such as direct sequence (DS) pseudorandom spreading have been used to create signaling methods that are much more difficult to intercept by an unintended receiver, or in other words, have a low probability of intercept (LPI).

By applying direct sequence spreading to a digital information sequence, and utilizing

bandwidth and power efficient multi-$h$ modulation, the work herein is an attempt to create a signaling technique that is immune to interception. This effort is a novel attempt to extend spread spectrum techniques to this bandwidth efficient modulation method.

By spreading a known bandwidth efficient modulation technique, a signal structure is created that should have a power density with a wide flat mainlobe and rapid sidelobe rolloff. At low signal-to-noise ratios, this spectrum will be difficult to detect, observe, and parameterize. Analytical expressions for the power spectral density of spread spectrum multi-$h$ signals with various parameters are derived and numerically simulated.

Coherent receiver structures to detect the transmitted information sequence will be derived, where it is assumed that the intended receiver knows the spreading sequence, the modulation index sequence, the carrier phase, and the symbol and chip timing. Performance analysis and simulation will be accomplished to verify the structure.

The issue of the detectability of the transmitted signal will also be addressed from an optimal intercept standpoint. Analysis will consider the best possible performance of an intercept receiver that knows all of the characteristics of the transmitted signal except the information sequence and the spreading sequence.

The current work is organized as follows. A historical perspective on which this research is founded will be followed in Chapter 3 by a succinct definition of the signals known collectively as spread spectrum multi-$h$ (SSMH) modulation along with some of their characteristics. Using the signal definition, a potential transmitter implementation follows in Chapter 4. The spectral characteristics of the transmitted signals are of vital importance in an LPI environment, hence the power spectral densities of these signals will be analytically derived and simulated in Chapter 5. Then receiver structures associated with the coherent reception of SSMH signals will be analytically derived in Chapter 6. The performance of these optimal receivers in an additive white Gaussian noise environment is then upper bounded in Chapter 7 and the system numerically simulated in Chapter 8. In Chapter 9, the detectability of these signals by an unintended receiver that has all the optimal information about the signal will be addressed. Lastly, Chapter 10 will summarize the results and conclusions of this work.

# CHAPTER 2

# Historical Perspective

The spectra of signals modulated by random or pseudorandom sequences was first investigated in 1961 by Titsworth and Welch[63]. They specifically considered discrete signaling and sinusoidal modulation. In 1963, Bennett and Rice concentrated on binary frequency shift keying techniques[17], and considered the spectral density and autocorrelation functions of sinusoidal segments leading to continuous and discontinuous phase/frequency shift keying. Their work was further amplified and optimum coherent reception of binary frequency shift keying (FSK) derived by deBuda[21], who showed that for low deviation ratios ($h = 1/2$), the radio frequency bandwidth of digital FM signals was smaller and performance better than conventional FSK.

In early 1974, Cahn extended the earlier work of Viterbi[68] and Forney[25] to show that digital sequences modulating either FSK or phase shift keying signals could be sequentially and maximum likelihood detected using the Viterbi Algorithm with an inherent detection delay[20]. Later in that year, Ungerboeck extended the approach to show that the Viterbi Algorithm could also be used to perform carrier phase tracking as well as detection by expanding the state definition[65].

Concurrently, Osborne and Luntz published a paper of major significance that derived the optimum maximum likelihood receivers for CPFSK under coherent and noncoherent conditions[45]. Additionally, high and low signal-to-noise ratio approximations were considered. Among their conclusions was the fact that noncoherent reception could perform as well as coherent detection.

In the same year, Bernstein extended the work of Urkowitz[66] on energy detection of deterministic signals, to derive the optimum energy detectors of pseudonoise waveforms[18]

for phase modulated signals. The work of Baker in October of 1974 to define the asymptotic behavior of digital FM spectra helped further define the low SNR properties of FM signals[16].

The power spectrum of digital continuous phase shift keying and frequency shift keying was considered later in 1975 by Rowe and Prabhu[53], who showed the time average autocorrelation method of spectral analysis of FSK including partial response signaling. Additionally, they derived conditions for the existence of discrete lines in the spectrum.

Multi-$h$ modulation was introduced in 1975 in a landmark paper by Miyakawa[42], who extended the continuous phase FSK techniques of deBuda by cyclically changing the modulation index to create 'multi-mode' binary CPFSK. By changing the modulation index from interval to interval, the distance characteristics of the continuous phase frequency shift keying signaling increased; the result was enhanced performance while at the same time maintaining bandwidth efficiency with the continuous phase property. He thus introduced a bandwidth efficient constant envelope signaling scheme.

At the same time, Garrison showed that the power spectra of digital FM could be calculated by making linear approximations to the input waveforms[26].

Continuous phase systems moved to the hardware implementation stage in 1976 when deBuda showed simple implementation of his Fast FSK system [22]. Additionally, Schonhoff extended the work of Osborne and Luntz to show that their results held for M-ary signaling as well as binary signaling, that M-ary systems outperformed binary schemes, and continuous phase systems outperformed conventional PSK systems[57].

Late in 1976, Anderson and deBuda showed that continuous phase or frequency shift keying systems displayed a trellis structure and could be detected using the Viterbi Algorithm[2]. In addition, if the modulation indices of Miyakawa's multi-mode (now multi-$h$) CPFSK were the ratio of small integers, then the CPFSK signals also had a trellis structure, which implied that they could be detected with the Viterbi Algorithm. In 1977, Anderson and Taylor exposed the characteristics of multi-$h$ signals by showing their spectral characteristics and showing that enhanced performance was obtained by the increased signal distance characteristics[5].

Coincident with the growth of multi-$h$ modulation was the maturation of spread spectrum techniques, which resulted from the desire to have anti-jam and anti-intercept com-

munications. An excellent review of the origins of spread spectrum systems was provided in the text by Simon, Omura, Scholtz, and Levitt, *Spread Spectrum Communications*[59].

In 1978, significant extension of multi-$h$ system theory was done by Anderson, Taylor, and Lereim[4,3]. Anderson and Taylor expanded their previous work to examine and report in a landmark paper[4] the signaling properties, distance properties, and detection performance by sequence estimation of multi-$h$ phase coding. Additionally, they included the spectral density findings of Lereim from his independent research[3,33]. Their results confirmed that multi-$h$ was indeed a bandwidth and power efficient modulation technique.

In 1979, Aulin, Rydbeck, and Sundberg used their previous work in partial response signaling, M-ary CPFSK, and pulse shaping in conjunction with multi-$h$ signaling to produce a combined modulation and coding scheme that provided power/bandwidth performance that exceeded conventional rectangular signaling multi-$h$ modulation[8].

In the early 1980's, multi-$h$ modulation reached a level of acceptance such that various attempts were made to begin implementation. Using the earlier work of Scharf[56], Wilson and Hsu devised a maximum *a posteriori* (MAP) sequence/phase estimator that utilized an expanded state vector and the Viterbi Algorithm to jointly estimate the data and phase of trellis coded systems[74,30]. Shortly thereafter (1981), Mazur and Taylor used a decision directed phase lock loop to establish synchronization and the Viterbi Algorithm to decode multi-$h$ phase coded signals[40].

Coincidently, Wilson and Gaus extended the earlier efforts of Lereim and generalized the power spectral calculations of multi-$h$ phase codes to include M-ary signals, pulse shaping, and arbitrary $h$ codes[72]. Their landmark paper investigated simulation, Markov chain, direct, and autocorrelation methods of spectral calculations as well as deriving the conditions for discrete spectral lines and spectral approximation methods.

In May of 1981, Anderson simulated the performance of multi-$h$ coded signals[1]. In the process of simulating additive white Gaussian noise channels, he devised a signal space receiver and confirmed that multi-$h$ was an attractive modulation technique for bandlimited channels. Simultaneously, Aulin and Sundberg were consolidating the work of Anderson, Baker, and Garrison to show numerical calculation methods for the spectra of multi-$h$ signals[14]. The following year they refined the autocorrelation method to generalize a direct numerical calculation method for the spectrum[9]. Later in the year,

they also used Baker's asymptotic approximations to estimate the tails of the spectra[12]. At the same time, they performed extensive analysis on the distance properties of multi-$h$ signals including bounding the Euclidean distance and confirming that M-ary signals outperformed binary signals[15]. They also concluded that quarternary, two $h$, systems performed the best[13].

During the same time frame, considerable work was performed in spread spectrum systems and the detection of digital signals. Pickholtz, Schilling, and Milstein summarized the state of spread spectrum in May of 1982 in a landmark paper[47] that complemented the theoretical work of Holmes[28] and Dixon[24]. Much of the work in spread spectrum concentrated on its low probability of intercept characteristics, which Krasner approached from the opposite view. He based his efforts on the earlier work of Dillard[23] on detectability and formulated the optimum receiver structures for digitally modulated signals when the data sequence was unknown[32]. His results followed closely the optimal receivers of Osborne and Luntz.

During mid 1982, Wilson, Highfill, and Hsu used the method of a difference state space to develop upper and lower bounds on the performance of multi-$h$ coding systems[73]. At the same time, Simmons and Wittke attempted to reduce the complexity of Viterbi Algorithm sequence detectors by using a reduced state space of received signals[58].

The following year saw increased efforts to perfect the implementation of multi-$h$ receivers. Wickert and Ziemer considered the practical aspects of bandlimiting and amplitude-limiting of multi-$h$ signals[70,71]. Additionally, they considered phase and timing errors, and found that there was minimal degradation in performance as a result of these factors.

Aulin and Sundberg also published a paper of major impact which summarized their earlier work on a general numerical method of calculation of the power spectrum of CPM signals[11]. Subsequent work by Maseng used the characteristic function of the phase change variable to calculate the autocorrelation function[38] and power spectrum[39] of multi-$h$ signals.

The year 1984 saw increased research and consideration of LPI signaling and signal detection. Detector structures for the reception of spread spectrum signals was the objective of an in depth study by Axiomatix Corporation[48]. The study concluded that

the radiometer energy detection of Dillard and Urkowitz may well be the best practical approach to detection of direct sequence spread spectrum systems. Subsequently, Torrieri addressed the transmission of LPI signals as well as their detection with similar conclusions[64]. Simon, Omura, Scholtz, and Levitt also addressed the issue in their definitive text on spread spectrum communications[59]. Meanwhile, Ziemer and Peterson were investigating the attributes of combining spread spectrum techniques with bandwidth efficient modulations[77]. In particular, they showed the extension and ease of implementation of spread spectrum minimum shift keying signaling.

At the same time, Anderson, Aulin, and Sundberg had consolidated their earlier research and produced a preeminent compendium entitled *Digital Phase Modulation*[6].

More recently, Ho and McLane used the autocorrelation method along with the Markov state characteristics of CPM signals to derive a recursive algorithm for the calculation of the power spectra of CPM signals with correlated input data symbols[27].

Receiver structures for multi-$h$ signals have also been maturing with the efforts of Liebetreu and Wickert[35,34]. Using the work of Scharf[56], Cahn[20], and Viterbi[68], Liebetreu developed a dynamic programing algorithm (i.e., Viterbi Algorithm) with expanded states to jointly estimate the data and phase state of multi-$h$ signals[34]. In 1986, he showed a simplification process of state reduction to reduce receiver complexity and computation time. Subsequently, both authors simulated the receiver performance and included practical aspects such as bandlimiting, timing errors, and decision depth[35].

Most recently, Premji and Taylor suggested alternate receiver structures that employed matched filters to perform maximum likelihood sequence estimation and jointly determine the carrier phase and symbol timing[51]. Additionally, Premji has shown the practical aspects of their receiver by using only an average $h$ value to reduce the state and matched filter structure and included synchronization effects with the result of minimum degradation in performance[50].

The concept of combining spread spectrum techniques with bandwidth efficient modulation schemes was initially considered by Sadr and Omura in January, 1988 [55] following their research efforts in 1983 [54]. They concluded that direct sequence spreading of a digital source prior to minimum shift keying modulation produced a signaling structure that was optimally detected using the Viterbi Algorithm with joint phase and data detection

from an expanded signal state vector.

The present work will extend this historical foundation by combining the power and bandwidth efficient characteristics of multi-$h$ modulation with the low probability of intercept attributes of spread spectrum techniques.

# CHAPTER 3

# Signal Description

This chapter defines the signals that will be collectively referred to as spread spectrum multi-$h$ signals. Some of the resulting properties and characteristics are discussed along with some of the limitations and assumptions used in this presentation.

## 3.1 Signal Definition

Spread spectrum multi-$h$ (SSMH) modulated signals are defined by a transmitted signal

$$s(t,\underline{\alpha},\underline{c},\underline{h}) = \sqrt{\frac{2E_c}{T_c}}\ \cos(2\pi f_0 t + \phi(t,\underline{\alpha},\underline{c},\underline{h}) + \theta_0), \tag{3.1}$$

where the information symbol, $\alpha_i$, is multiplied by a random/pseudorandom spreading sequence of $c_{ij}$ dibits, or chips, and modulated in the phase

$$\phi(t,\underline{\alpha},\underline{c},\underline{h}) = 2\pi \int_{-\infty}^{t} \sum_{i=-\infty}^{\infty} \sum_{j=0}^{N_c-1} \alpha_i h_{(i+j) \bmod H} c_{ij} g(\tau-(j+iN_c)T_c)d\tau;\ \ -\infty \le t \le \infty. \tag{3.2}$$

The data sequence, $\underline{\alpha}$, is an $M$-ary ($M$ is a power of 2) infinitely long sequence of uncorrelated equally likely data symbols; each with a value of $\alpha_i = \pm 1, \pm 3, \ldots, \pm(M-1)$, with $i = 0, \pm 1, \pm 2, \ldots$, and symbol duration $T_s$. The carrier frequency is $f_0$ and $\theta_0$ is an arbitrary constant initial phase which will be set to zero under the assumption of perfect coherency.

The spreading sequence, $\underline{c}$, is assumed to be an infinitely long sequence of uncorrelated equally likely chips, each with a value of $c_{ij} = \pm 1$. This sequence is presumed known *a priori* by both the transmitter and the receiver. Practical implementations require that this sequence become finite (implying correlated) with implementation via an m-sequence

generator for example. The present work will assume an infinitely long and uncorrelated sequence. Additionally, it will be assumed that there are an integer number of chips, $N_c$, per symbol interval such that $T_s = N_c T_c$.

The modulation index, $\underline{h}$, is a finite length sequence of cyclically varying fixed frequency deviations, such that

$$h_{i+j} = h_{i+j+H} = n_i/p, \text{ or,} \tag{3.3}$$

$$h_{i+j} = h_{(i+j) \bmod H}. \tag{3.4}$$

The numerators, $n_i$, and denominator, $p$, are fixed integer numbers. As a result, a finite state description for the signal structure can be made and can be reflected in finite state trellis structures.

While the number of frequency deviations is finite and fixed for a given modulation system, the number of deviations in the sequence can be variable and influences the resulting system performance. In general, it has been shown that up to a point, multi-$h$ systems with longer $h$ sequences perform better than systems with shorter $h$ codes [15]. The present work considers only systems with two modulation indices for simplicity. An obvious extension is to systems with longer frequency deviation codes.

The phase transitions in the signal definition to this point have been indexed on a bit basis for the information sequence and on a chip basis for the chip sequence. The application of the frequency deviation ratio, $h_{(i+j) \bmod H}$, on a chip basis will be referred to as *conventional* spread spectrum multi-$h$ modulation. This leads to the expression of the phase of the transmitted signal as

$$\phi(t, \underline{\alpha}, \underline{c}, \underline{h}) = 2\pi \sum_{i=-\infty}^{\infty} \sum_{j=0}^{N_c-1} \alpha_i c_{ij} h_{(i+j) \bmod H} q(t - (j + iN_c)T_c), \tag{3.5}$$

where $q(t)$ is the chip phase transition resulting from the frequency pulse shaping function $g(t)$.

At the same time, it should be noticed that the frequency deviation can be applied on a bit basis resulting in the ratio being indexed along with the bit sequence, i.e., $h_i$. This type of application will be referred to as *modified* spread spectrum multi-$h$ modulation.

In this situation, the phase is expressed as

$$\phi(t,\underline{\alpha},\underline{c},\underline{h}) = 2\pi \sum_{i=-\infty}^{\infty} \sum_{j=0}^{N_c-1} \alpha_i c_{ij} h_{i \bmod H} q(t-(j+iN_c)T_c). \tag{3.6}$$

The frequency smoothing pulse, $g(t)$, acts on the product of the chip and the data symbol to define the shape of the phase response, $q(t) = \int_{-\infty}^{t} g(\tau)d\tau$. Generally, $g(t)$ is a causal smoothing pulse of arbitrary form and length $LT_c$, where $L$ is a positive integer. When $L$ is greater than one, partial response signaling results. The pulse is normalized so that $q(LT_c) = 1/2$. For this work, it will be assumed that $g(t)$ is constant over a chip interval so that

$$g(t) = \begin{cases} \frac{1}{2T_c} & 0 \le t \le T_c \\ 0 & \text{otherwise,} \end{cases} \tag{3.7}$$

which results in a constant slope phase change over a chip interval as shown in Figure 3.1.

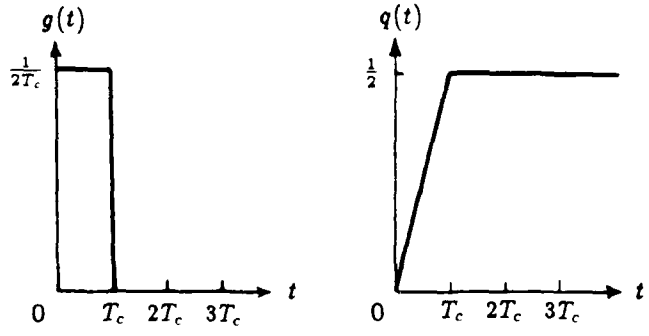


Figure 3.1: Chip Pulse Shaping Forms

With the smoothing pulse, $g(t)$, acting on each chip and data symbol, the characteristics of continuous phase systems are preserved by requiring that the phase transitions at chip intervals be a continuous function of time.

Following the lead of Anderson and others[6], the phase change during the $l$-th bit and $n$-th chip, can be expressed (assuming rectangular pulse shaping and fixed rational modulation indices) as

$$\phi(t,\underline{\alpha},\underline{c},\underline{h}) = 2\pi h_{(l+n) \bmod H} \alpha_l c_{ln} q(t) + \theta_{ln} = \theta(t,\alpha_l,c_{ln},h_{(l+n) \bmod H}) + \theta_{ln}, \tag{3.8}$$

where

$$\theta_{ln} = [\pi \sum_{i=-\infty}^{l} \sum_{j=0}^{n-1} h_{(i+j) \bmod H} \alpha_i c_{ij}] \bmod 2\pi. \tag{3.9}$$

As shown in *Digital Phase Modulation*[6], this expression describes a Markov state system with $p$ states. As a result, the signaling waveform will exhibit a periodic trellis structure. However, the inclusion of the cyclically changing modulation indices will alter the periodicity of the trellis as compared to fixed deviation continuous phase systems. Additionally, if m-sequences are used for the spreading code, an additional level (extremely long) of periodicity is introduced. The essence of the trellis structure remains the fixed repetitive Markov state structure. As mentioned above, simple examples of spread multi-$h$ trellis structures are shown in Figures 3.2 and 3.3 below. The diagrams illustrate the possible phase transitions according to the $c_{ij}$'s if viewed as if the information bit is a constant $+1$. Alternatively, if all of the dibits are $+1$, then the phase changes according to the information bits are shown.

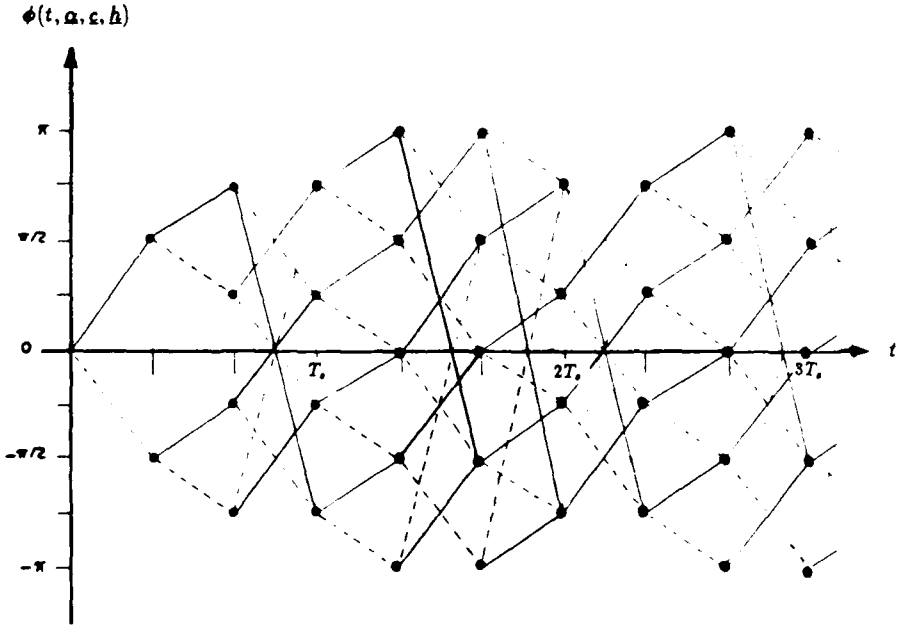


Figure 3.2: Conventional SSMH Trellis Structure; $h = \frac{1}{2}, \frac{1}{4}$

It is appropriate at this point to reiterate some of the characteristics of the SSMH trellis structure. For conventional spread spectrum multi-$h$, the essence of multi-$h$ signaling remains and the corresponding distinguishing features of the trellis remain intact; but

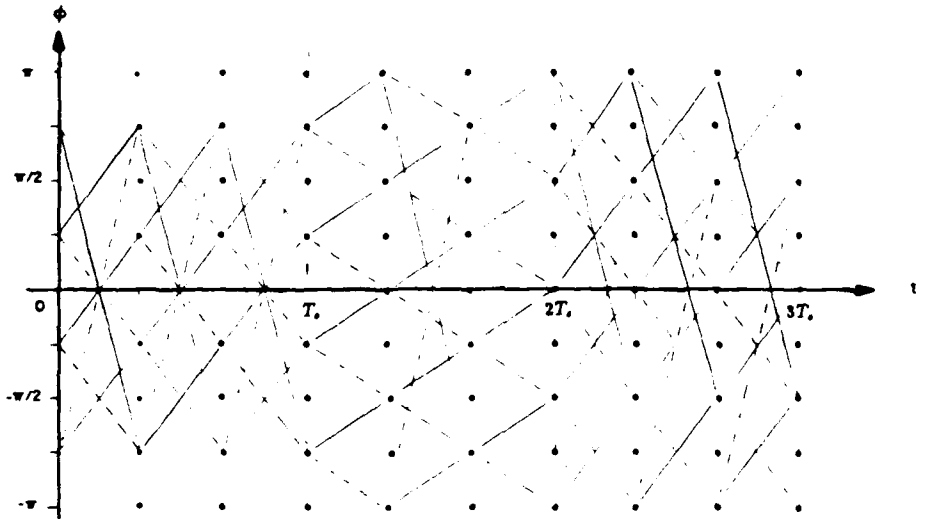


Figure 3.3: Modified SSMH Trellis Structure; $h = \frac{1}{2}, \frac{1}{4}$

the specific characteristics must be amended to account for the spreading sequence. As a result, the characteristics as delineated by Anderson and Taylor [4] must be refined to include the following,

- The minimum value of the binary unmerged interval is $C = H$ only if $p \geq 2^H$, and no subsets of $\{h_{ij}\}$ have an integer sum over $N_c$ chips.
- The period of the trellis remains $T_p = HT_c$ if $\sum_{i=1}^{H} n_i$ is even; and the period of the trellis is $T_p = 2HT_c$ if $\sum_{i=1}^{H} n_i$ is odd.
- The number of phase states is $p$ if the summation of the $n_i$ is even; or the number of states is $2p$ if the summation of the $n_i$ is odd, where $n_i$ are the numerators of the modulation indices.

When modified spread spectrum modulation is used, the characteristics change slightly and are,

- The minimum value of the binary unmerged interval is $C = H$ only if $p \geq 2^H$, and no subsets of $\{h_{ij}\}$ have an integer sum over $N_c$ chips.

- The period of the trellis is $T_p = HN_cT_c$ if $\sum_{i=1}^{H} n_i$ is even; and the period of the trellis is $T_p = 2HN_cT_c$ if $\sum_{i=1}^{H} n_i$ is odd.
- The number of phase states is $p$ if the summation of the $n_i$ is even; or the number of states is $2p$ if the summation of the $n_i$ is odd, where $n_i$ are the numerators of the modulation indices.

## 3.2 Assumptions

Prior to embarking on the analysis of SSMH systems, it is appropriate to first recount the assumptions that limit and define the scope of the modulation schemes to be considered.

These assumptions are as follows.

- Independent binary information sequence.
- Independent infinite length spreading code sequence.
- Perfect bit and chip synchronization and timing.
- Perfect coherent carrier phase reference.
- Integer number of chips per bit.
- Independent two index frequency deviation code.
- No filtering effects.
- Full response rectangular pulse shaping.
- Equal energy per chip.

# CHAPTER 4

## Transmitter Implementation

The concept of spread spectrum multi-$h$ signaling, as stated previously, is to apply direct sequence spreading to a digital information sequence prior to multi-$h$ modulation. The conceptual structure of the SSMH transmitter is shown in Figure 4.1. The binary ($\pm 1$) information bit is multiplied by a much higher rate dibit (value of $\pm 1$) to yield a digital binary input sequence that is input to a conventional multi-$h$ modulator.

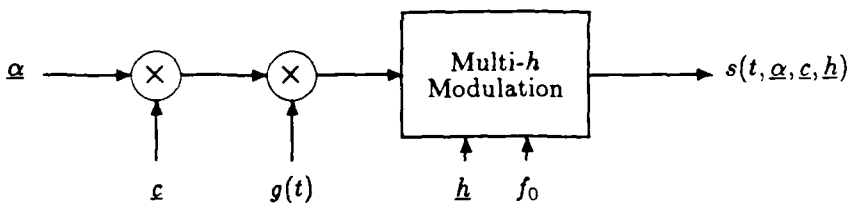


Figure 4.1: Spread Spectrum Multi-$h$ Transmitter

Using equations 3.1, 3.2, 3.5, and 3.6 as the definition of the desired transmitted signal, the transmitter structure can be further defined following trigonometric expansion and substitution. With the initial arbitrary phase set to zero and rectangular pulse shaping, the signal definition for the interval, $jT_c \leq t \leq (j+1)T_c$, may be expressed as

$$s(t,\alpha,c,h) = \sqrt{\frac{2E_c}{T_c}}\,[I(t)\cos\omega_0 t - Q(t)\sin\omega_0 t], \tag{4.1}$$

where the inphase term is

$$\begin{aligned} I(t) \;=\; & [\cos(2\pi h_{(i+j)\bmod H}\alpha_i c_{ij} q(t))]\cos\theta_{ij} - \\ & [\sin(2\pi h_{(i+j)\bmod H}\alpha_i c_{ij} q(t))]\sin\theta_{ij}, \end{aligned} \tag{4.2}$$

and the quadrature term is

$$Q(t) = [\sin(2\pi h_{(i+j) \bmod H} \alpha_i c_{ij} q(t))] \cos\theta_{ij} + [\cos(2\pi h_{(i+j) \bmod H} \alpha_i c_{ij} q(t))] \sin\theta_{ij}. \quad (4.3)$$

These equations form the basis of the quadrature transmitter structure of Figure 4.2 shown below.

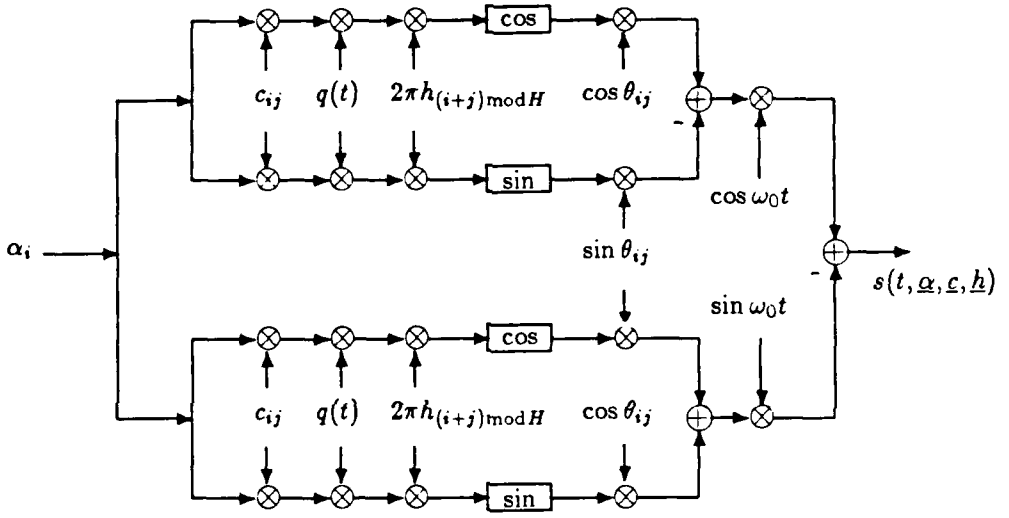


Figure 4.2: Quadrature Transmitter Structure

Since the phase states, $\theta_{ij}$, are fixed for rational modulation indices, and result from the previously discussed Markov description of the signaling waveform, it is apparent that the modulation process could be implemented in a recursive 'lookup table' fashion. Based on the current input data bit and the phase state after the last bit, a new transmitted waveform can be easily implemented in quadrature form prior to modulation by the carrier frequency.

Implementation of a similar form of a CPM transmitter using a read only memory (ROM) based signal generator has been shown by Anderson and others[6].

While not the subject of this work, it should be mentioned at this point that the dibits would be generated from pseudorandom generators of any appropriate type. It

is assumed here that the pseudorandom generation is such that the period is extremely long; in effect yielding a dibit sequence for which the individual chips can be considered to be independently generated plus or minus one. From the transmitter implementation standpoint, the pseudorandom generator is simply an independent component.

This same characteristic holds for the pulse shaping function. As previously delineated, this function may take on many forms with rectangular pulse shaping being the simplest case. Once again, from the transmitter implementation standpoint, it is a simple process to generate different pulse shaping functions, which will have a marked effect on the transmitted signal.

Finally, the ease with which it is possible to change the fundamental nature of the transmitted signal is shown in the ease with which the frequency deviation ratio sequence can be changed. It is obvious that the magnitude of these ratios can be readily changed. It should also be apparent that the method in which this frequency deviation is applied can be changed. In one case, the index can change during each chip interval; thereby resulting in *conventional* SSMH. On the other hand, it would be a simple matter to clock the sequence in accordance with the incoming data bit sequence and thereby produce *modified* SSMH, where the modulation indices change cyclically on a bit basis. Subsequent chapters will address the attributes of the signals produced by either of these methods.

# CHAPTER 5

# Spectral Analysis

One major purpose of spread spectrum multi-$h$ modulation is to create a signal waveform that presents a power density spectrum that has a wide flat mainlobe and rapid sidelobe rolloff. If transmitted at low signal-to-noise ratios, the broad flat spectrum becomes difficult to detect, observe, and characterize by unintended receivers. At the same time, finding analytical expressions and numerical results for digital FM signals has been referred to as 'analytically perverse' [26], due to the mathematical complexity and in general lack of closed form solutions. This results from the nonstationarity of random input waveforms, which means that direct autocorrelation methods do not apply[6]. However, average power spectra can be calculated. This chapter addresses the problem of analytically describing SSMH signal power density spectra.

Initially, the spectra for both conventional and modified SSMH are derived and it is shown that the spectra have the same characteristics as the original unspread multi-$h$ signals when normalized to the chip rate. It is also shown that from a spectral analysis standpoint, conventional and modified SSMH signals have the same spectral characteristics for consistent modulation indices. On the other hand, selection of the indices determines uniquely different spectra. As a result, control over the transmitted spectra can be obtained so that the resultant transmitted spectra may have the desired LPI characteristics.

Following a brief summary of the methods available for spectral analysis, the spectra for conventional SSMH signals are derived in Section 5.2, and the spectra for modified SSMH signals are derived in Section 5.4. Section 5.6 addresses common characteristics of the spectra, and finally the detectability of SSMH signal spectra will be addressed in Section 5.7.

## 5.1 Methods of Spectral Analysis

Various approaches to analytically deriving and describing the power density spectrum of phase/frequency modulated signals have been presented. These approaches generally fall into four categories,

1. Simulation[72],
2. Direct approach[17,63,72],
3. Markov chain approach[53,33], and
4. Autocorrelation approach[17,9,11,14].

The simulation method is straightforward application of the discrete Fourier transform. The complex envelope, $e^{j\phi(t_k)}$, is sampled and the spectrum estimated by[72]

$$S(f) = \mid X_N(f) \mid^2, \text{ where } X_N(f) = \sum e^{j\phi(t_k)} e^{-j2\pi f t_k}. \tag{5.1}$$

While uncomplicated, this approach may not give accurate results due to bias effects[72].

The direct approach is to take the Fourier transform of the autocorrelation of a deterministic signal, then average over the input sequence and the random phase. The spectrum can be expressed as[6]

$$S(f) = \lim_{N\to\infty} \frac{1}{NT} \mathcal{E}\{\mid S_N(f, \underline{\alpha}) \mid^2\}. \tag{5.2}$$

In the case of multi-$h$ signals, the period, $T$, is extended to $HT$ to account for the variation in $h$[72]. This method generally leads to complicated integrals, sometimes in two dimensions.

The Markov approach utilizes the Markov state description from the trellis diagram and computes the lowpass spectra for each state transition[72]. Hence, the spectrum is described via

$$S(f) = \frac{1}{T} \sum_{j=1}^{N} \sum_{k=1}^{N} \sum_{n=-\infty}^{\infty} \frac{1}{N} e^{-j2\pi f n T} P_{jk}^n S_j^*(f) S_k(f), \tag{5.3}$$

where $P_{jk}$ is the $jk$-element of the transition matrix, and $S_j$ and $S_k$ are the Fourier transforms of the lowpass complex envelopes of the $j$th and $k$th state waveforms[72]. Once again, the methodology is rather complicated.

Finally, the autocorrelation method for general CPM was derived by Anderson and others[6]. The procedure involves taking the product of $s(t,\underline{\alpha})$ and $s(t+\tau,\underline{\alpha})$, averaging over the input data sequence, time averaging the product over $T_s$, then Fourier transforming to obtain the average spectrum[6,14,9,11]. This general method has been applied to multi-$h$ signaling schemes by Anderson and others[6] by extending the time averaging over an interval $HT_s$. This is the approach taken in the current work.

The result is that the spectrum will be calculated from the expression

$$S(f) = 2\Re\int_0^\infty R(\tau)e^{-j2\pi f\tau}d\tau, \tag{5.4}$$

where $\Re$ is the real part, and

$$R(\tau) = \frac{1}{HN_cT_c}\int_0^{HN_cT_c} \mathcal{E}_{\underline{\alpha},\underline{c}}e^{j\phi(t+\tau,\underline{\alpha},\underline{c},\underline{h})}e^{-j\phi(t,\underline{\alpha},\underline{c},\underline{h})}\,dt. \tag{5.5}$$

Using these expressions, the analytical power density spectra for various parameter spread spectrum multi-$h$ signals will be derived. The first objective of the work will be accomplished with broad flat spectra with rapid sidelobe rolloff.

*Applying this methodology* to the current work requires two considerations. First, the random direct sequence of infinite duration can be handled by averaging over the sequence (equally probable $\pm 1$) assuming independent and identically distributed chips. Secondly, because the sequentially generated spreading code is considered to have an independent distribution, no consideration is given to the fact that in reality this sequence must be generated by a device that will have a fixed, but hopefully very long, period. This periodicity will introduce correlation in the spreading sequence that will not be considered.

The effect of the changing modulation index is to smooth the spectral density curves, which implies that better results may be obtained by applying the modulation index on a chip interval basis rather than on a bit interval basis. This issue will be addressed by analytically deriving the spectra for both modulation schemes and it is shown that the resulting spectra have essentially the same characteristics for a given modulation index code.

The general method of analysis then for the power spectral density is to obtain the autocorrelation of the signal expression, invoke the time averaged autocorrelation approach of Papoulis [46], and implement the Wiener-Khintchine Theorem to Fourier transform the

time averaged autocorrelation to obtain a 'probabilistic representation' [33] of the power spectral density.

The derivation begins by recalling that $s(t)$ can be represented in complex form by

$$s(t) = \Re\{u(t)\} = \sqrt{\frac{2E_c}{T_c}}\ \cos(2\pi f_0 t + \phi(t) + \theta_0), \tag{5.6}$$

where

$$u(t) = \sqrt{\frac{2E_c}{T_c}}\ \{e^{j(2\pi f_0 t + \phi(t) + \theta_0)}\} = \sqrt{\frac{2E_c}{T_c}}\ e^{j(2\pi f_0 t + \theta_0)} e^{j\phi(t)} \tag{5.7}$$

The autocorrelation function then can be expressed as

$$R(t_1, t_2) = \mathcal{E}\{s(t_1)s(t_2)\}, \tag{5.8}$$

where $\mathcal{E}\{\cdot\}$ represents the ensemble average. Using the fact that $\theta_0$ is randomly distributed on $2\pi$, and $\mathcal{E}\{\Re(u(t))\} = \mathcal{E}\{\Im(u(t))\}$, and following the procedure shown by Lereim [33], the autocorrelation function reduces to

$$R(t_1, t_2) = \frac{E_c}{T_c}\cos(2\pi f_0(t_1 - t_2))\mathcal{E}\{e^{j(\phi(t_1) - \phi(t_2))}\}. \tag{5.9}$$

Since this autocorrelation function is dependent on $t_1$ and is therefore not stationary, the power density spectrum and the autocorrelation do not form a Fourier transform pair. However, as shown by Papoulis [46] and Lereim [33], if $\phi(t)$ is a periodic function, a cyclostationary process results and the power density spectrum will form a Fourier transform pair with the 'time averaged' autocorrelation function.

Thus

$$R(\tau) = < \frac{E_c}{T_c}\cos(2\pi f_0 \tau)\mathcal{E}\{e^{j(\phi(t) - \phi(t+\tau))}\} >, \tag{5.10}$$

and by the Wiener-Khintchine Theorem

$$S(f) = \mathcal{F}\{R(\tau)\} = \frac{E_c}{T_c}G(f) * \{\frac{1}{2}\delta(f - f_0) + \frac{1}{2}\delta(f + f_0)\}, \tag{5.11}$$

where $G(f)$ is the spectrum of the lowpass process $e^{j(\phi(t) - \phi(t+\tau))}$, $*$ indicates the convolution process, and $\delta$ is the Kronecker delta function. Therefore,

$$G(f) = \mathcal{F}\{\mathcal{E}(e^{j(\phi(t) - \phi(t+\tau))})\} \tag{5.12}$$

Since the spectrum of the lowpass process characterizes the spectrum of the entire process, the remainder of this discussion will concentrate on the derivation of the lowpass spectra. Additionally, the application of the modulation indices now becomes a factor and the lowpass spectra for each type of SSMH signal must be derived separately.

## 5.2 Conventional Spread Spectrum Multi-$h$ Spectra

From Chapter 3, the information carrying phase of the lowpass process is expressed as

$$\phi(t) = 2\pi \sum_{i=-\infty}^{\infty} \sum_{j=0}^{N_c-1} \alpha_i c_{ij} h_{(i+j) \bmod H} q(t - (j + iN_c)T_c). \tag{5.13}$$

By expanding the series and regrouping terms, the lowpass autocorrelation function can be expressed as

$$r(t_1, t_2) = \mathcal{E}_{\alpha,c}\{e^{j2\pi \sum_{m=-\infty}^{\infty} \sum_{n=0}^{N_c-1} \alpha_m c_{mn} h_{(m+n) \bmod H}[q(t_1-(n+mN_c)T_c)-q(t_2-(n+mN_c)T_c)]}\}. \tag{5.14}$$

The summations in the exponentials become products of exponentials and this expression reduces to

$$r(t_1, t_2) = \prod_{m=-\infty}^{\infty} \prod_{n=0}^{N_c-1} \mathcal{E}_{\alpha,c}\{e^{j2\pi \alpha_m c_{mn} h_{(n+m) \bmod H}[q(t_1-(n+mN_c)T_c)-q(t_2-(n+mN_c)T_c)]}\}. \tag{5.15}$$

Since the information sequence is assumed independent and identically distributed, as well as the chip sequence being independent and identically distributed, the joint distribution for the product of $\alpha$ and $c$ is $f_{\alpha c} = \frac{1}{2}\delta(\alpha c + 1) + \frac{1}{2}\delta(\alpha c - 1)$. Therefore,

$$r(t_1, t_2) = \prod_{m=-\infty}^{\infty} \prod_{n=0}^{N_c-1} \cos[2\pi h_{(n+m) \bmod H}(q(t_1-(n+mN_c)T_c)-q(t_2-(n+mN_c)T_c))] \tag{5.16}$$

The modulation indices applied on a chip basis are from a finite set of $H$ values and applied cyclically. As a result, after expanding the products, the above equation becomes a periodic product over $HT_c$ and by Papoulis [46] yields a cyclostationary process. Then the time averaged autocorrelation becomes

$$r(\tau) = \frac{1}{HT_c} \int_0^{HT_c} \prod_{n=-\infty}^{\infty} \cos[2\pi h_{n \bmod H}(q(t - nT_c) - q(t + \tau - nT_c))]dt. \tag{5.17}$$

At this point, it is important to realize that $g(t) = 0$, for $t \leq 0$ and $q(T_c) = 1/2$. The result (as shown by Anderson [6] and Aulin [11]) is that the infinite product in equation 5.17 becomes a finite product. Then

$$r(\tau) = \frac{1}{HT_c} \int_0^{HT_c} \prod_{n=0}^{H(k+1)+1} \cos[2\pi h_{n \bmod H}(q(t + \tau - nT_c) - q(t - nT_c))]dt \quad k = 0, 1, 2, \ldots, \tag{5.18}$$

and for $\tau = \acute{\tau} + kHT_c \geq HT_c$, where $0 \leq \acute{\tau} < HT_c$,

$$r(\tau) = r(\acute{\tau} + kHT_c) \quad k = 1, 2, 3, \ldots \tag{5.19}$$

Considering $k \geq 1$ and following the procedure shown by Anderson to expand the product [6], the autocorrelation becomes

$$r(\tau) = C_\alpha^{k-1}\Psi(\acute{\tau}), \quad k = 1, 2, \ldots \tag{5.20}$$

$$C_\alpha = \prod_{j=0}^{H-1} \cos(\pi h_{j \bmod H}), \tag{5.21}$$

$$\Psi(\acute{\tau}) = \frac{1}{HT_c}\int_0^{HT_c} \prod_{j=0}^{H-1} \cos[2\pi h_{j \bmod H}(\frac{1}{2} - q(t - jT_c))] \times \prod_{j=0}^{H+1} \cos[2\pi h_{(j+kH) \bmod H}(q(t + \acute{\tau} - jT_c)]dt, \tag{5.22}$$

which indicates that the autocorrelation function can be expressed as a single integral term and a geometrically decaying multiplicative constant.

With this expression for the autocorrelation function, the lowpass power spectral density of the real signals can be obtained by using the Fourier transform as shown in equation 5.4. Again, following the procedure described by Anderson [6], after subdividing the interval of integration in the transform, expressing the integral from $HT_c$ to infinity as an infinite summation, and noting that the infinite sum is convergent, then the lowpass spectrum can be expressed as

$$G(f) = 2\Re\{\int_0^{HT_c} r(\tau)e^{-j2\pi f\tau}d\tau + \frac{e^{-j2\pi fHT_c}}{1 - C_\alpha e^{-j2\pi fHT_c}}\int_0^{HT_c} r(\tau + HT_c)e^{-j2\pi f\tau}d\tau\}. \tag{5.23}$$

After normalization by the chip duration, $T_c$; that is, $fT_c = f_n$, this expression for the lowpass spectrum reduces to

$$G(f_n) = 2\Re\{\int_0^{H} r(\tau)e^{-j2\pi f_n\tau}d\tau + \frac{e^{-j2\pi Hf_n}}{1 - C_\alpha e^{-j2\pi Hf_n}}\int_0^{H} r(\tau + H)e^{-j2\pi f_n\tau}d\tau\}. \tag{5.24}$$

After combining exponentials in the second integral, changing variables, and expanding the complex exponentials to obtain the real terms, the lowpass spectrum expressions become

$$
\begin{aligned}
G(f_n) &= 2\{\int_0^H r(\tau)\cos(2\pi f_n\tau)d\tau + \\
&\quad \frac{a}{c}\int_H^{2H} r(\tau)\cos(2\pi f_n\tau)d\tau - \\
&\quad \frac{b}{c}\int_H^{2H} r(\tau)\sin(2\pi f_n\tau)d\tau\}, \qquad (5.25)\\
a &= 1 - C_\alpha\cos(2\pi f_n H),\\
b &= C_\alpha\sin(2\pi f_n H),\\
c &= 1 + C_\alpha^2 - 2C_\alpha\cos(2\pi f_n H).
\end{aligned}
$$

It should be noticed that the maximum value of $\tau$ in the above integrals is equal to $2H$, which from equation 5.18 implies that the maximum value of $k$ is one. Therefore, the autocorrelation functions become finite length expressions. The final expressions for the conventional SSMH power spectral density then become

$$
\begin{aligned}
G(f_n) &= 2\{G_1(f_n) + \frac{a}{c}G_2(f_n) - \frac{b}{c}G_3(f_n)\}, \quad \text{with,} \qquad (5.26)\\
G_1(f_n) &= \frac{1}{H}\int_0^H\int_0^H \prod_{j=0}^{2H-1} r_c(t,\tau)\cos(2\pi f_n\tau)dtd\tau,\\
G_2(f_n) &= \frac{1}{H}\int_H^{2H}\int_0^H \prod_{j=0}^{2H+1} r_c(t,\tau)\cos(2\pi f_n\tau)dtd\tau,\\
G_3(f_n) &= \frac{1}{H}\int_H^{2H}\int_0^H \prod_{j=0}^{2H+1} r_c(t,\tau)\sin(2\pi f_n\tau)dtd\tau,\\
r_c(t,\tau) &= \cos[2\pi h_{j \bmod H}(q(t+\tau-j) - q(t-j))].
\end{aligned}
$$

This analysis reflects the application of the methodology of Anderson and Lereim to this new class of spread spectrum signals. It confirms the expected results that when normalized to the chip rate, *conventional* SSMH signals have the same spectra as their parent multi-$h$ signals. The next section considers some numerical evaluations of these expressions for comparison with known multi-$h$ signal spectra.

## 5.3 Numerical Evaluation of Conventional SSMH Spectra

Before numerically evaluating the spectra of selected conventional SSMH systems, it is necessary to comment on the normalization for the spectra. In addition to the normalization to the chip frequency as done in the previous section, the spectra have been normalized

to unity chip energy and the spectra have been normalized to zero decibels at the carrier frequency. Since the spectra for real signals are being displayed, it is also only necessary to display the single sided density.

The spectra of equations 5.26 were evaluated via FORTRAN implemented computer programs for selected values of modulation indices. These indices were selected based on the results from Hsu [30] and Lereim [33], which indicated the 'best' modulation codes for bandwidth efficient modulations in terms of coding gain and bandwidth efficiency. Additionally, the codes were selected based on the desire to have a spectrum with a flat mainlobe and rapid sidelobe rolloff.

In order to verify the validity of the numerical evaluations, the degenerate case of one chip per bit, i.e., conventional multi-$h$ signaling, and with modulation indices $h_1 = h_2 = 1/2$, i.e., standard Minimum Shift Keying (MSK) was plotted. Figure 5.1 displays the resulting spectral density and is wholly consistent with previous results [33].

The figures that follow are depictions of the spectra for the following modulation schemes.

| *Modulation Indices* | *Chips per Bit* | *Figure* |
|---|---|---|
| 0.5, 0.75 | 3 | 5.2 |
| 0.5, 0.625 | 3 | 5.3 |
| 0.5, 0.625 | 5 | 5.4 |
| 0.583, 0.667 | 3 | 5.5 |
| 0.583, 0.667 | 5 | 5.6 |
| 0.375, 0.5 | 3 | 5.7 |

Table 5.1: Conventional SSMH Spectra

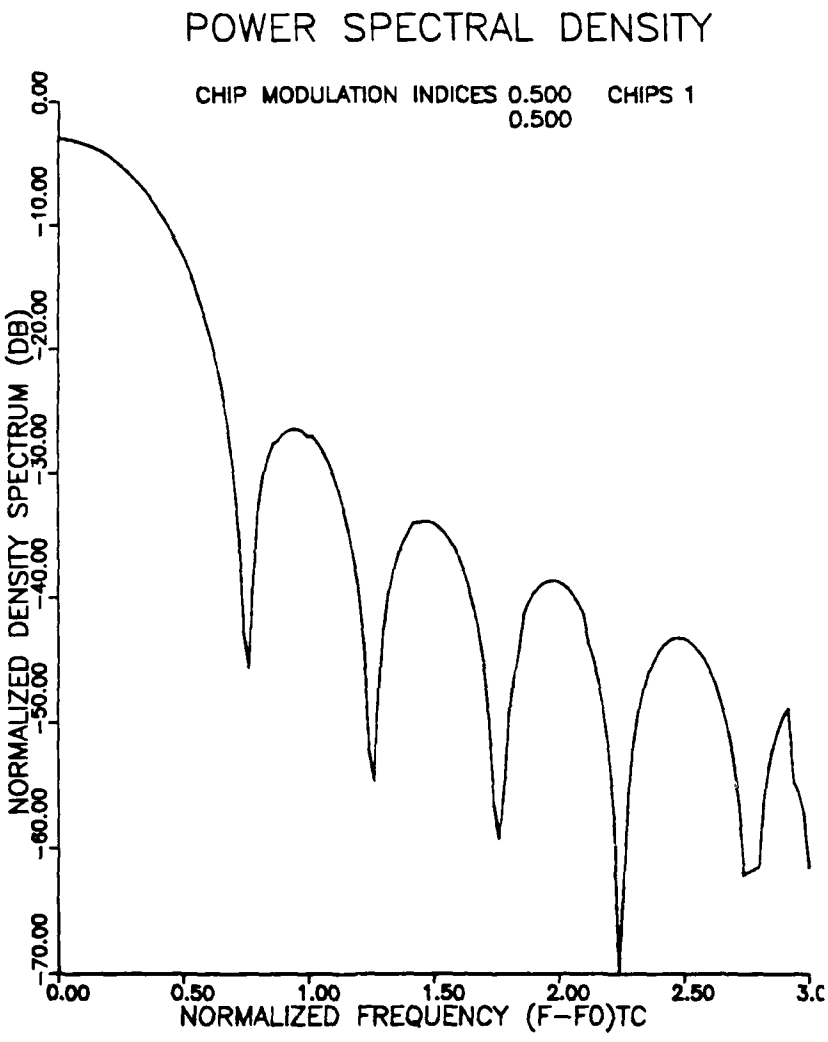


Figure 5.1: Minimum Shift Keying (MSK) Spectral Density

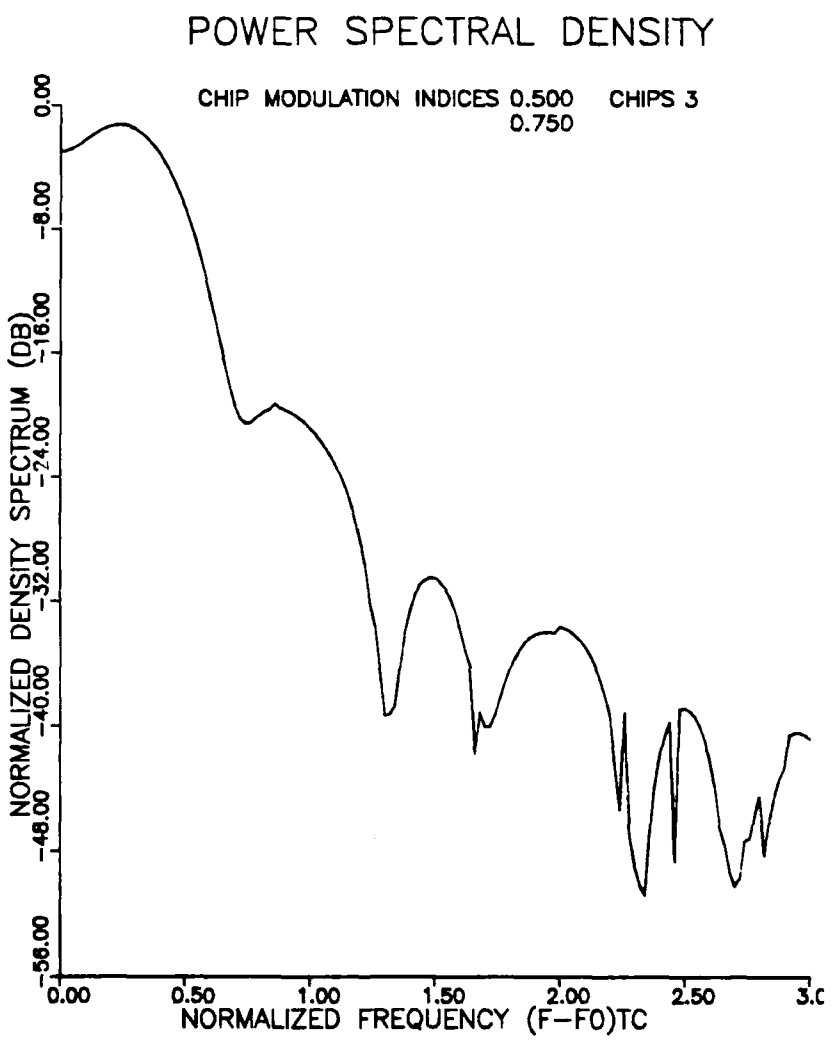


Figure 5.2: Conventional SSMH Spectrum for 0.5, 0.75 code; Chips per bit = 3

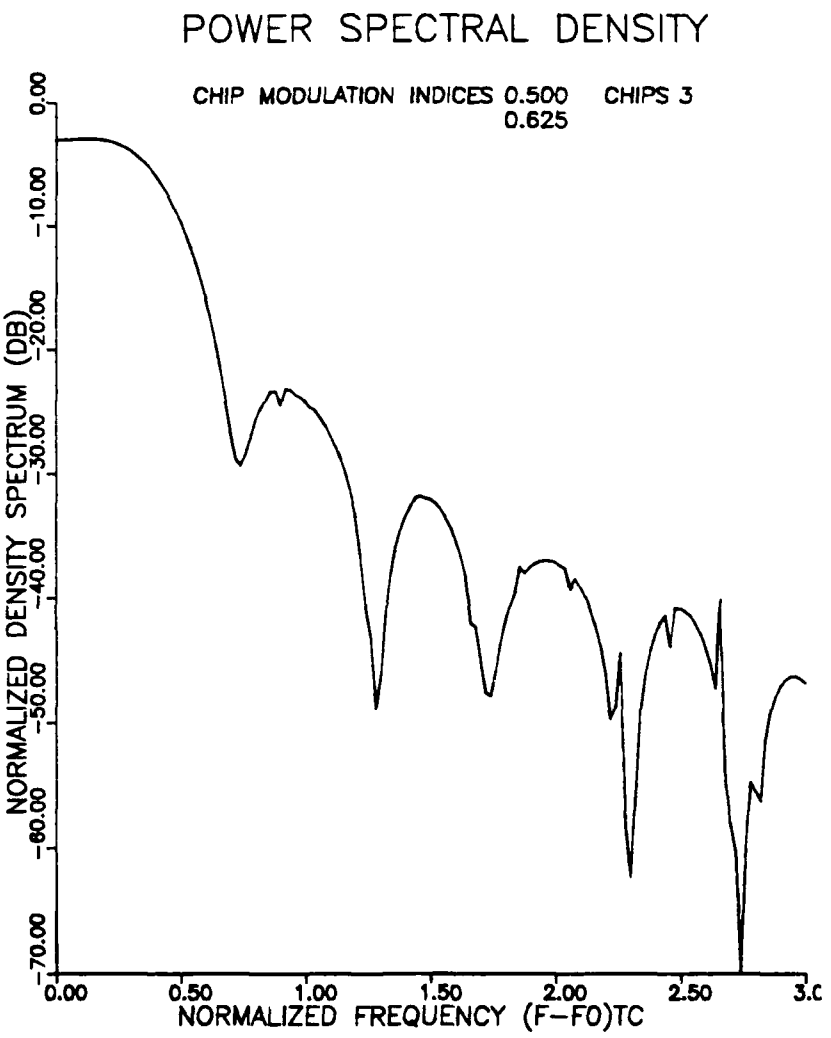


Figure 5.3: Conventional SSMH Spectrum for 0.5, 0.625 code; Chips per bit = 3

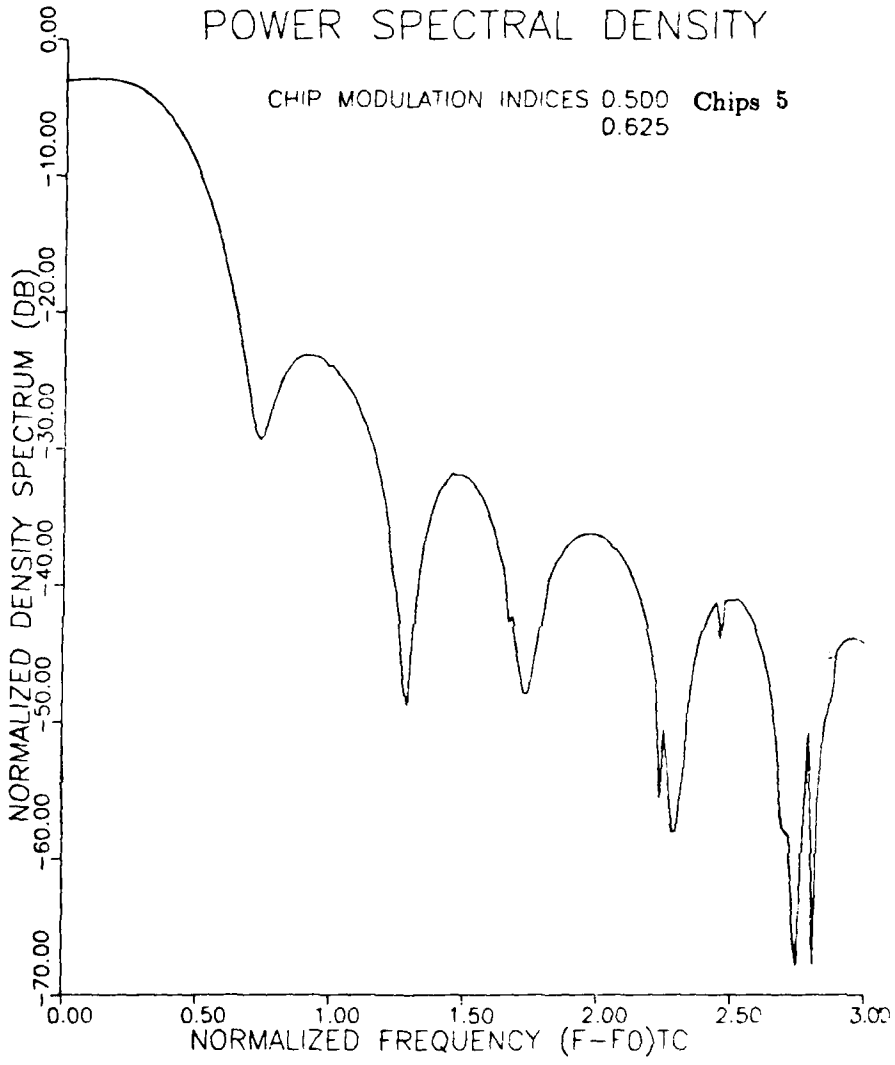


Figure 5.4: Conventional SSMH Spectrum for 0.5, 0.625 code; Chips per bit = 5

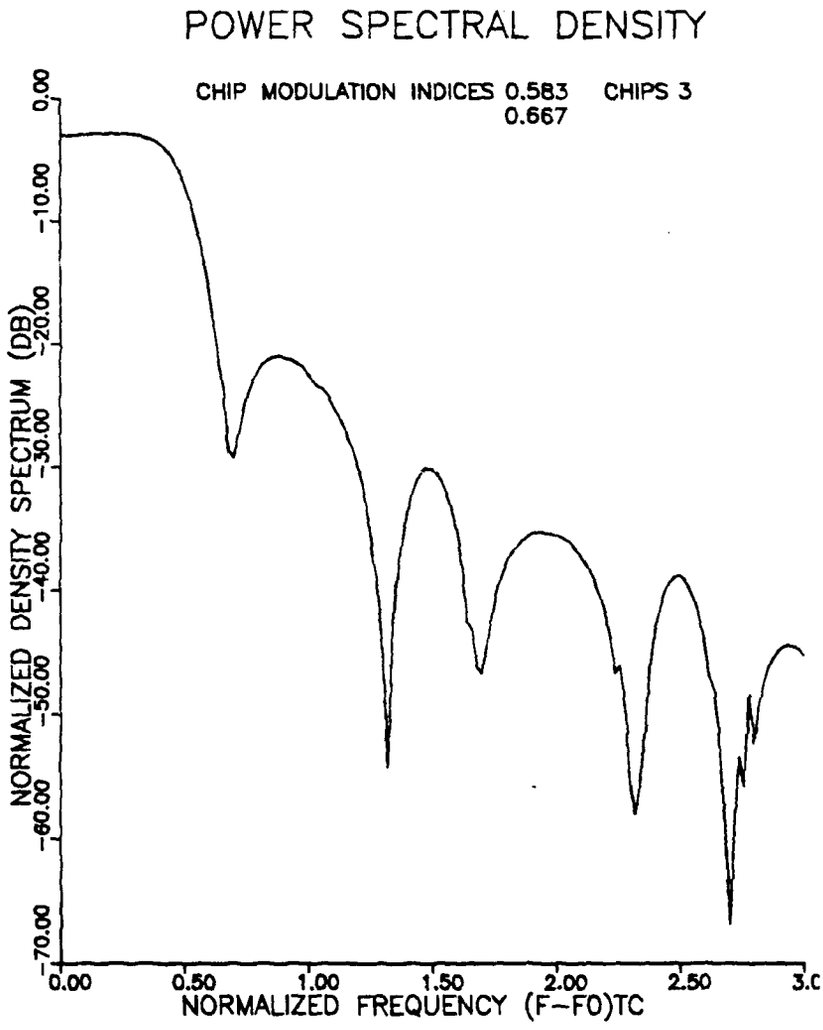


Figure 5.5: Conventional SSMH Spectrum for 0.583, 0.667 code; Chips per bit = 3

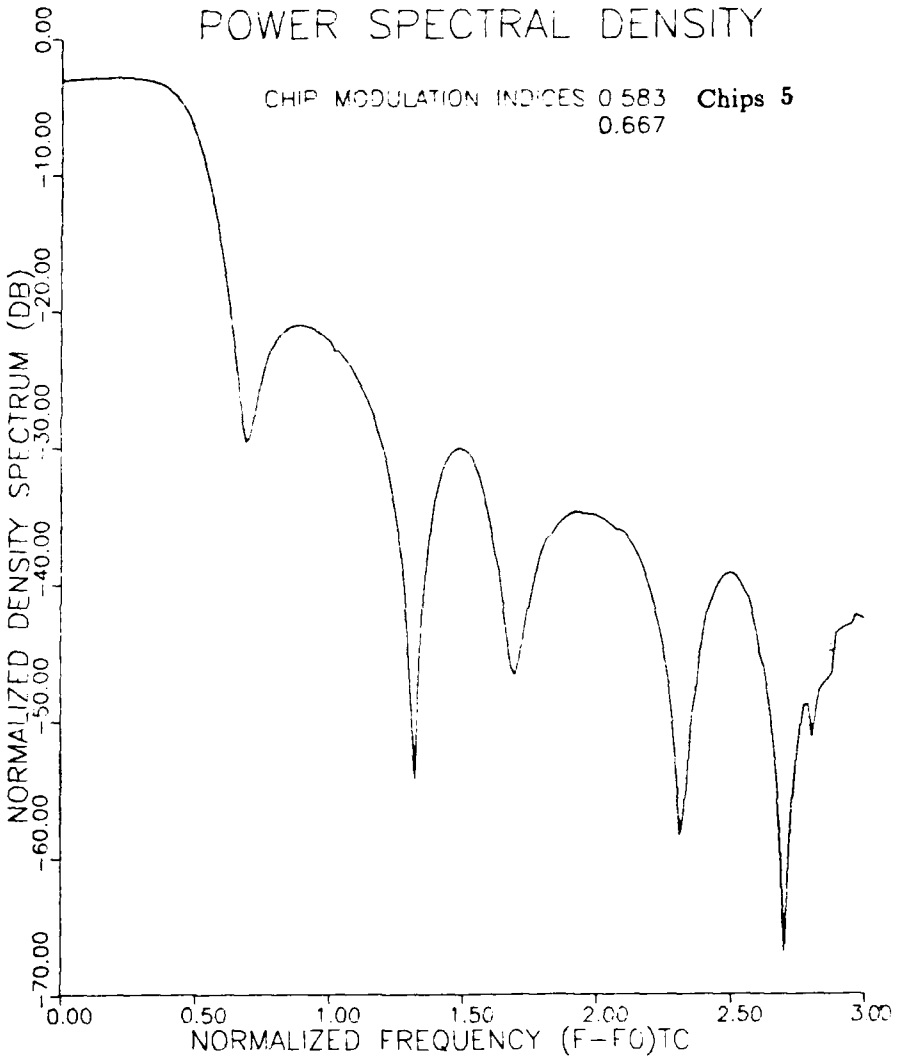


Figure 5.6: Conventional SSMH Spectrum for 0.583, 0.667 code; Chips per bit = 5

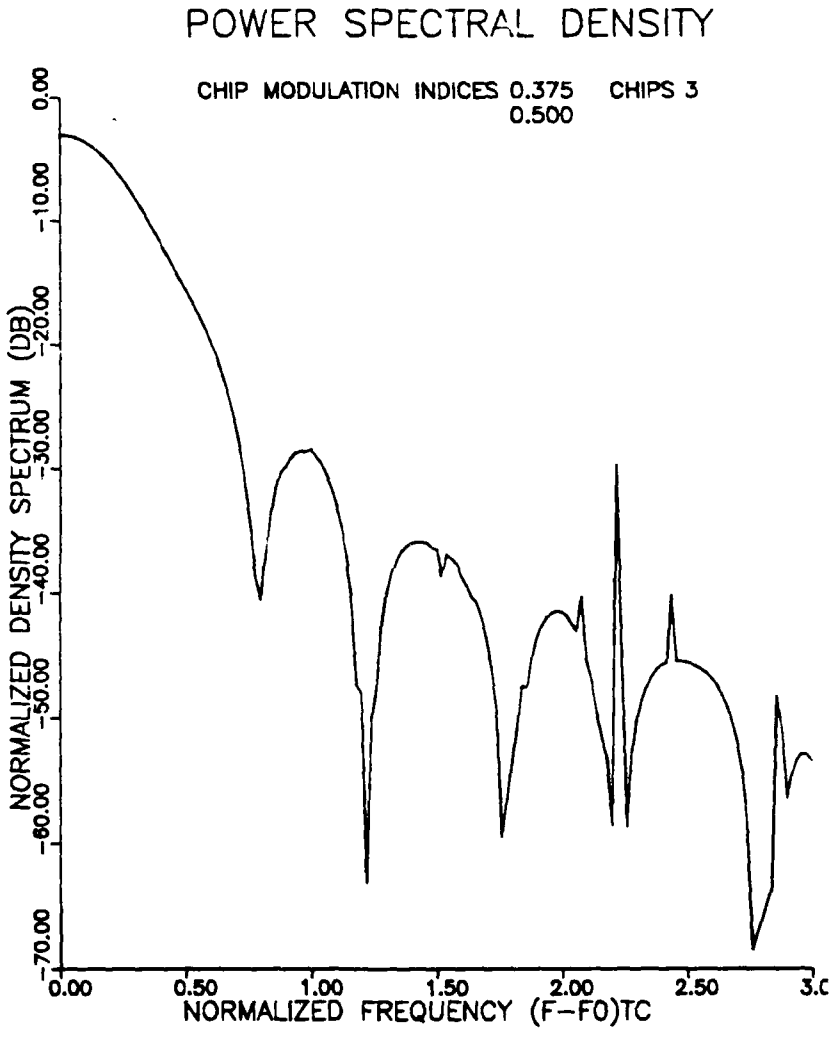


Figure 5.7: Conventional SSMH Spectrum for 0.375, 0.5 code; Chips per bit = 3

## 5.4 Modified Spread Spectrum Multi-$h$ Spectra

By changing the application of the modulation indices to a bit basis, the structure of the transmitted signal is much different. This section addresses the question of the resulting transmitted power density spectrum. The analysis is similar to the previous section, but with different final expressions for the spectra. Using the analytical results, numerical evaluation confirms that the spectra for modified SSMH signaling resemble very nearly those of conventional SSMH for the same modulation indices. This fact provides the communications engineer with a great deal of flexibility in designing the LPI system.

The derivation of the power density spectrum follows the same procedure as Section 5 2 above with the introduction of the phase as described by equation 3.6. As before, the autocorrelation function is

$$r(t_1,t_2) = \mathcal{E}\{e^{j\phi(t_1)}e^{-j\phi(t_2)}\}. \tag{5.27}$$

Following substitution of equation 3.6, expansion of the series, and collection of terms, the autocorrelation function can be expressed as

$$r(t_1,t_2) = \mathcal{E}_{\alpha,c,t_1,t_2}\{e^{j2\pi\sum_{m=-\infty}^{\infty}\sum_{n=0}^{N_c-1}\alpha_m h_{m \bmod H} c_{mn}[q(t_1-(n+mN_c)T_c)-q(t_2-(n+mN_c)T_c)]}\}. \tag{5.28}$$

Once again, the summations in the exponentials revert to the products of exponentials, and after taking the expectation with respect to $\alpha$ and $c$ ($f_{\alpha c} = \frac{1}{2}\delta(\alpha c+1)+\frac{1}{2}\delta(\alpha c-1)$) yields

$$r(t_1,t_2) = \prod_{m=0}^{\infty}\prod_{n=0}^{N_c-1}\cos[2\pi h_{m \bmod H}(q(t_2-(n+mN_c)T_c)-q(t_1-(n+mN_c)T_c))]. \tag{5.29}$$

As in the previous case, expansion of the products yields a function that is cyclostationary; this time over a period of $HN_cT_c$. Therefore, the time averaged autocorrelation is

$$r(\tau) = \frac{1}{HN_cT_c}\int_0^{HN_cT_c}\prod_{m=0}^{\infty}\prod_{n=0}^{N_c-1}\cos[2\pi h_{m \bmod H}(q(t+\tau-(n+mN_c)T_c)-q(t-(n+mN_c)T_c))]dt. \tag{5.30}$$

Similar to conventional SSMH, the pulse shaping function has a value of zero for $t \leq 0$ and a value of 1/2 for $t \geq T_c$, therefore the infinite product becomes finite. The

result is the autocorrelation can be written

$$r(\tau) = \frac{1}{HN_cT_c}\int_0^{HN_cT_c}\prod_{m=0}^{\lceil\frac{HN_c(k+1)+1}{N_c}\rceil}\prod_{n=0}^{N_c-1} r_1(t,\tau)dt, \text{ where} \quad (5.31)$$

$$r_1(t,\tau) = \cos[2\pi h_{m \bmod H}(q(t+\tau-(n+mN_c)T_c) - q(t-(n+mN_c)T_c))], \quad (5.32)$$

and $\lceil\cdot\rceil$ indicates the largest integer of the argument.

For $k \geq 1$ this equation becomes

$$r(\tau) = C_\alpha^{k-1}\Psi(\tau), \text{ where} \quad (5.33)$$

$$C_\alpha = \prod_{j=0}^{H-1}\{\cos(\pi h_{j \bmod H})\}^{N_c}, \quad \text{and} \quad (5.34)$$

$$\Psi(\tau) = \frac{1}{HN_cT_c}\int_0^{HN_cT_c}\prod_{j=0}^{HN_c-1}\cos[2\pi h_{\lfloor\frac{j}{N_c}\rfloor \bmod H}(\frac{1}{2} - q(t-jT_c))] \times \prod_{j=0}^{2HN_c-1}\cos[2\pi h_{\lfloor\frac{j}{N_c}\rfloor \bmod H} q(t+\tau-jT_c)]dt. \quad (5.35)$$

In this expression, the $\lfloor\cdot\rfloor$ indicates the smallest integer in the argument.

Following the same procedure as in Section 5.2, after Fourier transforming, expanding the integrals, converging the series, normalizing by the chip rate, and taking the real parts; the spectra can be expressed as

$$G(f_n) = 2\{\int_0^{HN_c} r(\tau)\cos(2\pi f_n\tau)d\tau + \frac{a}{c}\int_{HN_c}^{2HN_c} r(\tau)\cos(2\pi f_n\tau)d\tau - \frac{b}{c}\int_{HN_c}^{2HN_c} r(\tau)\sin(2\pi f_n\tau)d\tau, \text{ with} \quad (5.36)$$

$$a = 1 - C_\alpha\cos(2\pi f_n HN_c),$$

$$b = C_\alpha\sin(2\pi f_n HN_c),$$

$$c = 1 + C_\alpha^2 - 2C_\alpha\cos(2\pi f_n HN_c),$$

$$r(\tau) = \frac{1}{HN_c}\int_0^{HN_c}\prod_{m=0}^{2H+1}\prod_{n=0}^{N_c-1} r_1(t,\tau)dt, \quad (5.37)$$

$$r_1(t,\tau) = \cos[2\pi h_{m \bmod H}(q(t+\tau-(n+mN_c)) - q(t-(n+mN_c)))]. \quad (5.38)$$

## 5.5 Numerical Evaluation of Modified SSMH Spectra

As in Section 5.3 above, the analytic expressions for the spectra of modified SSMH signals are numerically evaluated for selected values of the modulation indices. The figures that follow are depictions of the spectra for the following modulation schemes.

| *Modulation Indices* | *Chips per Bit* | *Figure* |
|---|---|---|
| 0.5, 0.75 | 3 | 5.8 |
| 0.5, 0.75 | 7 | 5.9 |
| 0.5, 0.625 | 3 | 5.10 |
| 0.5, 0.625 | 7 | 5.11 |
| 0.583, 0.667 | 3 | 5.12 |
| 0.583, 0.667 | 5 | 5.13 |
| 0.583, 0.667 | 7 | 5.14 |
| 0.375, 0.5 | 3 | 5.15 |

Table 5.2: Modified SSMH Spectra

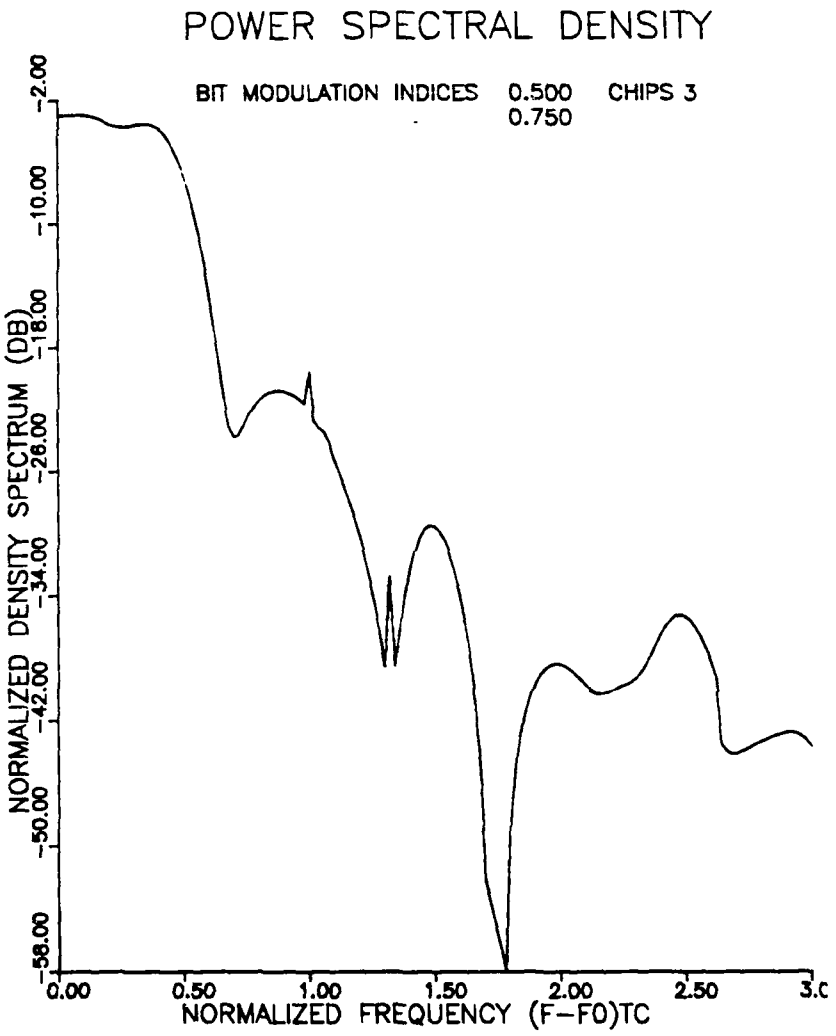


Figure 5.8: Modified SSMH Spectrum for 0.5, 0.75 code; Chips per bit = 3

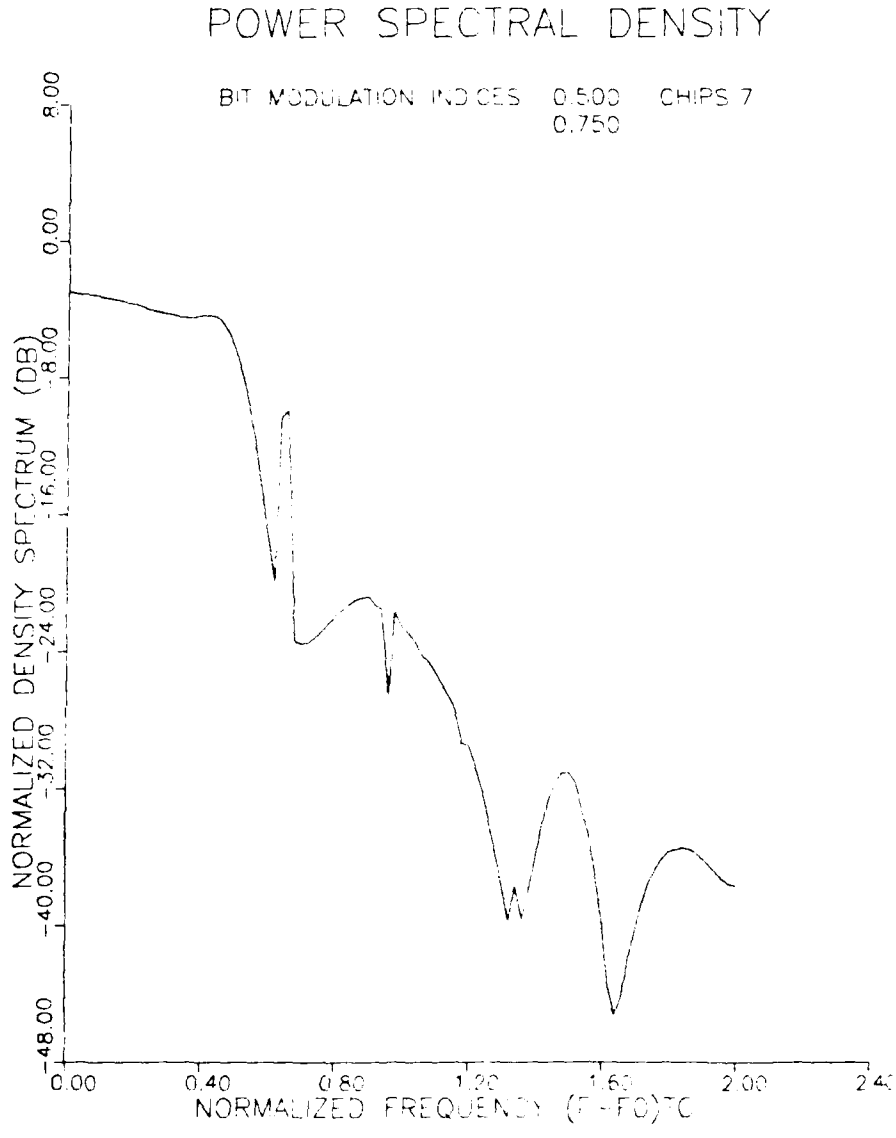


Figure 5.9: Modified SSMH Spectrum for 0.5, 0.75 code; Chips per bit = 7

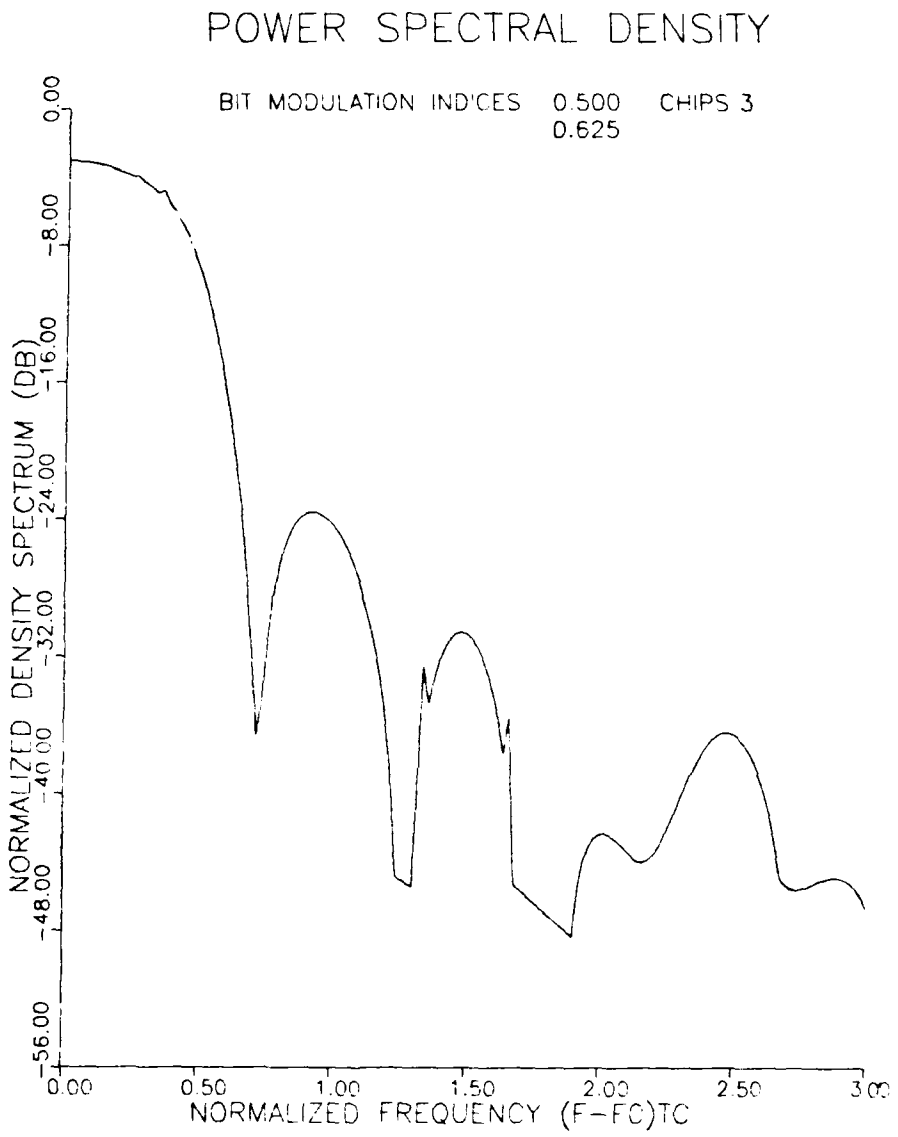


Figure 5.10: Modified SSMH Spectrum for 0.5, 0.625 code; Chips per bit = 3

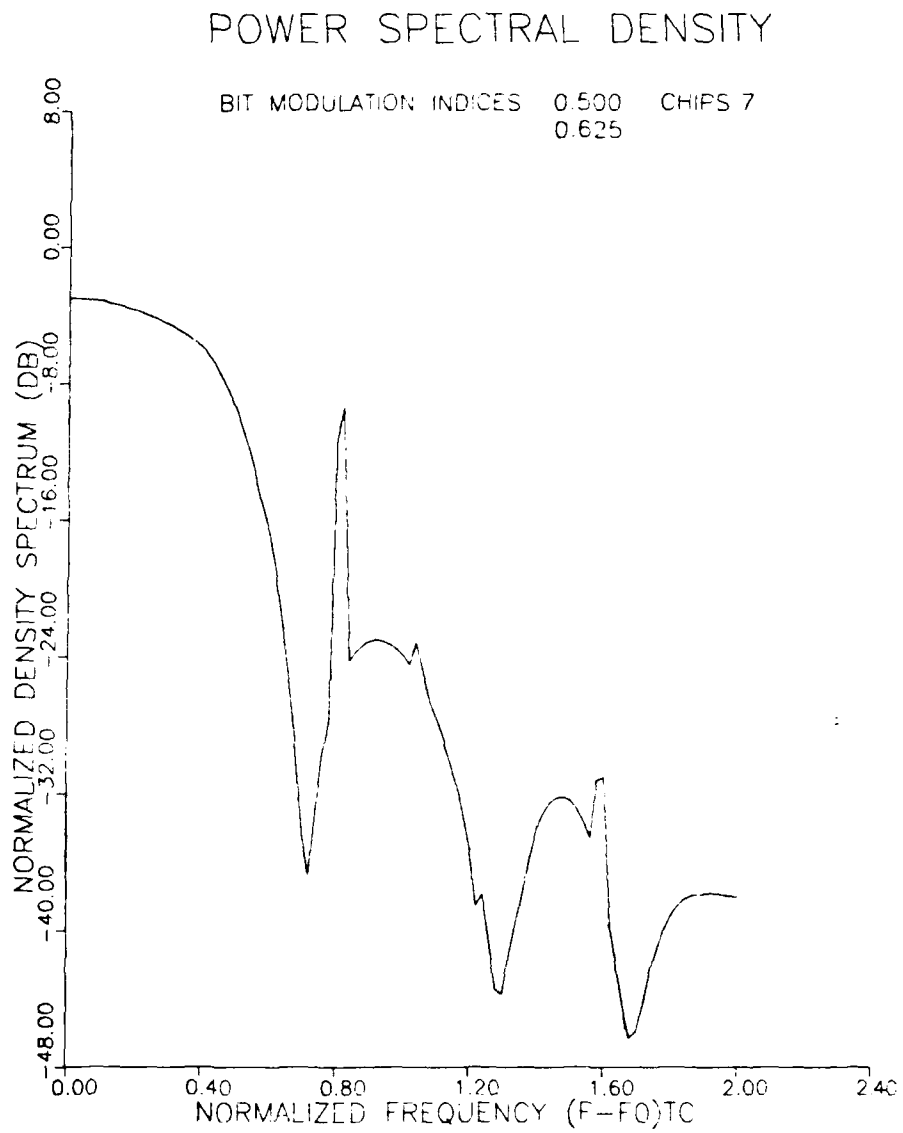


Figure 5.11: Modified SSMH Spectrum for 0.5, 0.625 code; Chips per bit = 7

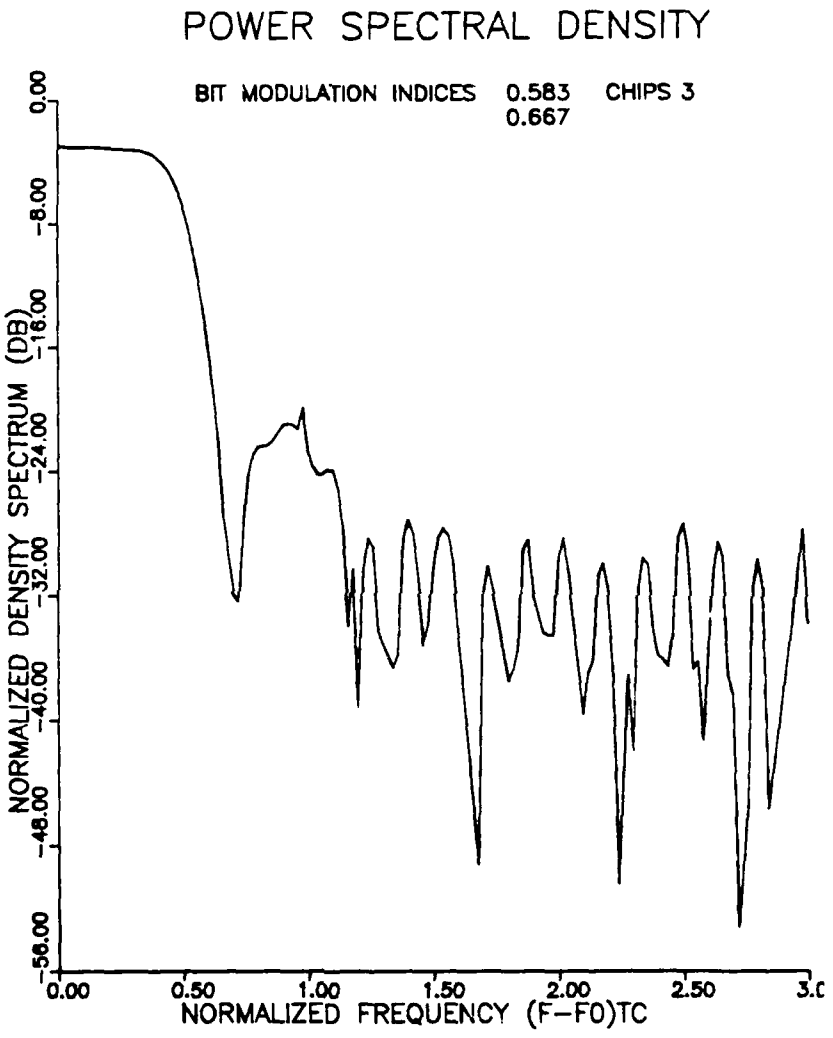


Figure 5.12: Modified SSMH Spectrum for 0.583, 0.667 code; Chips per bit = 3

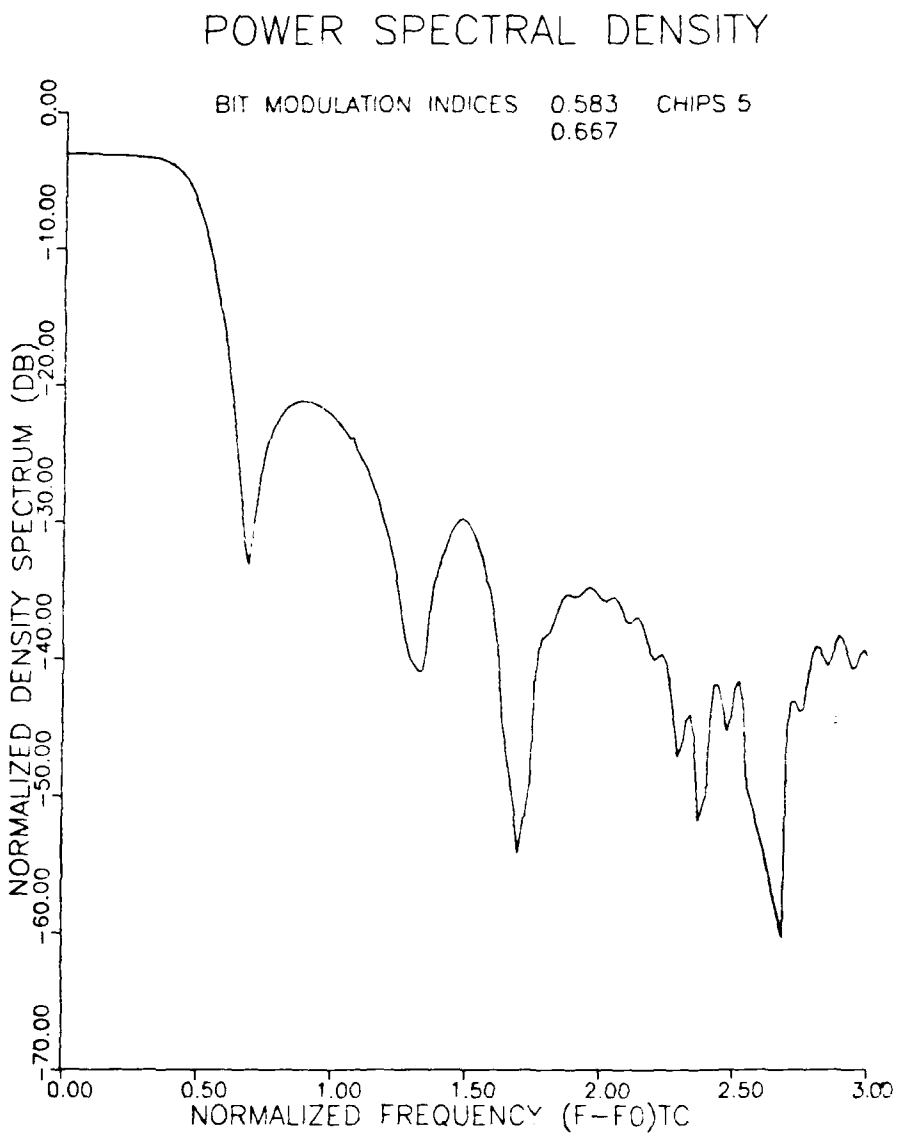


Figure 5.13: Modified SSMH Spectrum for 0.583, 0.667 code; Chips per bit = 5

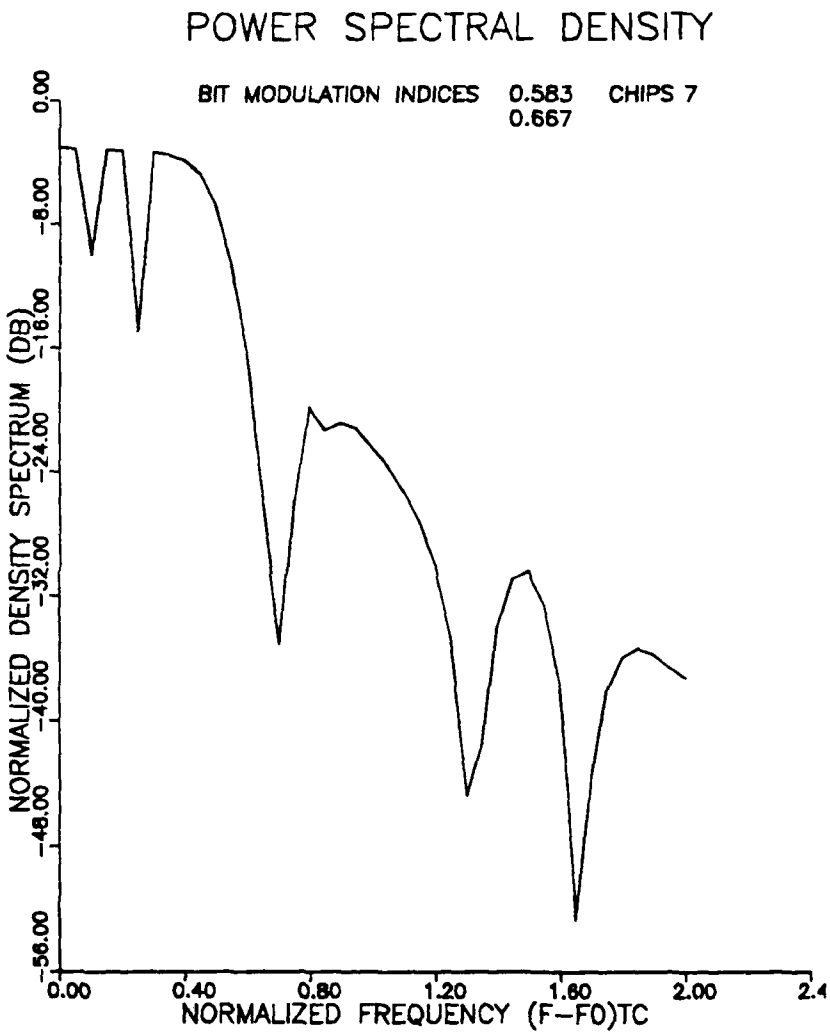


Figure 5.14: Modified SSMH Spectrum for 0.583, 0.667 code; Chips per bit = 7

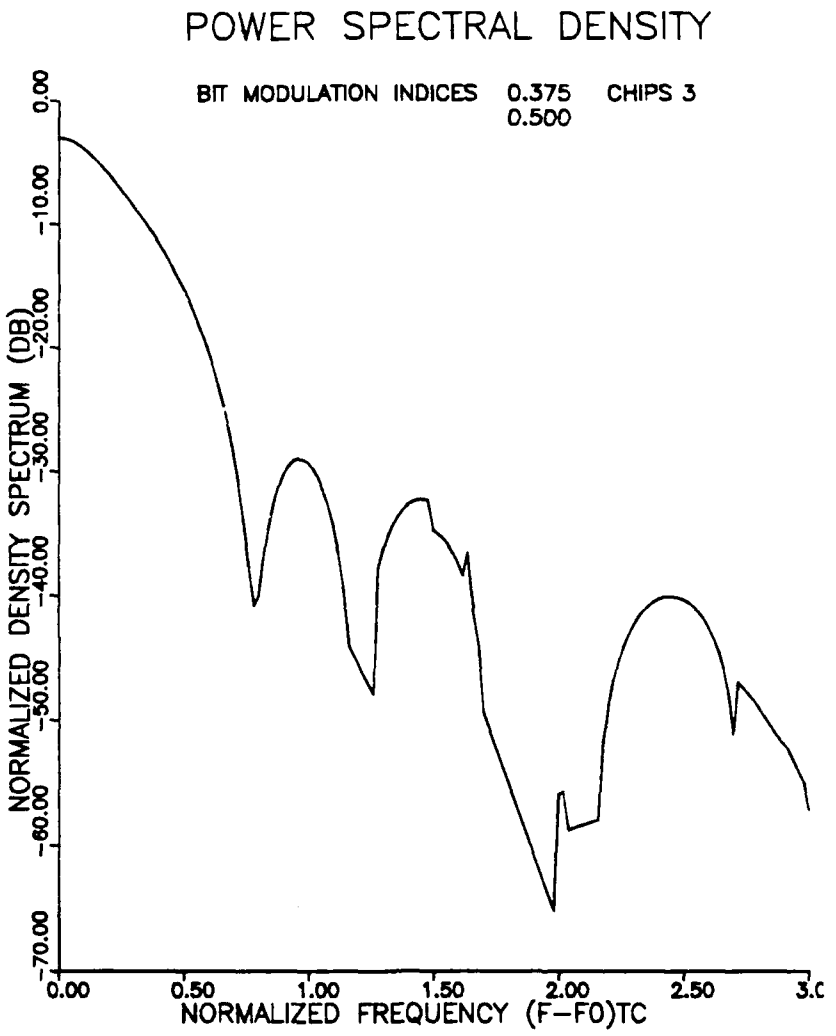


Figure 5.15: Modified SSMH Spectrum for 0.375, 0.5 code; Chips per bit = 3

## 5.6 Spread Spectrum Multi-$h$ Spectral Characteristics

Following the analysis and simulations of the previous sections, some conclusions and characterizations can be made regarding the spectra of this class of signals.

First and foremost is the fact that the spectra have similar characteristics to their parent multi-$h$ signals when normalized to the chip rate. This is seen by comparison of the evaluated spectra with previously derived spectra for multi-$h$ signals as shown by Lereim [30], Wilson [72], and Anderson, Aulin, and Sundberg [6]. Correspondingly, it also implies that the spectrum of the signals normalized to the bit rate will be spread by a factor of the number of chips per bit, while maintaining the shape characteristic of the multi-$h$ signal with the given modulation indices.

It is also apparent by comparison of the spectrum of modified versus conventional modulation that the method of modulation has little effect on the resulting spectrum. That is to say, the spectra of conventionally modulated and modified modulated spread spectrum signals with the same modulation indices closely resemble each other. This is a new and exciting result in that it characterizes the results of a new spread spectrum modulation technique, *modified* SSMH, in terms of existing spread spectrum signaling results. Thus, the designer has the option from a transmitted spectrum standpoint as to which modulation technique to use. It is also apparent, since the resulting spread spectra have the same appearance as the parent multi-$h$ signals, that considerable control over the spectrum is afforded by selection of the modulation indices, the spreading rate, and the other signaling parameters.

It is appropriate at this point to comment on the results in regard to the number of chips per bit and the apparent noisiness of the spectra. Equations 5.26 and 5.36 reveal that the spectra result from the product of a large number of cosine functions in the autocorrelation expressions. Implementation of this number of trigonometric functions by computer led to considerable truncation errors and rapid introduction of noise in the spectra. This factor prohibited simulation at chip rates more appropriate to spread spectrum signaling and introduced many numerical inconsistencies. However, the issues of spectrum definition and characterization were accomplished.

Prior to discussing the detectability of SSMH signals, it is instructive to examine the

spectrum of 'normal' direct sequence binary phase shift keying (DS/BPSK) systems and normal direct sequence spreading applied to multi-$h$ signals. In this situation the random spreading sequence is applied after the modulation process as shown in Figure 5.16.

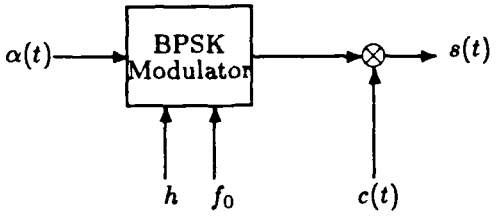


Figure 5.16: Traditional Direct Sequence Modulation

In the case of multi-$h$ signaling, the transmitted signal would be expressed as

$$s(t) = c(t)\sqrt{\frac{2E}{T}}\cos(\omega_0 t + \phi(t) + \theta_0), \tag{5.39}$$

where $\phi(t)$ is the phase transition expression

$$\phi(t) = 2\pi \sum_{i=-\infty}^{\infty} \alpha_i h_i q(t - iT_c), \tag{5.40}$$

and $c(t)$ is the pseudorandom spreading sequence. For DS/BPSK, the phase modulation expression is removed and instead the signal is simply a cosinusoidal function premultiplied by the data sequence.

The power density spectrum for these signals can be expressed as

$$S(f) = \frac{1}{T_c}\text{sinc}^2(\frac{f}{T_c}) * \{\frac{E}{T_c}(G(f + f_0) + G(f - f_0))\}, \tag{5.41}$$

where $G(f)$ is the lowpass spectrum of the modulation process.

From equation 5.41, it is obvious that the spectrum for these signals will result from the convolution of a $\text{sinc}^2(x)$ envelope with the spectrum of the modulation process. In the case of DS/BPSK, it is seen that the spectrum of the modulation process is simply an impulsive function resulting from the cosinusoidal term in equation 5.41. As a result, the spectra of the spread signals will have nulls at multiples of the chip rate. When processed by radiometer detection, these nulls will produce discrete components and thus give a great deal of information about the transmitted signal. Neither discrete elements nor nulls are present in the spectrum of SSMH signals. The following section addresses the issue of spectrum detectability.

## 5.7 Spectrum Detectability

The issue of spectrum detectability must be addressed in any LPI environment. In this regard, there are a two issues that are important in detecting SSMH signals.

The first is the absence of any discrete components in the SSMH spectra. Similar to other multi-$h$ spectral characteristics, equations 5.26 and 5.36 reveal that as long as $\mid C_\alpha \mid$ is less than one, which will always be the case since the modulation indices are rational values less that one, the spectrum will not have any discrete components. This fact is essential in a LPI environment.

The second factor is the requirement of an unintended receiver to raise the received signal to the power of the denominator of the modulation index sequence in order to extract any discrete components. While it is possible for this to occur, it requires the commitment of the interceptor to perform a great deal of signal processing in order to extract the discrete components.

For example, the normal intercept detector may employ radiometer detection as a first option. If the SSMH signal is squared, the following expression describes the signal,

$$x^2(t) = \frac{E_c}{T_c}[1 + \cos(2\omega_0 t + 2\phi(t))]. \tag{5.42}$$

This signal has the same form as the original SSMH signal with the addition of a dc bias and at twice the original frequencies. The equations of Section 5.2 apply directly after incorporating the factor of two in the amplitude of the pulse shaping function and operating at a carrier frequency of twice the previous value. Figure 5.17 shows the spectrum of this signal and can be compared with the spectrum of the transmitted signal in Figure 5.2. Obviously, there are no discrete components in either.

Similar analysis applies to signals raised to greater powers until the signal is raised to the $p$-th power (recall that $p$ is the denominator of the set of modulation indices). At this point discrete components appear at $p$ times the carrier frequency and multiples depending on the modulation index. As a result, the spectrum is much more detectable and an unintended receiver can gain at least partial parameterization.

With the transmitted spectrum characterized, it is now appropriate to determine if the signal can be transmitted at sufficiently low signal-to-noise ratios to take advantage of

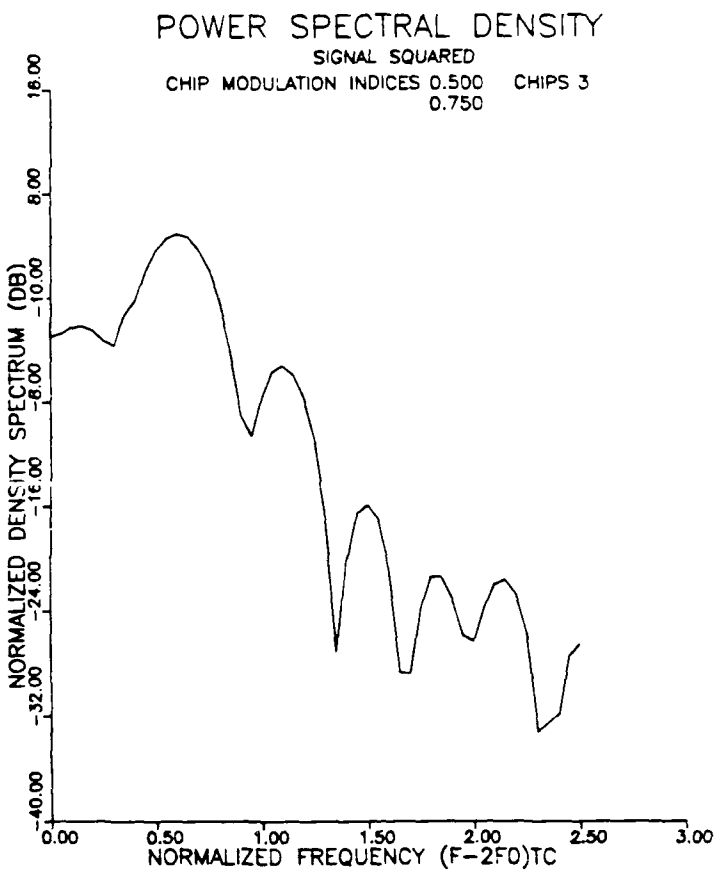


Figure 5.17: Signal Squared Spectrum

the spectral characteristics and still be detected by an intended receiver. The next chapter addresses the issues of receiver design and signal detection.

# CHAPTER 6

# Receiver Structure

This chapter addresses the issues incumbent in detecting spread spectrum multi-$h$ signals in an additive white Gaussian noise (AWGN) environment and decoding the transmitted information. While significant research has been done on multi-$h$ receiver structures as a generalization of CPM signaling, the addition of another level of detection and synchronization is novel. The bit and chip synchronization and timing are assumed to be known exactly. Additionally, the intended receiver is assumed to have complete knowledge of the spreading code and the modulation index code. The receiver still must detect and decode the chip sequence and ultimately the transmitted data. This can be done either coherently, if full knowledge of the arbitrary initial phase offset is assumed, or noncoherently, if the phase offset is assumed to be random. For this work, it is assumed that complete coherency can be established and the phase offset is assumed to be zero.

Following a maximum *a posteriori* probability derivation, it is shown that the SSMH signal sequence can be detected using the Viterbi Algorithm with bit metrics that are the sum of the chip metrics for that bit. A simple receiver structure is derived and numerically evaluated in Chapter 8 following derivation of the performance bounds of this signaling structure (Chapter 7). It is shown that SSMH signals can be successfully detected at 'low' signal-to-noise ratios thereby creating a viable LPI signaling structure.

## 6.1 Coherent Receiver Structure

The work of Osborne and Luntz[45] first derived the maximum likelihood (ML) decision statistics for continuous phase frequency shift keying (CPFSK) signals. Assuming equally

likely transmitted digital sequences, the received signal can be expressed as

$$r(t) = s(t) + n(t), \tag{6.1}$$

where $n(t)$ is white Gaussian noise with a two sided variance of $N_0/2$. Following the derivations of Viterbi and Omura [69], Jackson showed [31] that a digital sequence is maximum likelihood detected with a decision metric

$$\mathcal{L} = p(\underline{r}(t) \mid s(t, \underline{\alpha}, \underline{h}, \underline{c})) \gtrless p(\underline{r}(t) \mid s(t, \underline{\acute{\alpha}}, \underline{h}, \underline{c})), \tag{6.2}$$

where $p(\underline{r}(t) \mid s(t, \underline{\alpha}, \underline{h}, \underline{c}))$ is the probability distribution (density) of the received sequence, $\underline{r}(t)$, given the transmitted sequence resulting from $\underline{\alpha}$, $\underline{c}$, and $\underline{h}$.

For a sequence of N symbols (bits) and the white Gausssian noise distribution, this decision metric reduces to a log-likelihood metric of

$$l = \frac{2}{N_0} \int_0^{NT_s} \underline{r}(t) s(t, \underline{\alpha}, \underline{h}, \underline{c}) dt \gtrless \frac{2}{N_0} \int_0^{NT_s} \underline{r}(t) s(t, \underline{\acute{\alpha}}, \underline{h}, \underline{c}) dt. \tag{6.3}$$

This decision metric for SSMH signals can be expressed

$$l = \sum_{i=0}^{N} \sum_{j=0}^{N_c-1} \int_{jT_c}^{(j+1)T_c} r(t - (j + iN_c)T_c) s(t - (j + iN_c)T_c, \alpha_i, h_{(i+j) \bmod H}, c_{ij}) dt. \tag{6.4}$$

Thus, the decision metric for a sequence of $N$ bits is

$$\lambda = \sum_{i=0}^{N-1} \lambda_i, \tag{6.5}$$

where the individual bit metrics are

$$\lambda_i = \sum_{j=0}^{N_c-1} \int_{jT_c}^{(j+1)T_c} r(t - jT_c) s(t - jT_c, \alpha_i, h_{(i+j) \bmod H}, c_{ij}) dt. \tag{6.6}$$

These expressions indicate that the overall decision metric is the result of the sum of bit metrics, which in turn are the sum of 'chip' metrics. Equation 6.6 also indicates that the metrics are the correlation of the received signal with the possible transmitted signals. Hence, the optimal receiver computes the maximum correlation over all possible received sequences. Forney [25] and others [6,30] have shown that for sequences from a finite-state Markov process, such as the multi-$h$ signals defined in Chapter 3, the Viterbi Algorithm is a recursive method to exhaustively search for the optimal sequence.

The final receiver structure is defined after determining the correlation filter structure. First, the chip metrics for rectangular signaling over the $i$th bit and $j$th chip can be written in the following manner,

$$\lambda(\alpha_i = +1, c_{ij}, \theta_{ij}) = \int_0^{T_c} r(t)\cos(2\pi f_0 t + \frac{\pi c_{ij} h_{ij} t}{T_c} + \theta_{ij})dt, \tag{6.7}$$

$$\lambda(\alpha_i = -1, c_{ij}, \theta_{ij}) = \int_0^{T_c} r(t)\cos(2\pi f_0 t - \frac{\pi c_{ij} h_{ij} t}{T_c} + \theta_{ij})dt. \tag{6.8}$$

These expressions indicate an array of $2H$ times the number of states correlators. Expanding these expressions on the initial phase angle yields quadrature forms of the correlators. That is,

$$\begin{bmatrix} \lambda(+\alpha_i, c_{ij}, \theta_{ij}) \\ \lambda(-\alpha_i, c_{ij}, \theta_{ij}) \end{bmatrix} = \begin{bmatrix} I_1 & -Q_1 \\ I_2 & -Q_2 \end{bmatrix} \begin{bmatrix} \cos\theta_{ij} \\ \sin\theta_{ij} \end{bmatrix}, \tag{6.9}$$

where over a chip interval

$$I_1 = \int_0^{T_c} r(t)\cos(2\pi f_0 t + \frac{\pi c_{ij} h_{ij} t}{T_c})dt, \tag{6.10}$$

$$Q_1 = \int_0^{T_c} r(t)\sin(2\pi f_0 t + \frac{\pi c_{ij} h_{ij} t}{T_c})dt, \tag{6.11}$$

$$I_2 = \int_0^{T_c} r(t)\cos(2\pi f_0 t - \frac{\pi c_{ij} h_{ij} t}{T_c})dt, \tag{6.12}$$

$$Q_2 = \int_0^{T_c} r(t)\sin(2\pi f_0 t - \frac{\pi c_{ij} h_{ij} t}{T_c})dt. \tag{6.13}$$

These equations imply a bank of $4H$ correlators and a phase rotation network to account for the allowable phases at the start of each chip interval.

The final requirement in defining the receiver architecture is to account for the changes in the modulation indices and the chip sequence. Minor modification to the simple switching circuitry shown by Sadr [54] allows proper multiplexing of the quadrature elements to select the appropriate modulation index and the known chip sequence. The resulting multiplexing circuit is shown in Figure 6.1, where $h_{ij} = \text{logic}(+1)$ for modulation index $h_1$, $h_{ij} = \text{logic}(0)$ for modulation index $h_2$, $c_{ij} = \text{logic}(+1)$ for $c_{ij} = +1$, and $c_{ij} = \text{logic}(0)$ for $c_{ij} = -1$.

The flexibility of the modulation scheme and receiver structure is noted here where clocking both the chip and modulation indices at the chip rate will give conventional SSMH, while clocking the modulation indices at the bit rate (still maintaining the chip rate on the chips) will give modified SSMH.

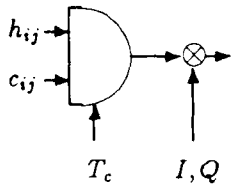


Figure 6.1: Receiver Multiplexer Circuit

The receiver architecture in toto is shown in Figure 6.2.

It should be noted at this point that the quadrature components can also be obtained on a baseband basis as shown by Mazur [41] by heterodyning the received signal with quadrature signals at the carrier frequency and lowpass filtering. This is accomplished by expanding the arguments in equation 6.13 as

$$I_1 = IC - QS, \tag{6.14}$$

$$Q_1 = QC + IS, \tag{6.15}$$

$$I_2 = IC + QS, \tag{6.16}$$

$$Q_2 = QC - IS \quad \text{where,} \tag{6.17}$$

$$IC = \int_0^{T_c} r(t)\cos(2\pi f_0 t)\cos(\frac{\pi h_{ij} t}{T_c})dt, \tag{6.18}$$

$$QS = \int_0^{T_c} r(t)\sin(2\pi f_0 t)\sin(\frac{\pi h_{ij} t}{T_c})dt, \tag{6.19}$$

$$IS = \int_0^{T_c} r(t)\cos(2\pi f_0 t)\sin(\frac{\pi h_{ij} t}{T_c})dt, \quad \text{and} \tag{6.20}$$

$$QC = \int_0^{T_c} r(t)\sin(2\pi f_0 t)\cos(\frac{\pi h_{ij} t}{T_c})dt. \tag{6.21}$$

The bandpass version is shown in Figure 6.3.

Prior to evaluating this receiver structure, the analytic performance bounds to the modulation technique are derived in the following chapter. The receiver derived in this chapter is then numerically evaluated by computer and the performance compared to the bounds.

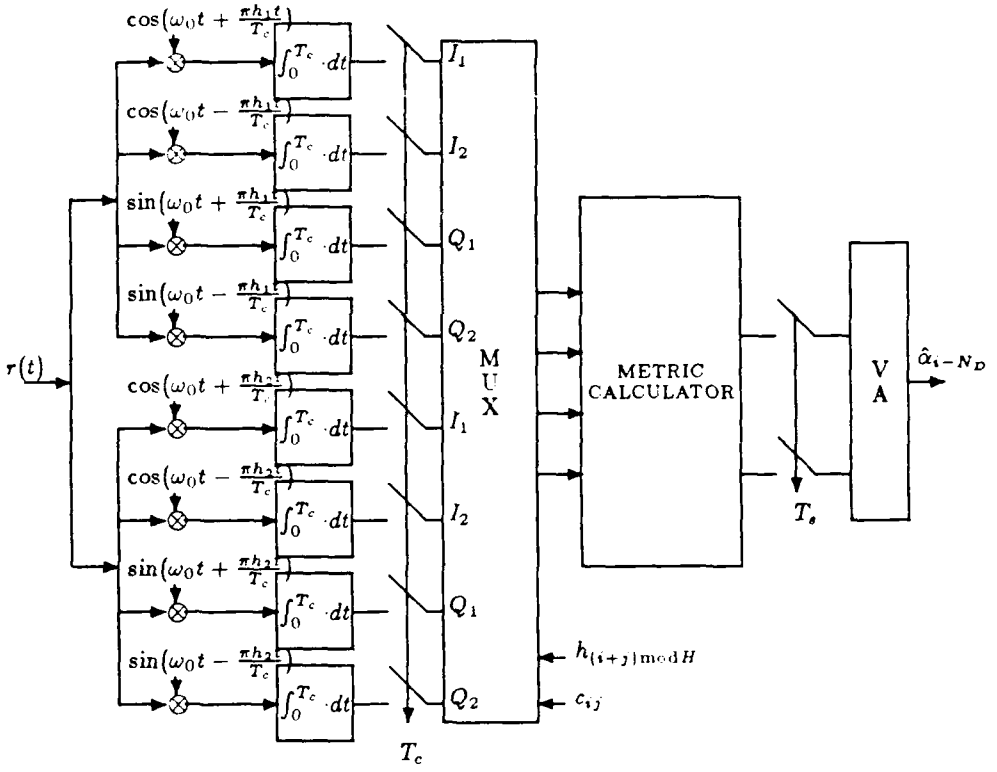


Figure 6.2: Maximum Likelihood Receiver Structure

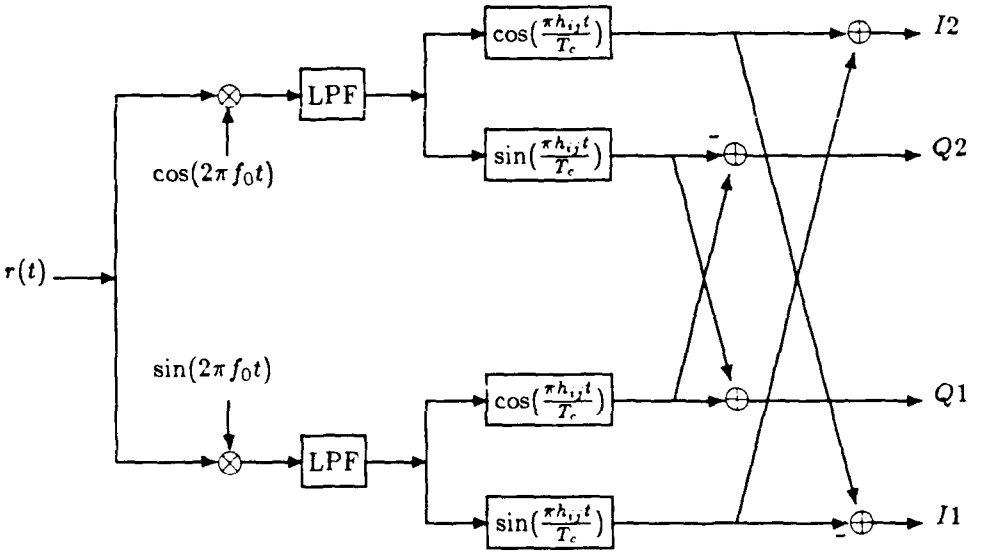


Figure 6.3: Lowpass Quadrature Implementation

# CHAPTER 7

# Performance Bounds

The error performance of the maximum likelihood receiver of the previous chapter is dependent on the distance properties and performance bounds for the signaling structure. In this chapter, it is shown that the error performance is dependent not only on the minimum distance of the signaling structure, but also on the complete signal phase transition structure. The distance properties are shown to result from the sum of the distance properties of the chip intervals. Upper bounds to the bit error probability are analytically derived and shown to be dependent on the modulation code and the spreading code. It is shown that SSMH performance can exceed that of conventional signaling schemes such as DS/BPSK.

## 7.1 Performance Bound Analysis

The analysis of receiver performance begins with the approach of Wozencraft [75], who showed that the probability of error in deciding between any two signals, $s_1(t)$ and $s_2(t)$, in AWGN is dependent on the Euclidean distance, $d_{12}$, separating the two signals. Thus

$$P_e(s_2 \mid s_1) = \int_{\frac{d_{12}/2}{\sqrt{N_0/2}}}^{\infty} \frac{1}{\sqrt{2\pi}} e^{-\frac{n^2}{2}} dn, \tag{7.1}$$

$$P_e(s_2 \mid s_1) = Q(\sqrt{\frac{d_{12}^2}{2N_0}}), \tag{7.2}$$

where

$$Q(x) = \frac{1}{\sqrt{2\pi}} \int_x^{\infty} e^{-\frac{t^2}{2}} dx. \tag{7.3}$$

Expanding this concept to more than two signals and incorporating the total probability theorem yields

$$P_e = \sum_{i=1}^{K} P(e \mid s_i)P(s_i). \tag{7.4}$$

Viterbi [69] extended this concept to a digital sequence of $N$ bits with the result that the pairwise probability of error between any two sequences of length $N$ bits is expressed as

$$P_e(\alpha_N, \hat{\alpha}_N) = Q(\sqrt{\frac{d^2(N)}{2N_0}}). \tag{7.5}$$

This expresses the probability of error between two sequences that separate at some point, $nT_s$, and merge again after $N$ bits at $(n+N)T_s$.

The complete probability of error is found by ensemble averaging over all possible error event sequences. This average is difficult to calculate and as a result is generally upper bounded by the union bound

$$P_e \leq \sum_{\hat{\alpha}_N} \sum_{\alpha_N} Q(\sqrt{\frac{d^2(N)}{2N_0}})P(\alpha_N). \tag{7.6}$$

Equation 7.6 reflects the fact that the error probability is found by fixing the error sequence and averaging over all possible transmitted sequences. This is the same approach taken by Hsu [30] for multi-$h$ phase coding and by Zehavi [76] for trellis codes.

The result for equally likely transmitted signals is the total error probability and is found by summing the probabilities of error for all possible error sequences against all possible transmitted sequences. This is expressed as

$$P_e \leq \sum_{\text{all errors}} Q(\sqrt{\frac{d_i^2}{2N_0}})P(\alpha_N), \tag{7.7}$$

where $d_i$ is the Euclidean distance separating two signals of a particular error event length.

Equation 7.7 also reflects the fact that the probability of error for each error event is simply a pairwise comparison of two sequences over a given length. This implies the implementation of the 'difference' sequence approach as shown by Hsu [30] and Anderson [6]. Since the phase changes of the signaling scheme correspond directly to the information sequences, the difference phase state approach can be invoked where

$$\Delta\theta(i+1) = [\Delta\theta(i) + \sum_{j=0}^{N_c-1} \pi h_{ij}\gamma_{ij}] \bmod 2\pi, \tag{7.8}$$

and $\gamma_{ij}$ is the difference,

$$\gamma_{ij} = c_{ij}\alpha_i - c_{ij}\hat{\alpha}_i. \tag{7.9}$$

The all zero path then corresponds to error free transmission.

Equation 7.9 illustrates a key and essential difference between the current analysis and that of Hsu and Anderson. Although the chip sequence is known *a priori* by the transmitter and receiver, the chip values help determine the phase changes on a chip basis and hence contribute to the difference state transitions. The Markov process structure is not disturbed indicating that the phase changes over a bit interval are the sum of the changes over each chip interval. Hence equation 7.8 can be written

$$\Delta\theta(i+1) = [\Delta\theta(i) + \sum_{j=0}^{N_c-1} \Delta\theta_{ij}] \bmod 2\pi, \tag{7.10}$$

where,

$$\Delta\theta_{ij} = \pi h_{(i+j) \bmod H} \gamma_{ij}. \tag{7.11}$$

The result of this analysis is that a 'difference' state structure and analysis can now be followed similar to Anderson and Hsu, but the state diagram must account for all possible chip sequences. Additionally, the analysis must include all possible transmitted phase states.

To perform the difference state analysis, equation 7.7 must be modified in two ways. The first reflects the fact that the bit error sequences, $\gamma_i = \alpha_i - \hat{\alpha}_i$, can occur in different ways and must be appropriately weighted. That is, the values of $\gamma_i$ can occur as follows.

$$\gamma_i = \begin{cases} 0, & \text{if } \alpha = 1, \hat{\alpha} = 1 \\ 0, & \text{if } \alpha = -1, \hat{\alpha} = -1 \end{cases} \tag{7.12}$$

$$\gamma_i = +2, \text{ if } \alpha = 1, \hat{\alpha} = -1 \tag{7.13}$$

$$\gamma_i = -2, \text{ if } \alpha = -1, \hat{\alpha} = +1 \tag{7.14}$$

Since $\gamma_i = 0$ can occur twice as often as $\gamma_i = +2$ or $\gamma_i = -2$, equation 7.7 must be modified to reflect this weighting.

Secondly, equation 7.7 must account for the different possibilities for the chip interval dibits. For bit interval differences of $\gamma_i = 0$, there is no effect since no error is made, but for $\gamma_i = +2$ or $\gamma_i = -2$ all of the possible chip values and sequences must be considered.

For example, for a three chip per bit sequence, and $\alpha = 1, \hat{\alpha} = -1$ ($\gamma_i = +2$), there are $2^3 = 8$ possible $\gamma_{ij}$ sequences for the set of three chips depending on the values of the chips. Hence,

| $c_{i1}$ | $c_{i2}$ | $c_{i3}$ | $\gamma_{i1}$ | $\gamma_{i2}$ | $\gamma_{i3}$ |
|---|---|---|---|---|---|
| -1 | -1 | -1 | -2 | -2 | -2 |
| -1 | -1 | +1 | -2 | -2 | +2 |
| -1 | +1 | -1 | -2 | +2 | -2 |
| -1 | +1 | +1 | -2 | +2 | +2 |
| +1 | -1 | -1 | +2 | -2 | -2 |
| +1 | -1 | +1 | +2 | -2 | +2 |
| +1 | +1 | -1 | +2 | +2 | -2 |
| +1 | +1 | +1 | +2 | +2 | +2 |

Table 7.1: Chip Difference Sequences

These chip difference sequences have a substantial effect on the phase transitions and on the distance characteristics, which is a significant new finding in this research.

The end result is equation 7.7 modified to be

$$P_e \leq \sum_{i=1}^{\infty} \nu_i Q(\sqrt{\frac{d_i^2}{2N_0}}), \tag{7.15}$$

where,

$$\nu_i = \prod_{i=1}^{N} \prod_{j=1}^{N_c} Pr(\gamma_{ij} \mid \gamma_i) Pr(\gamma_i). \tag{7.16}$$

It should be noted here that since the weighting for the bit difference, $\gamma_i$, is $\gamma_i = 1/2$ for both $\gamma_i = +2$ and $\gamma_i = -2$, and coupled with the fact that the phase transition diagrams are symmetric, this weighting will reduce to only the conditional probability of the chip difference sequence. (Viewing Table 7.1 in reverse order for $\gamma_i = -2$ gives the same results as for $\gamma_i = +2$.)

The resulting bit error probability is then

$$P_b \leq \sum_{i=1}^{\infty} \nu_i \mu_i Q(\sqrt{\frac{d_i^2}{2N_0}}), \tag{7.17}$$

where $\mu_i$ is the number of bit errors in each error sequence with separation distance, $d_i$.

Prior to concluding the bit error analysis it is necessary to digress for a moment to consider the methods in determining the distances, $d_i$, in equation 7.17.

## 7.2 Distance Analysis

The previous section showed that the error probability of an error event over $N$ symbols, is (from equation 7.1)

$$P(s_2(t) \mid s_1(t)) = P[\int_0^{NT_s} s_2(t)r(t)dt > \int_0^{NT_s} s_1(t)r(t)dt] \tag{7.18}$$

$$= Q(\sqrt{\frac{d_{12}^2}{2N_0}}), \tag{7.19}$$

where $d_{12}$ is the Euclidean distance between the two signals.

The squared distance can be expressed as

$$d_{12}^2(N) = \int_0^{NT_s} (s_1(t) - s_2(t))^2 dt, \tag{7.20}$$

but this distance is cumulative over bit intervals as seen by expanding the integral to

$$d_{12}^2(N) = \int_0^{T_s} (s_1 - s_2)^2 dt + \int_{T_s}^{2T_s} (s_1 - s_2)^2 dt + \ldots + \int_{(N-1)T_s}^{NT_s} (s_1 - s_2)^2 dt. \tag{7.21}$$

For SSMH signals these integrals over a bit interval can be further expanded to

$$d_{12}^2(N) = \int_0^{N_c T_c} (s_1 - s_2)^2 dt + \int_{N_c T_c}^{2N_c T_c} (s_1 - s_2)^2 dt + \ldots, \tag{7.22}$$

which can be rewritten

$$d_{12}^2(N) = \sum_{i=0}^{N} \sum_{j=0}^{N_c-1} \int_{jT_c}^{(j+1)T_c} (s_{1ij}(t) - s_{2ij}(t))^2 dt; \tag{7.23}$$

and implies that the distance squared on a bit basis is cumulative and also cumulative over the chips per bit.

Recalling from Chapter 3 that the signal over bit $i$ and chip $j$ is defined as

$$s_1(\alpha_i, h_{ij}, c_{ij}, \theta_{ij}, t) = \sqrt{\frac{2E_c}{T_c}} \cos(\omega_0 t + 2\pi h_{ij}\alpha_i c_{ij} q(t) + \theta_{ij}) \tag{7.24}$$

$$s_2(\hat{\alpha}_i, h_{ij}, c_{ij}, \theta_{ij}, t) = \sqrt{\frac{2E_c}{T_c}} \cos(\omega_0 t + 2\pi h_{ij}\hat{\alpha}_i c_{ij} q(t) + \theta_{ij}), \tag{7.25}$$

and since $c_{ij}, h_{ij}$, and $q(t) = t/2T_c$ are known, substitution yields

$$d_{12}^2(N) = 2E_c \sum_{i=1}^{N} \sum_{j=0}^{N_c-1} \frac{1}{T_c} \int_{jT_c}^{(j+1)T_c} 1 - \cos[2\pi h_{ij} c_{ij} (\alpha_i - \hat{\alpha}_i) q(t - jT_c) + (\theta_{ij} - \hat{\theta}_{ij})] dt. \quad (7.26)$$

Letting $\Delta\theta_{ij} = \theta_{ij} - \hat{\theta}_{ij}$ and $\Delta\theta_{i,j+1} = \Delta\theta_{ij} + \pi h_{ij} c_{ij} (\alpha_i - \hat{\alpha}_i)$, and substituting for $q(t - jT_c)$ yields

$$d_{12}^2(N) = \begin{cases} 2E_c \sum_{i=1}^{N} \sum_{j=0}^{N_c-1} 1 - \frac{\sin(\Delta\theta_{i,j+1}) - \sin(\Delta\theta_{ij})}{\Delta\theta_{i,j+1} - \Delta\theta_{ij}}, & \text{if } \Delta\theta_{i,j+1} \neq \Delta\theta_{ij}, \\ 2E_c \sum_{i=1}^{N} \sum_{j=0}^{N_c-1} 1 - \cos(\Delta\theta_{i,j+1}), & \text{if } \Delta\theta_{i,j+1} = \Delta\theta_{ij}. \end{cases} \quad (7.27)$$

The result of this investigation is the fact that on a bit basis the distance between two signals is cumulative from bit to bit. In addition, the bit distances are the incremental sum of distances over the chip intervals. Coincidently, the chip distances are directly dependent on the differences of phase states at the chip boundaries.

For large signal-to-noise ratios, and as the number of bits considered grows large, the probability of error will be dominated by a few error events with small distances. Hence, a minimum distance between any two signals will dominate and be defined as the 'free' distance, where

$$d_{\text{free}}^2(N) = \lim_{N \to \infty} \min d_{mn}^2(N) \quad m \neq n. \quad (7.28)$$

Finding this distance requires the exhaustive search of all signals whose phase paths split at some point and remerge at a future point. However, Aulin [15] and Hsu [30] have shown that the Viterbi Algorithm, as a dynamic programming technique, can be used to find the minimum distance in a trellis structure of the difference states of the original state trellis structure. Hence, a comparison of all signals that depart from the error free path and remerge at a future point will characterize the distance distribution. The current work can not take advantage of this methodology however, since the bit differences are not constant over a bit interval due to the spreading sequence as discussed in the previous section.

However, assuming all signal paths in the trellis structure begin at some point $nT_s$, that is, assuming error free transmission up to time $nT_s$, the state transition diagrams can be used to determine the shortest distance to return to the all zero path. This distance will become the minimum distance for the code and determine the constraint length.

The determination of the minimum distance is important for several reasons. First, from equation 7.17 for high signal-to-noise ratios the free distance term will dominate the error probability. Secondly, the depth, or number of bits required to obtain the free distance, will determine the minimum decoding delay for a Viterbi Algorithm processor to obtain maximal performance. Finally, if the entire distance distribution for a given code is known, the performance in relation to the minimum distance can be determined. For example, if a code has a significant number of error events at distances that are close to the minimum distance, its performance may be worse than a code with a single but rarely occuring minimum distance.

It should be noted that as shown by Hsu [30], the starting index will affect the distance metrics for multi-$h$ signals; therefore, the minimization of distance must also include a minimization over all possible starting indices. This is accomplished by assuming that it is equally likely that each index will be chosen first; therefore, the minimum distance is chosen from all distances that arise from a given modulation index code.

## 7.3 Probability of Error Upper Bounds

Having established that the separation distance between two error sequences is cumulative over chip and bit intervals, and having defined the free distance, we return to the determination of the upper bound on the probability of bit error.

From equation 7.17 and equation 7.27, the probability of bit error is upper bounded by

$$P_b \leq \sum_{i=1}^{\infty} \mu_i \nu_i Q\left(\sqrt{\frac{2E_c d_i^2}{2N_0}}\right), \tag{7.29}$$

$$P_b \leq \sum_{i=1}^{\infty} \mu_i \nu_i Q\left(\sqrt{\frac{d_i^2 E_c}{N_0}}\right). \tag{7.30}$$

Introducing the term, $d_f^2 E_c/N_0$, and using the equality $Q(\sqrt{x+y}) \leq Q(\sqrt{x})e^{-y/2}$, $x, y > 0$, this becomes

$$P_b \leq Q\left(\sqrt{\frac{d_f^2 E_c}{N_0}}\right) e^{\frac{d_f^2 E_c}{2N_0}} \sum_{i=1}^{\infty} \mu_i \nu_i e^{-\frac{d_i^2 E_c}{2N_0}}. \tag{7.31}$$

At this junction, the signal flow graph and difference state analysis of Hsu [30] and Anderson [6] are invoked. The split bit difference state transition diagram for a given

modulation index code describes the possible phase difference transitions. For an error event beginning at $nT_s$ then returning to the all zero path at $(n+N)T_s$, the overall path gain is

$$T = \sum_{i=1}^{N} \nu_i D^{d_i^2} E^{\mu_i} L. \tag{7.32}$$

As shown by Hsu, if $T_A$ represents the split difference state transition for a particular bit modulation coding over one bit, then $T_A T_A$ represents the error transition over two bits, and by extension

$$T = T_A + T_A T_A + T_A T_A T_A + \ldots.$$

represents the error transitions over an infinite length. This situation reflects a decoder with unlimited memory. For multi-$h$ codes the bit modulation coding changes from bit to bit; i.e., for a two index code there are two bit transition matrices, $T_A$ and $T_B$. Therefore, the unlimited length transition becomes

$$T = T_A + T_A T_B + T_A T_B T_A + \ldots.$$

Since the modulation indices and transition matrices are periodic, this reduces to

$$T = \sum_{k=0}^{\infty} (T_A T_B)^k (T_A + T_A T_B), \tag{7.33}$$

$$T = (1 - T_A T_B)^{-1} (T_A + T_A T_B), \tag{7.34}$$

and the upper right corner term of this transition matrix represents the sum of all the branch gains, i.e.,

$$T(1, p+1) = \sum_{i=1}^{\infty} \nu_i D^{d_i^2} E^{\mu_i} L. \tag{7.35}$$

Since the error events could begin during either coding interval, two possiblities for the transitions occur; thus

$$T_1 = (1 - T_A T_B)^{-1} (T_A + T_A T_B), \tag{7.36}$$

$$T_2 = (1 - T_B T_A)^{-1} (T_B + T_B T_A). \tag{7.37}$$

Applying these results to equation 7.17 results in

$$P_{e|1} \leq Q\left(\sqrt{\frac{d_f^2 E_c}{N_0}}\right) e^{\frac{d_f^2 E_c}{2N_0}} \sum_{i=1}^{\infty} \mu_i e^{-\frac{d_i^2 E_c}{2N_0}}, \tag{7.38}$$

$$P_{e|1} \leq Q\left(\sqrt{\frac{d_f^2 E_c}{N_0}}\right) e^{\frac{d_f^2 E_c}{2N_0}} T_1 \,|_{D=e^{-E_c/2N_0}, E=1, L=1}, \tag{7.39}$$

and

$$P_{b|1} \leq Q(\sqrt{\frac{d_f^2 E_c}{N_0}}\,) e^{\frac{d_f^2 E_c}{2N_0}} \frac{\partial T_1}{\partial E} \mid_{D=e^{-E_c/2N_0}, E=1, L=1} . \tag{7.40}$$

Alternatively,

$$P_{b|2} \leq Q(\sqrt{\frac{d_f^2 E_c}{N_0}}\,) e^{\frac{d_f^2 E_c}{2N_0}} \frac{\partial T_2}{\partial E} \mid_{D=e^{-E_c/2N_0}, E=1, L=1} . \tag{7.41}$$

Since it is equally likely that the receiver will begin decoding on either modulation code sequence, the total probability of bit error is the average of the individual code bit error probabilities. Hence,

$$P_b = \frac{1}{2}(P_{b|1} + P_{b|2}). \tag{7.42}$$

As a final note, equation 7.40 can be rewritten

$$P_{b|i} \leq \frac{1}{2}\mathrm{erfc}(\sqrt{\frac{d_f^2 E_c}{2N_0}}\,) e^{\frac{d_f^2 E_c}{2N_0}} \frac{\partial T_i}{\partial E} \mid_{D=e^{-E_c/2N_0}, E=1, L=1} . \tag{7.43}$$

Additionally, using the approximation $Q(x) \leq e^{-\frac{x^2}{2}}/\sqrt{2\pi}\, x$, then

$$P_{b|i} \leq \frac{\frac{\partial T_i}{\partial E}}{\sqrt{\frac{2\pi d_f^2 E_c}{N_0}}}. \tag{7.44}$$

In the following section, equation 7.43 and equation 7.44 are used to determine the upper bound to the bit error for selected SSMH coding schemes.

## 7.4 Selected SSMH Performance Bounds

In order to implement the analytically determined bound expressions of the previous section, it is first necessary to determine the bit transition diagram for the specific modulation scheme and code selected. For illustrative purposes, the $\frac{1}{2}, \frac{3}{4}$ and $\frac{4}{8}, \frac{5}{8}$ modulation codes were selected. The first was used because it is the simplest, and the second was selected due to its flat spectral characteristics and coding gain as shown by Lereim [33].

A recursive FORTRAN implemented routine was used to determine the distance over a bit interval and difference phase transitions for all possible beginning difference phases and all possible chip difference sequences, where there are $2^{N_c}$ possible sequences if the bit difference is not zero. The following figures show the resulting bit difference transition diagrams.

| *Modulation Indices* | *Figure* |
|---|---|
| Conventional | |
| .5, .75 | 7.1 |
| .75, .5 | 7.2 |
| .5, .625 | 7.3 |
| .625, .5 | 7.4 |
| Modified | |
| .5 (4 state) | 7.5 |
| .5 (8 state) | 7.7 |
| .625 | 7.8 |
| .75 | 7.6 |

Table 7.2: Selected SSMH State Transition Diagrams; $N_c = 3$

As was inferred in the previous section, inspection of the state transition diagrams reveals the minimum distance required to leave the all zero path during an initial bit interval and after a free distance minimum to return to the all zero path. For example, examination of Figure 7.2 shows that an error event over just one bit interval will return to the all zero path with a minimum distance of 2.79. On the other hand, if the opposite order of modulation indices were considered as the first bit interval, it would require alternation

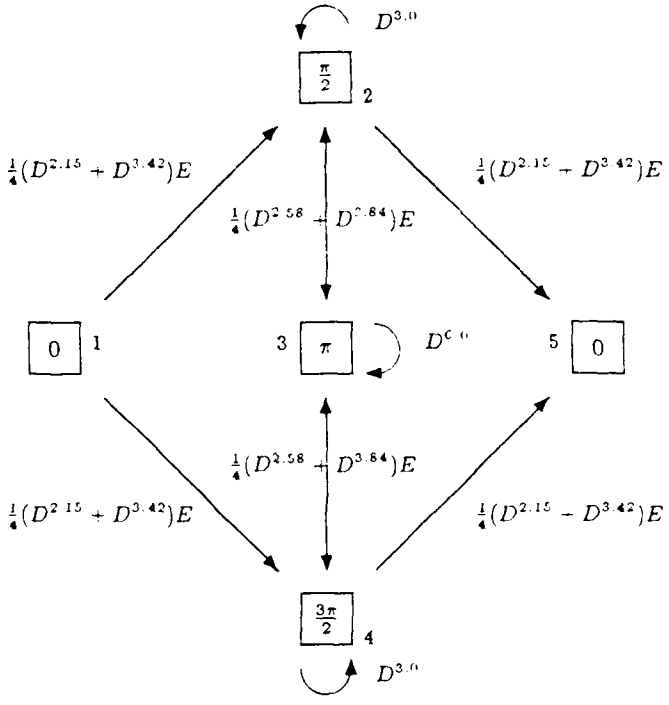


Figure 7.1: Conventional $\frac{1}{2}$, $\frac{3}{4}$ SSMH Code; $N_c = 3$, Difference States

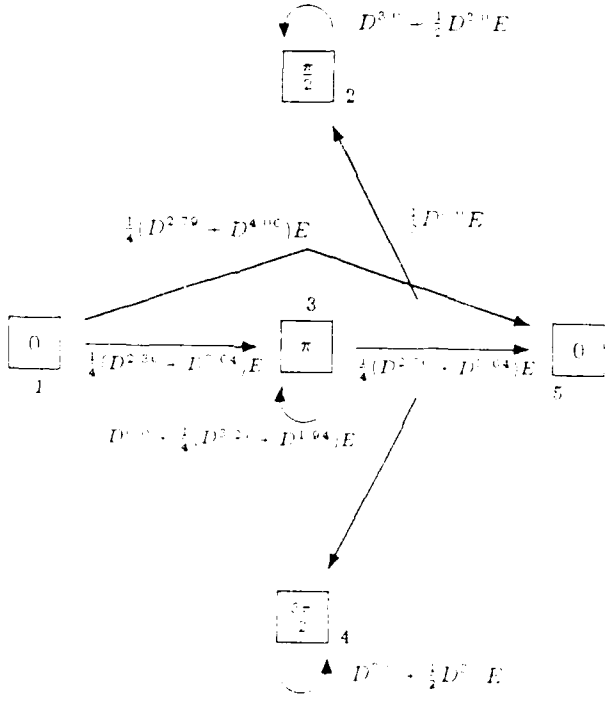


Figure 7.2: Conventional $\frac{3}{4}$, $\frac{1}{2}$ SSMH Code: $N_c = 3$, Difference States

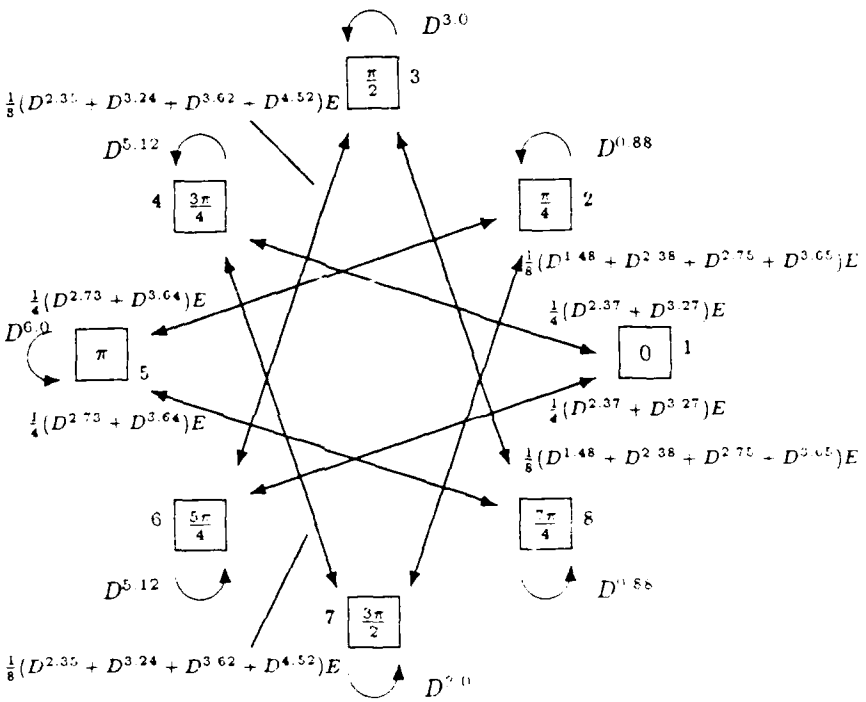


Figure 7.3: Conventional $\frac{1}{2}$, $\frac{5}{8}$ SSMH Code; $N_c = 3$, Difference States

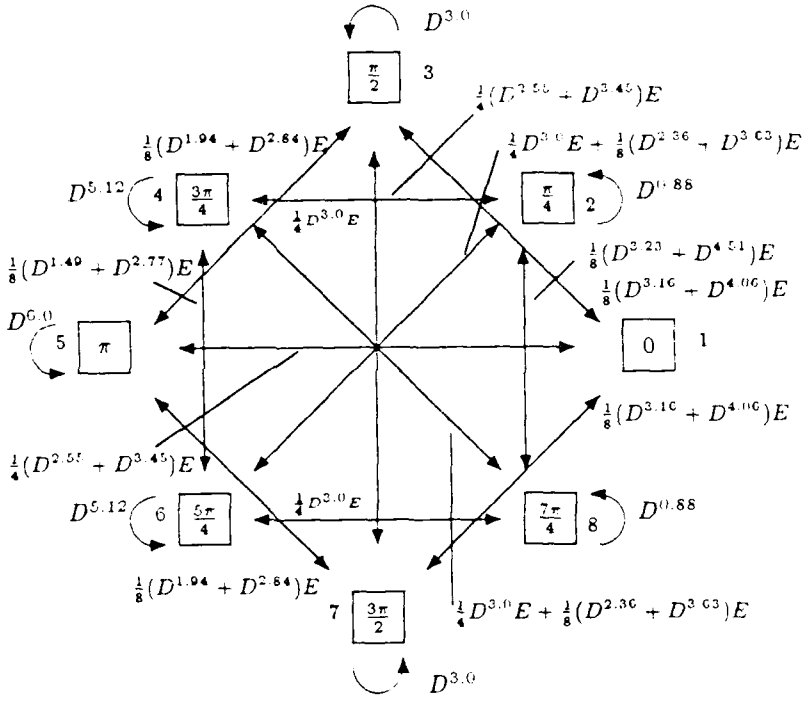


Figure 7.4: Conventional $\frac{5}{8}$, $\frac{1}{2}$ SSMH Code; $N_c = 3$, Difference States

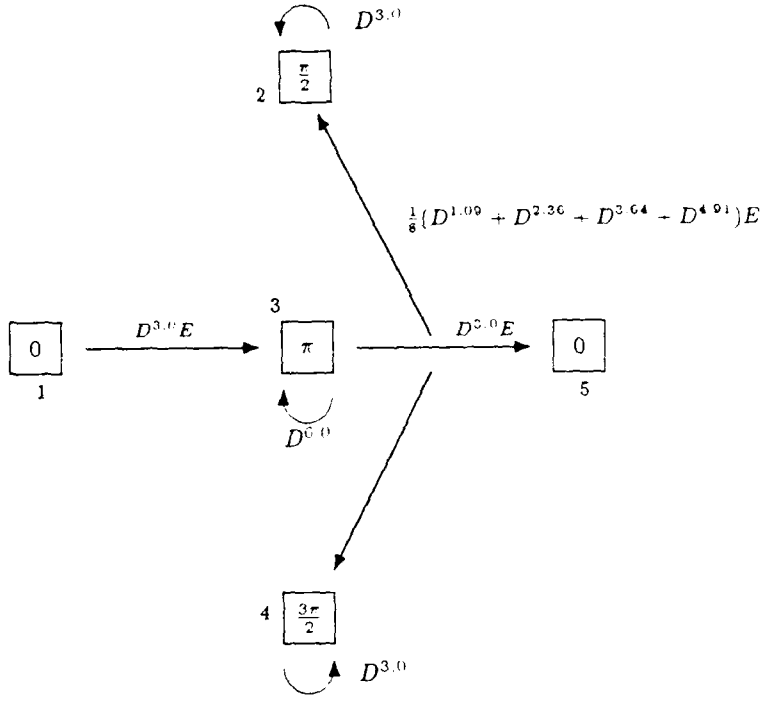


Figure 7.5: Modified $\frac{1}{2}$ SSMH Code; $N_c = 3$, Difference States

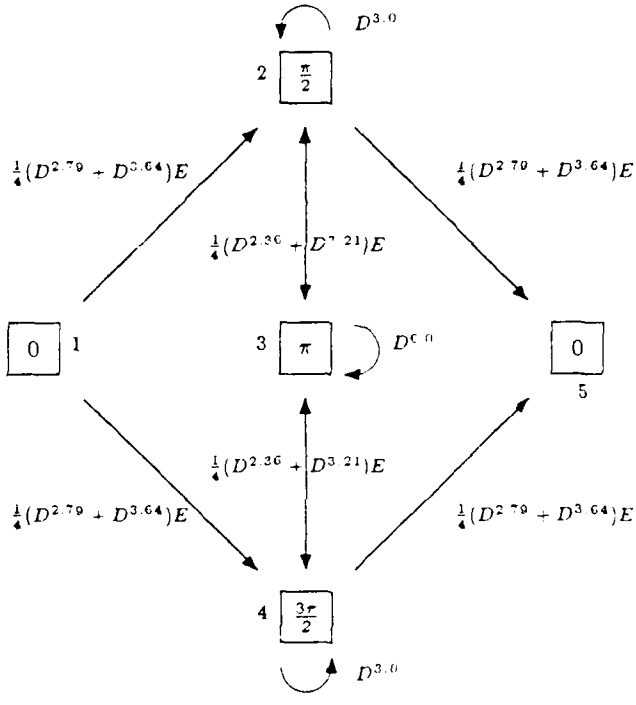


Figure 7.6: Modified $\frac{3}{4}$ SSMH Code; $N_c = 3$, Difference States

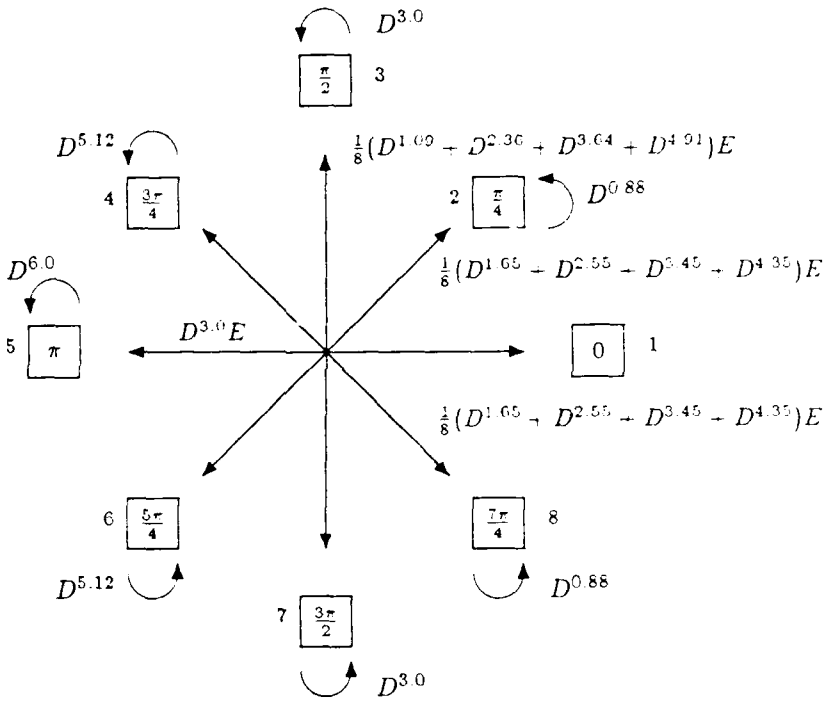


Figure 7.7: Modified $\frac{1}{2}$ SSMH Code; $N_c = 3$, Eight Difference States

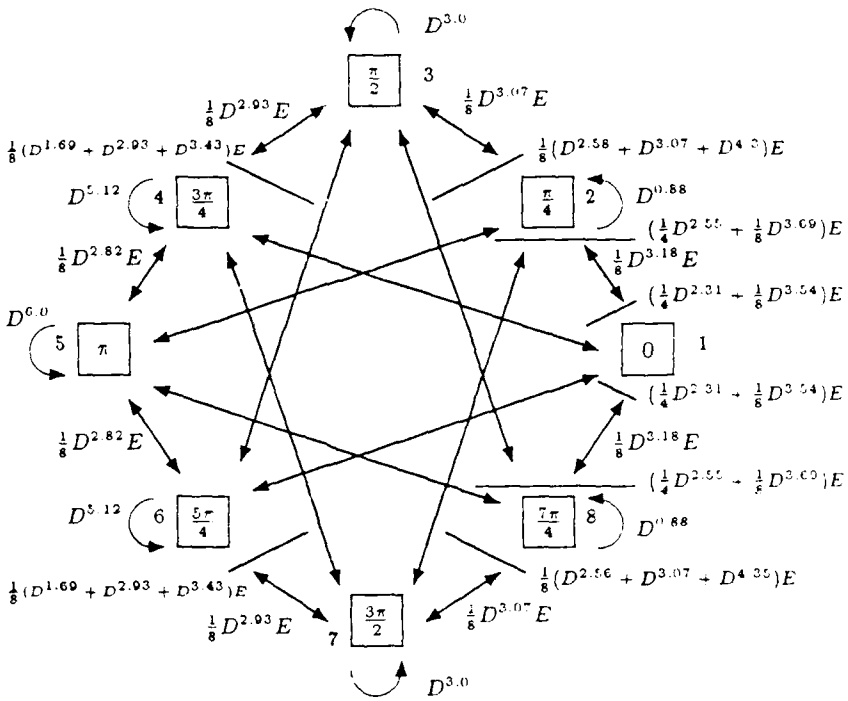


Figure 7.8: Modified $\frac{5}{8}$ SSMH Code; $N_c = 3$, Difference States

between the two state diagrams (Figure 7.1 and Figure 7.2) over 3 bits for the error event to terminate and obtain the minimum distance of 7.3.

After inspection of the transition diagrams, the minimum distances for both modulation schemes with a spreading code of three chips were determined. Table 7.3 below summarizes these important figures of merit.

| *Modulation Indices* | *Spread Rate* | $D^2_{\min}$ | *Depth* |
|---|---|---|---|
| Conventional | | | |
| .5, .75 | 3 | 7.30 | 3 |
| .75, .5 | 3 | 2.79 | 1 |
| .5, .625 | 3 | 6.23 | 3 |
| .625, .5 | 3 | 9.37 | 4 |
| Modified | | | |
| .5, .75 | 3 | 12.00 | 3 |
| .75, .5 | 3 | 6.67 | 3 |
| .5, .625 | 3 | 9.51 | 4 |
| .625, .5 | 3 | 7.24 | 3 |

Table 7.3: Selected SSMH Minimum Distances

With the difference state transitions as shown above and the free distances, equation 7.43 or equation 7.44 can now be solved to determine the upper bound to the bit error probability. Once again, these equations were numerically implemented via FORTRAN code with the partial differentiation accomplished with numerical differencing. Figure 7.9 below shows the resultant upper bounds to the bit error probability for the selected modulation indices with a spreading rate of three chips per bit, and Figure 7.10 reflects the bit error probability bounds for seven chips per bit. The circled path reflects Conventional .5, .75 coding, the triangle path is for Conventional .5, .625 coding, the plus path delineates Modified .5, .75 coding, and Modified .5, .625 coding is shown by x's. The unmarked path corresponds to DS/BPSK.

At this point it is appropriate to comment on the relative merits of these findings vis-a-vis more realistic spreading rates. The results above incorporated a spreading rate

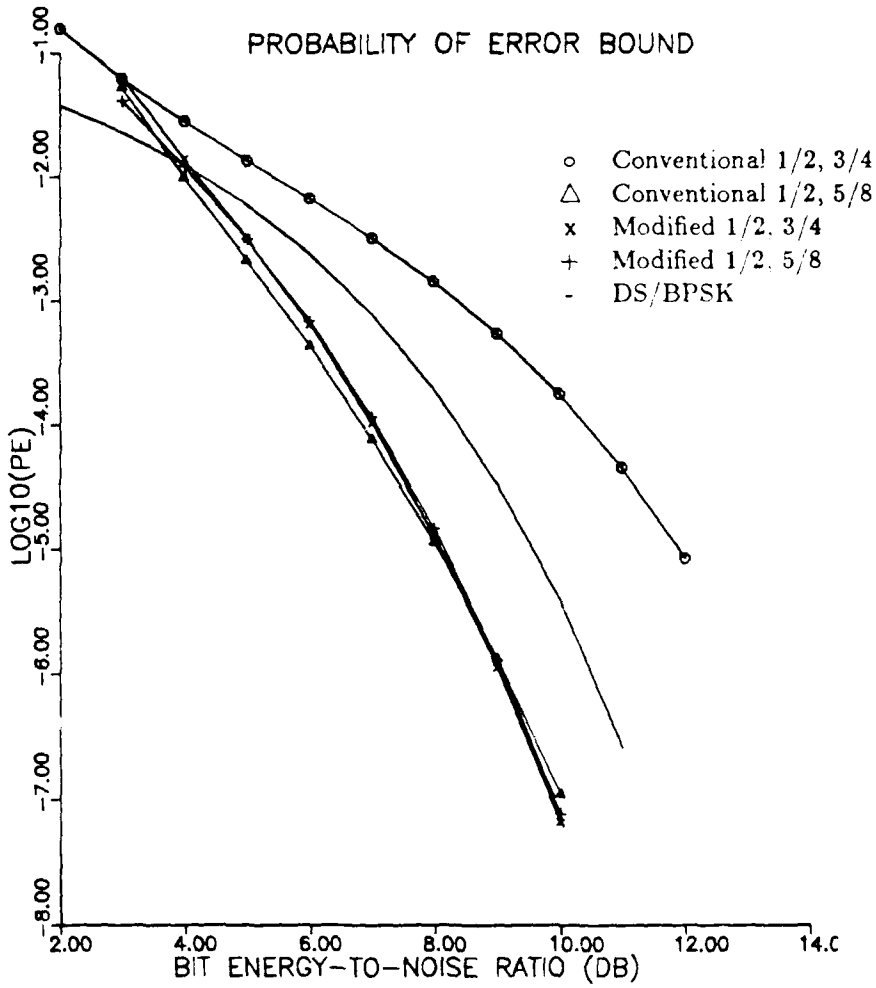


Figure 7.9: Probability of Bit Error Bounds, $N_c = 3$

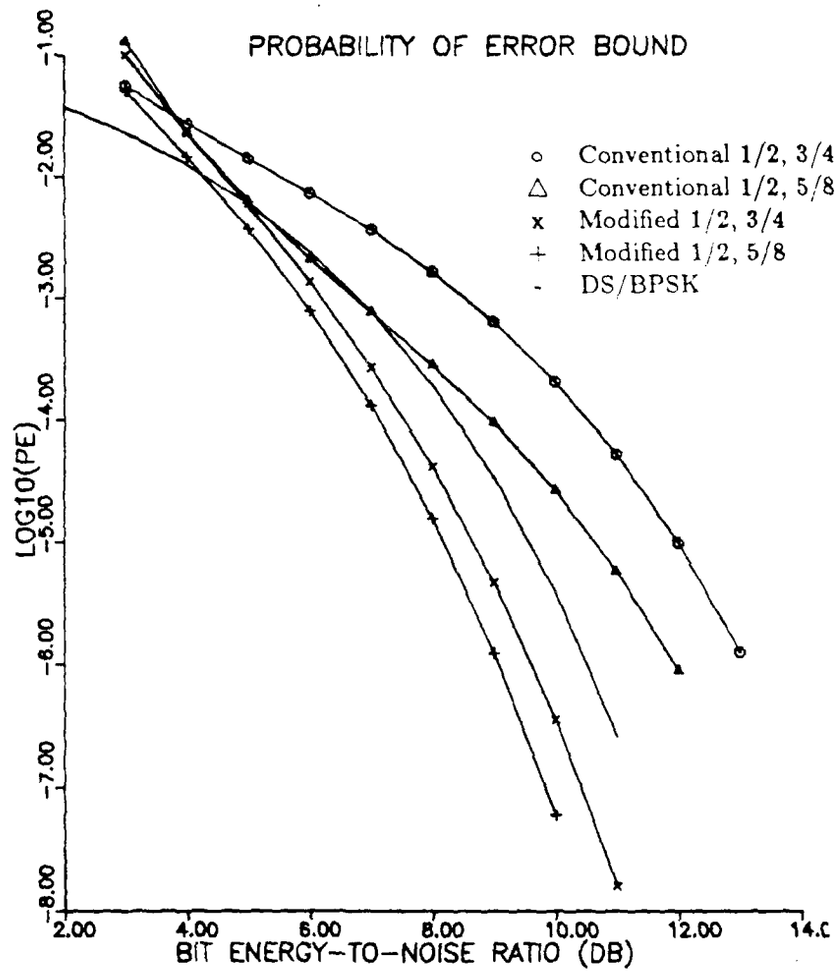


Figure 7.10: Probability of Bit Error Bounds, $N_c = 7$

of three chips per bit while normal spreading rates are on the order of one thousand chips per bit. However, the number of possible chip difference sequences is on the order of $2^{N_c}$ implying that for a chip rate of 1000 chips per bit, an unreasonably large number of chip difference sequences would have to be considered for each starting phase. As a result, only small order chip rates were considered in this work to verify the procedure. Numerical evaluations in Chapter 8 will consider more reasonable figures of 127 and 1023 chips per bit.

With the analytical bounds to the performance of the modulation scheme established, it is appropriate to consider the receiver structure of Chapter 6. The following chapter discusses the numerical evaluation of this receiver and comparisons can be made with the established bounds.

# CHAPTER 8

# Receiver Evaluation

In Chapter 6 the receiver structure and maximum likelihood receiver metrics for a SSMH receiver were derived. This chapter numerically evaluates the analytically derived receiver in an additive white Gaussian noise environment. The individual chip metrics are represented as sampled outputs from matched correlation filters with correlated noise samples added to the noise free filter outputs. This arrangement represents the received signal corrupted by white noise and the received signal processed by correlation filters. The remainder of the receiver is shown to consist of a Viterbi Algorithm processor, which uses the sum of chip metrics over a bit interval to form the bit branch metrics. The receiver is shown to perform within the bounds established in Chapter 7.

With the groundwork of Chapter 6, the signal components of the chip metric calculators are first derived. The correlated noise samples are then determined using uncorrelated white noise samples as a source and a linear transformation to achieve the appropriate correlated noise samples. With the appropriate multiplexing to insure the proper chip and modulation index alignment, the chip metrics are then summed to form individual bit metrics over a bit interval. A state traceback implementation of the Viterbi Algorithm then forms the decision processing. Throughout the evaluation, perfect phase synchronization, bit and chip timing, and modulation index synchronization are assumed.

## 8.1 Correlation Filters

Equations 6.5 and 6.6 from Chapter 6 a. repeated here to recall the maximum likelihood chip and bit metrics on which the decision making process is based. The bit metrics over

bit interval $i$ are the sum of the chip metrics, hence

$$\lambda_i = \sum_{j=0}^{N_c-1} \lambda_j, \tag{8.1}$$

where the chip metrics are

$$\lambda_j = \int_{jT_c}^{(j+1)T_c} r(t - jT_c) s(t - jT_c, \alpha_i, h_{(i+j) \bmod H}, c_{ij}) dt. \tag{8.2}$$

These expressions reveal two key factors; first, that the bit metrics result simply from the sum of chip metrics, and, secondly, that the chip metrics are obtained from the correlation of the noise corrupted received signal with all of the possible transmitted signals.

It should be noted at this point that previous works in this area have taken the approach of orthonormalizing the signal structure and adding independent white noise samples to create the noise corrupted received signal. An alternate approach is taken here for the first time with this class of signals. Correlated noise samples generated by linear transformation of independent noise samples will be added to the noise free samples of the output of the correlation filters. The signal components of the filter outputs are addressed in this section and the following section addresses the noise components.

As shown in Chapter 6, expansion of the metric expressions above for binary signaling and the possible beginning phase states yields over each chip interval

$$\begin{aligned} \lambda(\alpha_i = +1, c_{ij}, \theta_{ij}) &= \int_0^{T_c} r(t) \cos(2\pi f_0 t + \frac{\pi c_{ij} h_{ij} t}{T_c} + \theta_{ij}) dt, \\ \lambda(\alpha_i = -1, c_{ij}, \theta_{ij}) &= \int_0^{T_c} r(t) \cos(2\pi f_0 t - \frac{\pi c_{ij} h_{ij} t}{T_c} + \theta_{ij}) dt. \end{aligned} \tag{8.3}$$

These expressions indicate an array of $2H$ times the number of states correlators. Expanding these expressions on the initial phase angle yields quadrature forms of the correlators. That is,

$$\begin{bmatrix} \lambda(+\alpha_i, c_{ij}, \theta_{ij}) \\ \lambda(-\alpha_i, c_{ij}, \theta_{ij}) \end{bmatrix} = \begin{bmatrix} I_1 & -Q_1 \\ I_2 & -Q_2 \end{bmatrix} \begin{bmatrix} \cos\theta_{ij} \\ \sin\theta_{ij} \end{bmatrix}, \tag{8.4}$$

where

$$I_1 = \int_0^{T_c} r(t) \cos(2\pi f_0 t + \frac{\pi c_{ij} h_{ij} t}{T_c}) dt, \tag{8.5}$$

$$Q_1 = \int_0^{T_c} r(t)\sin(2\pi f_0 t + \frac{\pi c_{ij} h_{ij} t}{T_c})dt, \tag{8.6}$$

$$I_2 = \int_0^{T_c} r(t)\cos(2\pi f_0 t - \frac{\pi c_{ij} h_{ij} t}{T_c})dt, \tag{8.7}$$

$$Q_2 = \int_0^{T_c} r(t)\sin(2\pi f_0 t - \frac{\pi c_{ij} h_{ij} t}{T_c})dt. \tag{8.8}$$

These equations imply a bank of $4H$ correlators and a phase rotation network to account for the allowable phases at the start of each chip interval.

*The received signal is*

$$r(t) = s(t) + n(t),$$

where $n(t)$ is AWGN with variance, $N_0/2$, and $s(t)$ is the transmitted signal

$$s(t) = \sqrt{\frac{2E_c}{T_c}}\cos(2\pi f_0 t + \frac{\pi h_{ij}\alpha_i c_{ij} t}{T_c} + \psi_{ij}(t)). \tag{8.9}$$

This expression represents a signal transmitted over any bit interval, $i$, and chip interval, $jT_c$ to $(j+1)T_c$, with chip multiplier, $c_{ij}$, data bit, $\alpha_i$, modulation index, $h_{(i+j) \bmod H} = h_{ij}$, and initial phase angle, $\psi_{ij}(t)$.

Substitution in equations above gives

$$I_1 = \int_0^{T_c} [s(t) + n(t)]\cos(2\pi f_0 t + \frac{\pi c_{ij} h_{ij} t}{T_c})dt, \tag{8.10}$$

$$Q_1 = \int_0^{T_c} [s(t) + n(t)]\sin(2\pi f_0 t + \frac{\pi c_{ij} h_{ij} t}{T_c})dt, \tag{8.11}$$

$$I_2 = \int_0^{T_c} [s(t) + n(t)]\cos(2\pi f_0 t - \frac{\pi c_{ij} h_{ij} t}{T_c})dt, \tag{8.12}$$

$$Q_2 = \int_0^{T_c} [s(t) + n(t)]\sin(2\pi f_0 t - \frac{\pi c_{ij} h_{ij} t}{T_c})dt. \tag{8.13}$$

After multiplication of terms, these equations are expressed as

$$I_1 = S1C + N1C, \tag{8.14}$$

$$Q_1 = S1S + N1S, \tag{8.15}$$

$$I_2 = S2C + N2C, \tag{8.16}$$

$$Q_2 = S2S + N2S, \tag{8.17}$$

where

$$S1C = \int_0^{T_c} s(t)\cos(2\pi f_0 t + \frac{\pi c_{ij} h_{ij} t}{T_c})dt, \tag{8.18}$$

$$
\begin{aligned}
N1C &= \int_0^{T_c} n(t)\cos(2\pi f_0 t + \frac{\pi c_{ij} h_{ij} t}{T_c})dt, \\
S1S &= \int_0^{T_c} s(t)\sin(2\pi f_0 t + \frac{\pi c_{ij} h_{ij} t}{T_c})dt, \\
N1S &= \int_0^{T_c} n(t)\sin(2\pi f_0 t + \frac{\pi c_{ij} h_{ij} t}{T_c})dt, \\
S2C &= \int_0^{T_c} s(t)\cos(2\pi f_0 t - \frac{\pi c_{ij} h_{ij} t}{T_c})dt, \\
N2C &= \int_0^{T_c} n(t)\cos(2\pi f_0 t - \frac{\pi c_{ij} h_{ij} t}{T_c})dt, \\
S2S &= \int_0^{T_c} s(t)\sin(2\pi f_0 t - \frac{\pi c_{ij} h_{ij} t}{T_c})dt, \\
N2S &= \int_0^{T_c} n(t)\sin(2\pi f_0 t - \frac{\pi c_{ij} h_{ij} t}{T_c})dt.
\end{aligned}
$$

For a given $\alpha_i$, $c_{ij}$, and $h_{ij}$, the expected value of these expressions will give the signal components of the correlation filters (Note an alternate approach is to assume simply a noise free situation). As an example,

$$\mathcal{E}\{I_1\} = \mathcal{E}\{S1C + N1C\}, \tag{8.19}$$

$$\mathcal{E}\{I_1\} = \mathcal{E}\{S1C\} + \mathcal{E}\{N1C\}, \tag{8.20}$$

$$\mathcal{E}\{I_1\} = S1C, \tag{8.21}$$

since $n(t)$ is white Gaussian noise of mean zero and variance $N_0/2$.

Following this procedure for each term, eliminating the double frequency terms, and normalizing the time interval yields for $\alpha_i c_{ij} = +1$,

$$\mathcal{E}\left\{\begin{array}{c} I_1 \\ Q_1 \\ I_2 \\ Q_2 \end{array}\right\}_{|\alpha_i c_j = +1, h_{ij}} = \sqrt{\frac{E_c}{2}} \left\{\begin{array}{c} \cos(\psi(0)) \\ -\sin(\psi(0)) \\ \frac{\sin(2\pi h_{ij})}{2\pi h_{ij}}\cos(\psi(0)) - \frac{[1-\cos(2\pi h_{ij})]}{2\pi h_{ij}}\sin(\psi(0)) \\ -\frac{[1-\cos(2\pi h_{ij})]}{2\pi h_{ij}}\cos(\psi(0)) - \frac{\sin(2\pi h_{ij})}{2\pi h_{ij}}\sin(\psi(0)) \end{array}\right\} \tag{8.22}$$

and for $\alpha_i c_{ij} = -1$,

$$\mathcal{E}\left\{\begin{array}{c} I_1 \\ Q_1 \\ I_2 \\ Q_2 \end{array}\right\}_{|\alpha_i c_j = -1, h_{ij}} = \sqrt{\frac{E_c}{2}} \left\{\begin{array}{c} \frac{\sin(2\pi h_{ij})}{2\pi h_{ij}}\cos(\psi(0)) + \frac{[1-\cos(2\pi h_{ij})]}{2\pi h_{ij}}\sin(\psi(0)) \\ \frac{[1-\cos(2\pi h_{ij})]}{2\pi h_{ij}}\cos(\psi(0)) - \frac{\sin(2\pi h_{ij})}{2\pi h_{ij}}\sin(\psi(0)) \\ \cos(\psi(0)) \\ -\sin(\psi(0)) \end{array}\right\} \tag{8.23}$$

These equations form the basis of the noise free signal components at the output of the correlation filters. The next section continues the analysis to derive the correlated noise samples to be added to these signal components.

## 8.2 Correlated Noise Samples

The determination of the correlated noise samples begins with equations 8.18 from the previous section. However, now we seek the covariance matrix, $\underline{C}$, of the four Gaussian signals $I_1$, $Q_1$, $I_2$, and $Q_2$.

An example will illustrate the procedure. Hence,

$$\begin{aligned} C_{I_1I_1} &= \mathcal{E}\{(I_1)^2\} - \mathcal{E}^2\{I_1\}, \\ &= \mathcal{E}\{(S1C + N1C)^2\} - \mathcal{E}^2\{I_1\}, \\ &= \mathcal{E}\{S1C^2 + 2(S1C)(N1C) + (N1C)^2\} - \mathcal{E}^2\{I_1\}, \\ &= \mathcal{E}\{S1C^2\} + 2\mathcal{E}\{(S1C)(N1C)\} + \mathcal{E}\{N1C^2\} - \mathcal{E}^2\{I_1\}. \end{aligned} \tag{8.24}$$

Using the results of the previous section, the signal terms cancel and the since the mean of $n(t)$ is zero, the product term is zero. Therefore,

$$C_{I_1I_1} = \mathcal{E}\{N1C^2\}. \tag{8.25}$$

After substitution for $N1C$, normalization by $T_c$, and neglecting the double frequency terms, this expression reduces to

$$\begin{aligned} C_{I_1I_1} &= \mathcal{E}\{\int_0^{T_c} n(u)\cos(2\pi f_0 u + \frac{\pi h_{ij} u}{T_c})du \int_0^{T_c} n(v)\cos(2\pi f_0 v + \frac{\pi h_{ij} v}{T_c})dv\}, \\ &= \int_0^{T_c}\int_0^{T_c} \mathcal{E}\{n(u)n(v)\}\cos(2\pi f_0 u + \frac{\pi h_{ij} u}{T_c})\cos(2\pi f_0 v + \frac{\pi h_{ij} v}{T_c})dudv, \\ &= \frac{N_0}{2}\int_0^{T_c}\int_0^{T_c} \delta(u-v)\cos(2\pi f_0 u + \frac{\pi h_{ij} u}{T_c})\cos(2\pi f_0 v + \frac{\pi h_{ij} v}{T_c})dudv, \\ &= \frac{N_0}{2}\int_0^{T_c} \cos^2(2\pi f_0 v + \frac{\pi h_{ij} v}{T_c})dv, \\ &= \frac{N_0}{4}. \end{aligned} \tag{8.26}$$

The result of following this procedure for all of the autocovariance and cross-covariance terms is the covariance matrix below for the multivariant Gaussian random variables for

the outputs of the correlation filters,

$$\underline{C} = \frac{N_0}{4}\begin{bmatrix} 1 & 0 & \frac{\sin(2\pi h_{ij})}{2\pi h_{ij}} & \frac{-1+\cos(2\pi h_{ij})}{2\pi h_{ij}} \\ 0 & 1 & \frac{1-\cos(2\pi h_{ij})}{2\pi h_{ij}} & \frac{\sin(2\pi h_{ij})}{2\pi h_{ij}} \\ \frac{\sin(2\pi h_{ij})}{2\pi h_{ij}} & \frac{1-\cos(2\pi h_{ij})}{2\pi h_{ij}} & 1 & 0 \\ \frac{-1+\cos(2\pi h_{ij})}{2\pi h_{ij}} & \frac{\sin(2\pi h_{ij})}{2\pi h_{ij}} & 0 & 1 \end{bmatrix}. \tag{8.27}$$

Examination of this covariance matrix reveals that the values are constant over a chip interval and depend on the modulation index. As a result, the evaluation need only maintain proper index synchronization and this covariance can be used to determine the correlated noise samples.

This covariance matrix gives the relationship that must exist between samples of the random quadrature components at the output of the correlation filters. The previous section gave the noise free signal components that would appear at the outputs. Now using the covariance matrix, a method can be established to add correlated noise samples to the noise free signal components so that the random variable signal components have the appropriate covariance.

As shown by Papoulis [46] and others, including Stark and Woods [61], if selected properly, a linear transformation on a correlated Gaussian process could yield an uncorrelated Gaussian process. The inverse approach is taken here, where now four uncorrelated Gaussian random variables are transformed by linear transformation to a multi-variant Gaussian random variable with a known covariance.

Following the derivation of Stark and Woods [61], if $\underline{Y} = \underline{D}\underline{X}$, where $\underline{X}$ is a correlated multi-variant Gaussian random variable and $\underline{Y}$ is an uncorrelated multi-variant Gaussian random variable, then

$$\underline{C}_Y = \underline{D}\underline{C}_X\underline{D}^T = \underline{I}, \tag{8.28}$$

where $\underline{I}$ is the identity matrix of order equal to the number of random variables, $\underline{C}_X$ is the covariance of the random variable $\underline{X}$, and $\underline{C}_Y$ is the covariance of the random variable $\underline{Y}$. Then $\underline{D} = \underline{Z}\underline{U}^T$, where

$$\underline{Z} = \underline{\Upsilon}^{-\frac{1}{2}} = \begin{bmatrix} \upsilon_{11}^{-\frac{1}{2}} & 0 & \cdots \\ 0 & \upsilon_{22}^{-\frac{1}{2}} & \vdots \\ \vdots & \cdots & \end{bmatrix}, \tag{8.29}$$

with $v_{ii}$ the eigenvalues of matrix $\underline{C}_X$, and $\underline{U}$ is the corresponding eigenvector matrix of $\underline{C}_X$.

This implies that

$$\underline{X} = \underline{D}^{-1}\underline{Y} \tag{8.30}$$

will transform uncorrelated random variables $\underline{Y}$ to correlated random variables $\underline{X}$ with covariance $\underline{C}_X$ and

$$\underline{C}_X = \underline{D}^{-1}\underline{C}_Y(\underline{D}^{-1})^T \tag{8.31}$$

$$\underline{C}_X = \underline{D}^{-1}\underline{I}(\underline{D}^{-1})^T, \tag{8.32}$$

where

$$\begin{aligned} \underline{D}^{-1} &= (\underline{Z}\underline{U}^T)^{-1} \\ &= (\underline{U}^T)^{-1}\underline{Z}^{-1} \\ &= \underline{U}\underline{Z}^{-1} \end{aligned} \tag{8.33}$$

since $\underline{U}$ is unitary ($\underline{U}^T = \underline{U}^{-1}$), and now

$$\underline{Z}^{-1} = \begin{bmatrix} \sqrt{v_{11}} & 0 & \cdots \\ 0 & \sqrt{v_{22}} & \vdots \\ \vdots & \cdots & \end{bmatrix}. \tag{8.34}$$

Then

$$(\underline{D}^{-1})^T = \underline{Z}^{-1}\underline{U}^T, \tag{8.35}$$

and

$$\underline{C}_X = (\underline{U}\underline{Z}^{-1})\underline{I}(\underline{Z}^{-1}\underline{U})^T. \tag{8.36}$$

This equation indicates that a linear transformation of $\underline{D}^{-1}$ applied to uncorrelated random variables $\underline{Y}$ will yield correlated random variables $\underline{X}$ with known covariance $\underline{C}_X$, if $\underline{D}$ is the matrix

$$\underline{D} = \begin{bmatrix} \sqrt{v_{11}} & 0 & \cdots \\ 0 & \sqrt{v_{22}} & \vdots \\ : & \cdots & \end{bmatrix} \underline{U}, \tag{8.37}$$

where $v_{ii}$ are the eigenvalues of $\underline{C}_X$, and $\underline{U}$ is the eigenvector matrix of $\underline{C}_X$.

Applying these results to the evaluation at hand implies that a linear transformation applied to four uncorrelated equal variance Gaussian random noise variables will yield four Gaussian random variables of known covariance, if the linear transformation is the inverse of the matrix product of the eigenvalues and eigenvectors of the covariance matrix. Since equation 8.27 delineates the desired covariance matrix, the necessary transformation can be obtained from the eigenvalues and eigenvectors.

A FORTRAN program was used to determine the eigenvalues and eigenvectors from each of the covariance matrices for the selected modulation indices. Then using a random Gaussian generator with a variance of 1, ($N_0 = 2.0$) the transformation matrices were determined. The tables that follow show the values of the covariance matrices and the transformation matrices.

| *Covariance Matrix* | | | |
|---|---|---|---|
| .5 | 0 | 0 | -.3183 |
| 0 | .5 | .3183 | 0 |
| 0 | .3183 | .5 | 0 |
| -.3183 | 0 | 0 | .5 |
| *Linear Transformation Matrix* | | | |
| -.0218 | .3010 | 0 | -.6388 |
| -.3010 | -.0219 | .6388 | 0 |
| .3010 | .0219 | .6388 | 0 |
| -.0219 | .3010 | 0 | .6388 |

Table 8.1: SSMH Modulation Index $\frac{1}{2}$ Transformation Matrices

The correlated noise samples, $N1C$, $N1S$, $N2C$, and $N2S$ can now be added to the noisefree signal outputs of the correlation filters to produce noise corrupted correlation metrics. The next section addresses the calculation of the chip metrics to produce bit metrics and the subsequent decision making process.

| *Covariance Matrix* | | | |
|---|---|---|---|
| .5 | 0 | -.0900 | -.2174 |
| 0 | .5 | .2174 | -.0900 |
| -.0900 | .2174 | .5 | 0 |
| -.2174 | -.0900 | 0 | .5 |
| *Linear Transformation Matrix* | | | |
| .1392 | .3361 | -.2320 | -.5602 |
| -.3361 | .1392 | .5602 | -.2320 |
| .3638 | 0 | .6063 | 0 |
| 0 | .3638 | 0 | .6063 |

Table 8.2: SSMH Modulation Index $\frac{5}{8}$ Transformation Matrices

| *Covariance Matrix* | | | |
|---|---|---|---|
| .5 | 0 | -.1061 | -.1061 |
| 0 | .5 | .1061 | -.1061 |
| -.1061 | .1061 | .5 | 0 |
| -.1061 | -.1061 | 0 | .5 |
| *Linear Transformation Matrix* | | | |
| .2958 | .2958 | -.4031 | -.4031 |
| -.2958 | .2958 | .4031 | -.4031 |
| .4183 | 0 | .5701 | 0 |
| 0 | .4183 | 0 | .5701 |

Table 8.3: SSMH Modulation Index $\frac{3}{4}$ Transformation Matrices

## 8.3 Metric Calculations

With the noise corrupted outputs of the correlation filters, the chip metrics can be calculated from equation 8.3 and must be accomplished for each possible phase state. Hence,

$$\lambda(\alpha_i = +1, c_{ij}, \theta_{ij}) = \int_0^{T_c} r(t)\cos(2\pi f_0 t + \frac{\pi c_{ij} h_{ij} t}{T_c} + \theta_{ij})dt, \quad (8.38)$$

$$\lambda(\alpha_i = -1, c_{ij}, \theta_{ij}) = \int_0^{T_c} r(t)\cos(2\pi f_0 t - \frac{\pi c_{ij} h_{ij} t}{T_c} + \theta_{ij})dt. \quad (8.39)$$

A phase rotation network accomplishes this calculation for each state, $\theta_{ij}$.

The overall bit metrics from equation 6.5 are just the sum of the chip metrics over a bit interval. This summation is accomplished by performing the chip metric calculations during each chip interval and adding the appropriate metric to the partial sum metric from the previous interval. This process requires determining the next phase state for the given modulation index, chip and bit values. The partial sum metrics, $\lambda^+_{\theta_{ij}}$ and $\lambda^-_{\theta_{ij}}$, for each next state can be found by adding the chip metrics to the partial sum metrics of the previous beginning state. After $N_c$ chips, the bit metrics are determined at each phase state as the metric sums $\sum_{j=0}^{N_c-1} \lambda_j^+$ and $\sum_{j=0}^{N_c-1} \lambda_j^-$. The phase transitions from bit beginning phase to bit ending phase are calculated knowing the chip sequence.

The random input data is generated by a uniform random number generator and each chip value is randomly generated by a uniform and independent random number generator. Since the receiver is assumed to know the chip sequence along with the transmitter, these values are maintained throughout the bit interval.

## 8.4 Evaluation Implementation and Results

Using the bit metrics as determined in the previous section, a Viterbi Algorithm processor makes a bit decision after a delay of $N_D$ bits. The algorithm was implemented using the state traceback method in FORTRAN to make a majority logic decision after observation over the predetermined bit delay. This delay was selected to exceed the minimum distance for optimal performance from Chapter 7 for the modulation indices in use.

An overview diagram of the evaluation receiver is shown below in Figure 8.1.

The figures that follow show the evaluation receiver bit error rate performance and

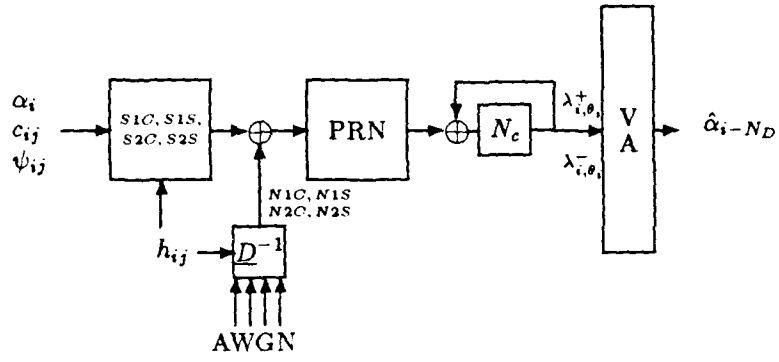


Figure 8.1: Evaluation Receiver

the analytically determined performance bound for the indicated modulation criteria. It should be noted that the degenerate case of one chip per bit was used to verify the validity of the evaluation routine. The results agreed completely with those of Hsu [30] and Anderson [1]. The curves reflect 90% confidence intervals on the observed data that were obtained using the weak law of large numbers; and depict the exact bit error performance of DS/BPSK as a baseline comparison. As mentioned previously in Chapter 7, evaluations for 127 chips per bit are shown without bounds. Additionally, isolated samples for 1023 chips per bit are shown with the evaluations for 127 chips per bit. Only selected values of these evaluations are available due to the extended amount of processing time required. A value of five decibels in signal-to-noise ratio was selected as a reasonable received value and the results are consistent with results obtained for lower values of chips per bit.

| *Modulation Indices* | *Spreading Rate* | *Figure* |
|---|---|---|
| Conventional | | |
| .5, .75 | 3 | 8.2 |
| .5, .625 | 3 | 8.3 |
| .5, .75 | 7 | 8.4 |
| .5, .625 | 7 | 8.5 |
| .5, .75 | 127 | 8.6 |
| .5, .625 | 127 | 8.7 |
| Modified | | |
| .5, .75 | 3 | 8.8 |
| .5, .625 | 3 | 8.9 |
| .5, .75 | 7 | 8.10 |
| .5, .625 | 7 | 8.11 |
| .5, .75 | 127 | 8.12 |
| .5, .625 | 127 | 8.13 |

Table 8.4: Spread Spectrum Multi-$h$ Evaluations

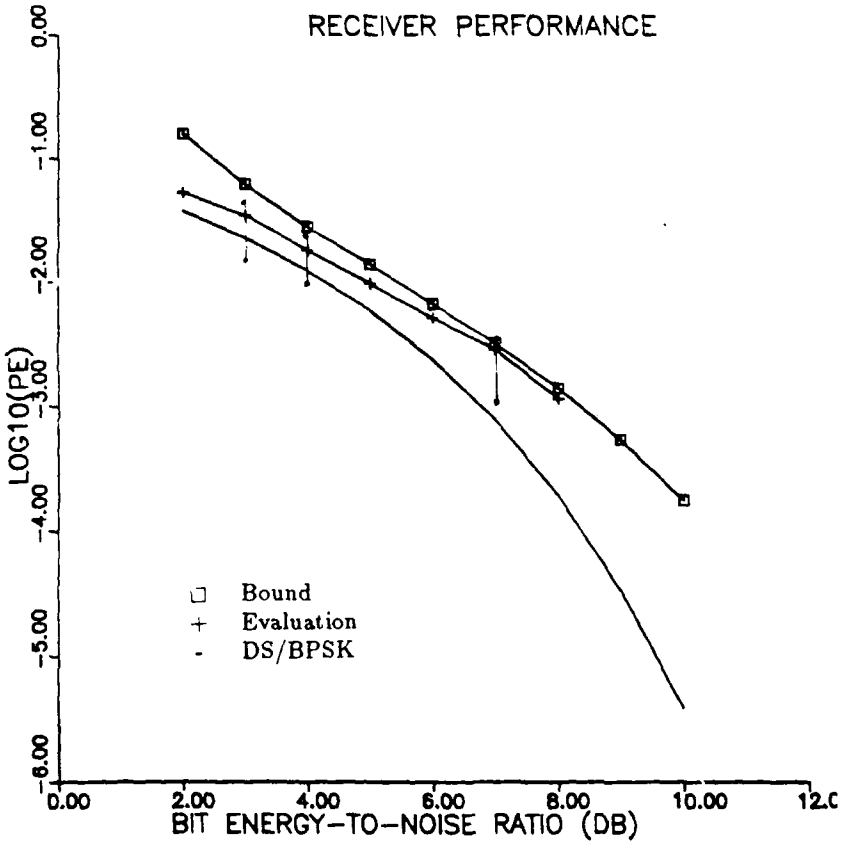


Figure 8.2: Conventional $\frac{1}{2}$, $\frac{3}{4}$ SSMH Code; $N_c = 3$ Evaluation

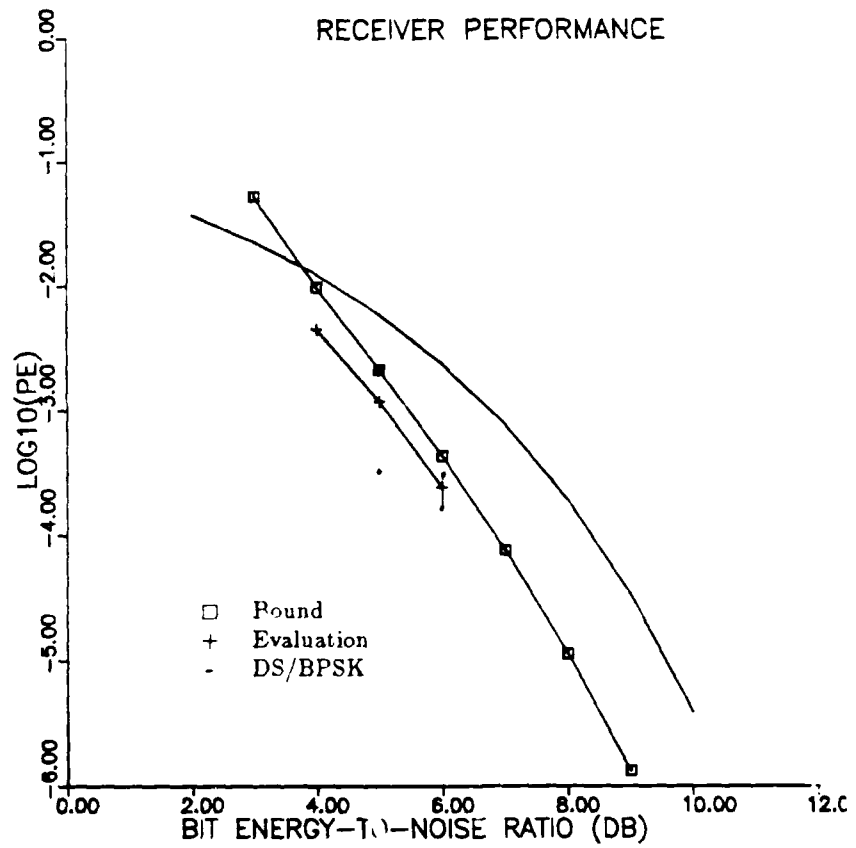


Figure 8.3: Conventional $\frac{1}{2}$, $\frac{5}{8}$ SSMH Code; $N_c = 3$ Evaluation

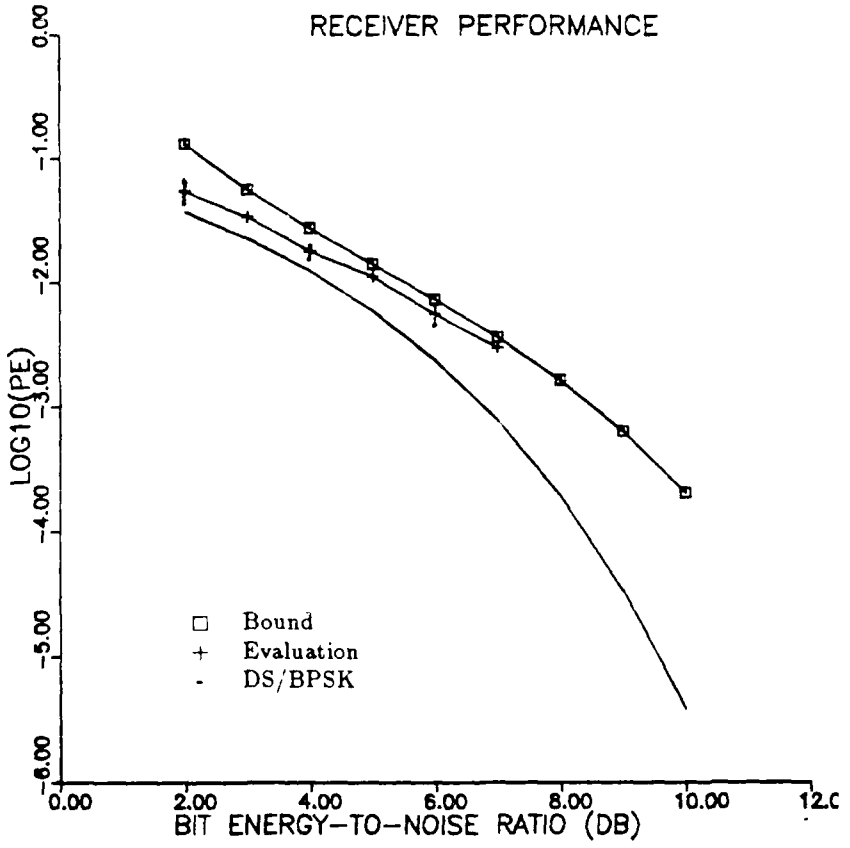


Figure 8.4: Conventional $\frac{1}{2}$, $\frac{3}{4}$ SSMH Code; $N_c = 7$ Evaluation

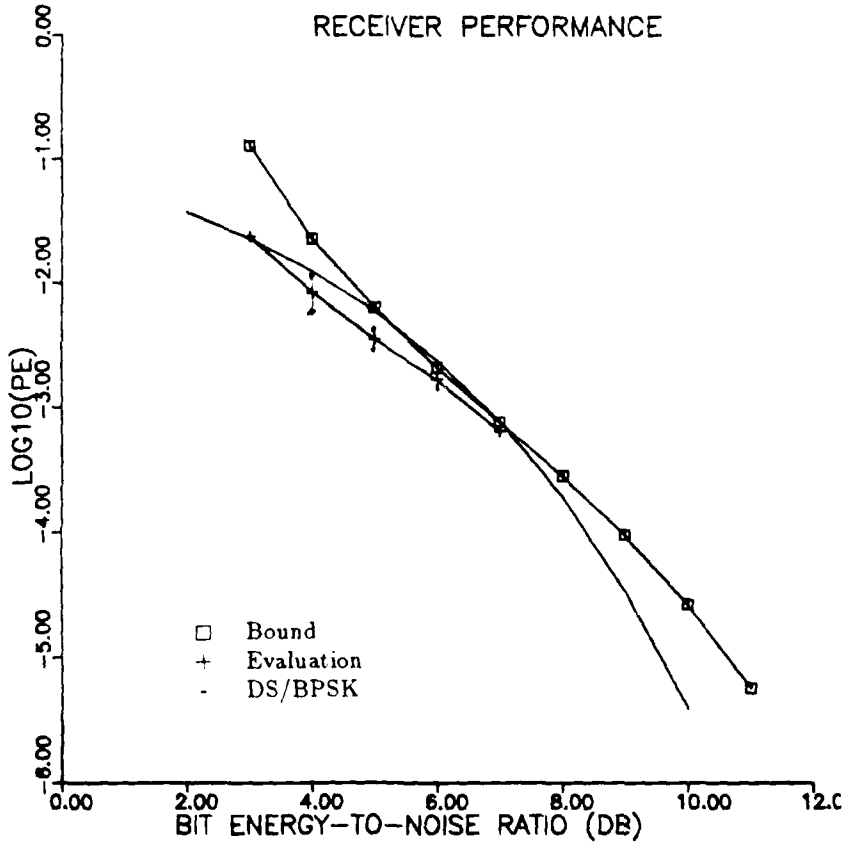


Figure 8.5: Conventional $\frac{1}{2}$, $\frac{5}{8}$ SSMH Code; $N_c = 7$ Evaluation

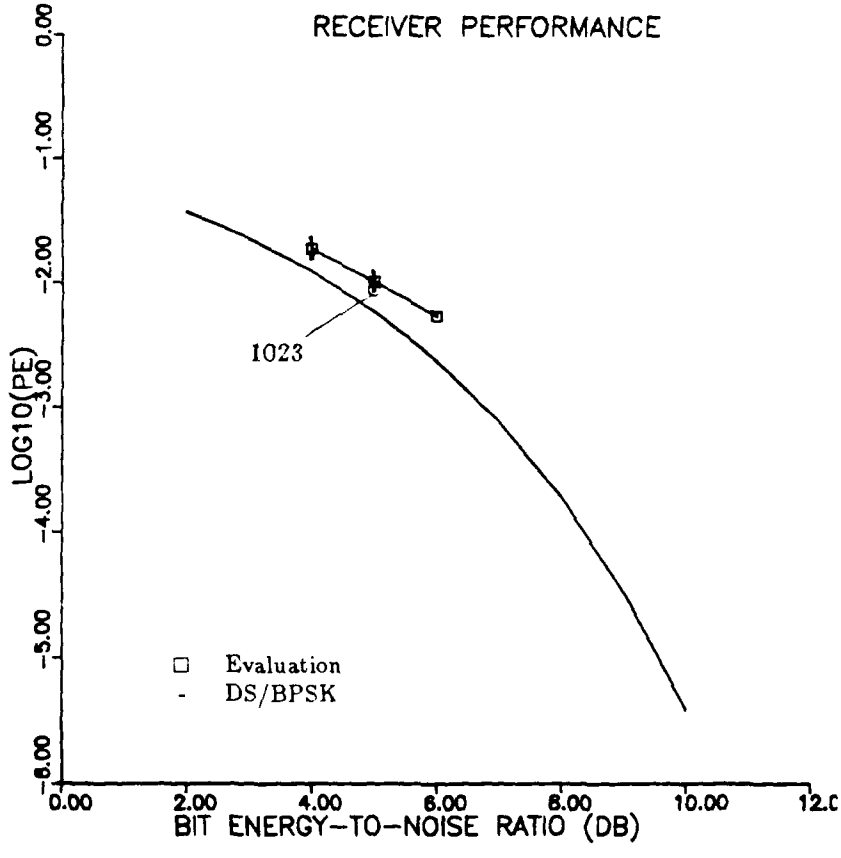


Figure 8.6: Conventional $\frac{1}{2}$, $\frac{3}{4}$ SSMH Code; $N_c = 127$ Evaluation

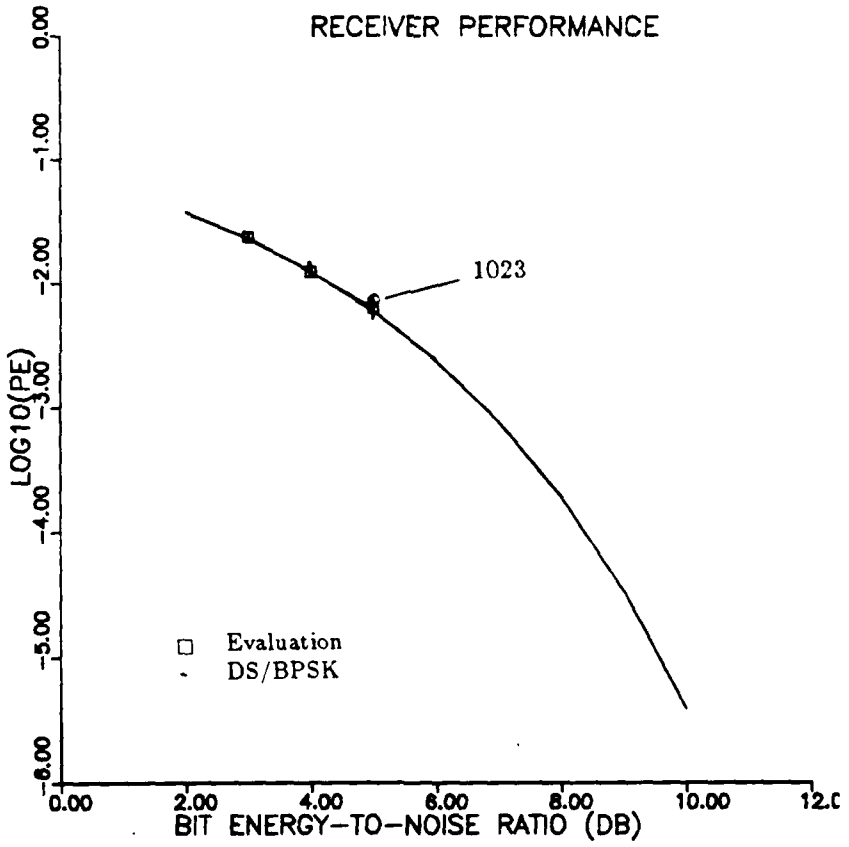


Figure 8.7: Conventional $\frac{1}{2}$, $\frac{5}{8}$ SSMH Code; $N_c = 127$ Evaluation

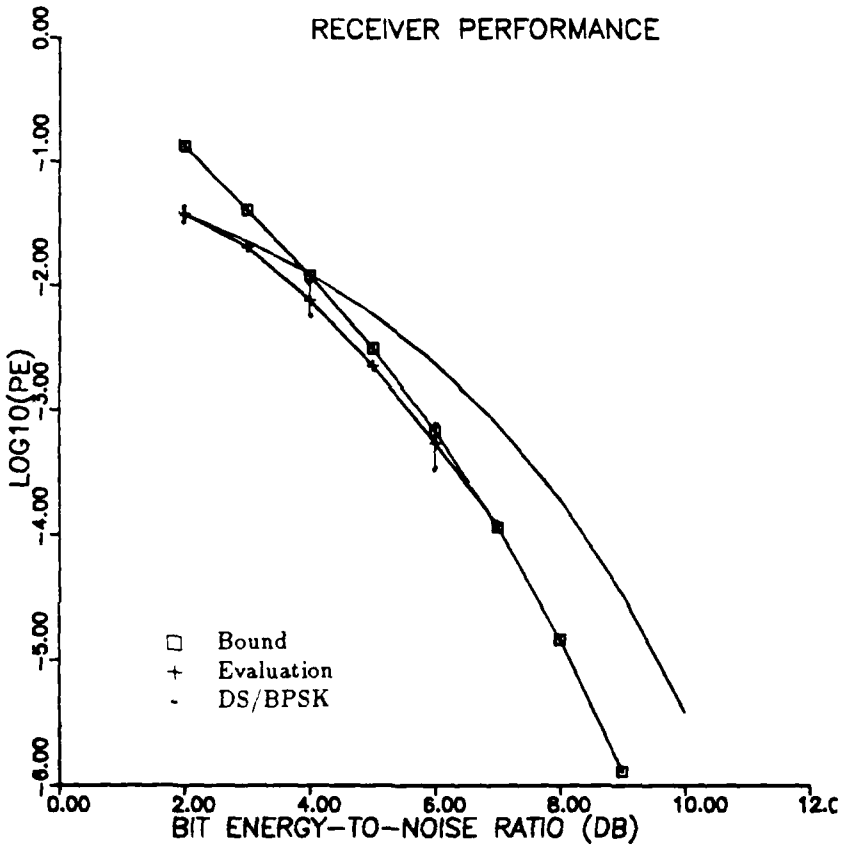


Figure 8.8: Modified $\frac{1}{2}$, $\frac{3}{4}$ SSMH Code; $N_c = 3$ Evaluation

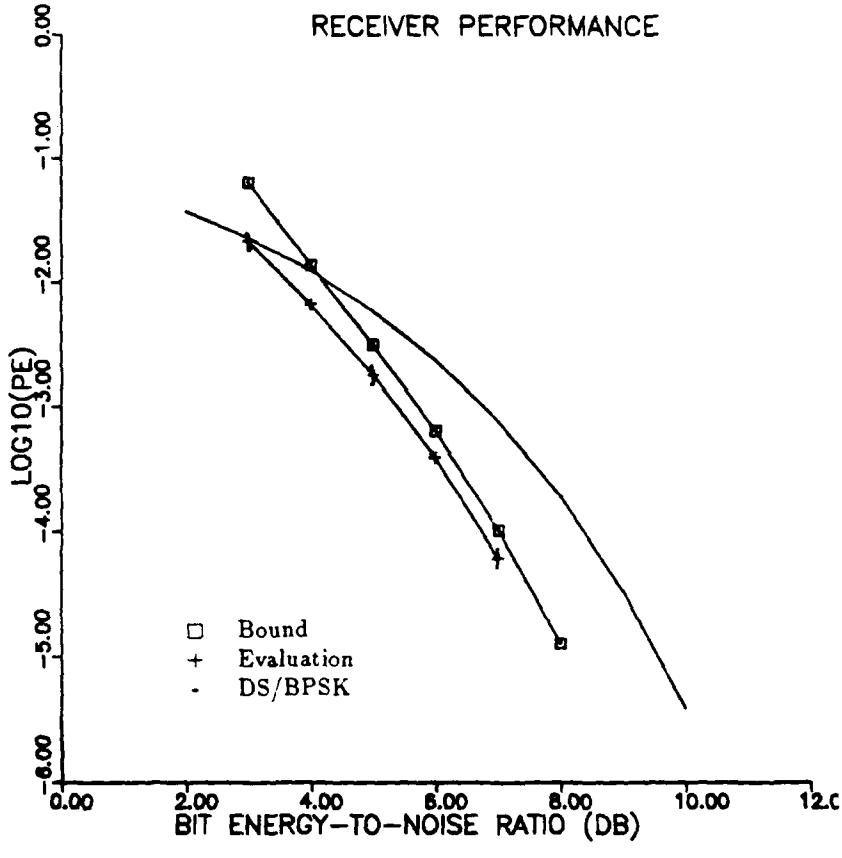


Figure 8.9: Modified $\frac{1}{2}$, $\frac{5}{8}$ SSMH Code; $N_c = 3$ Evaluation

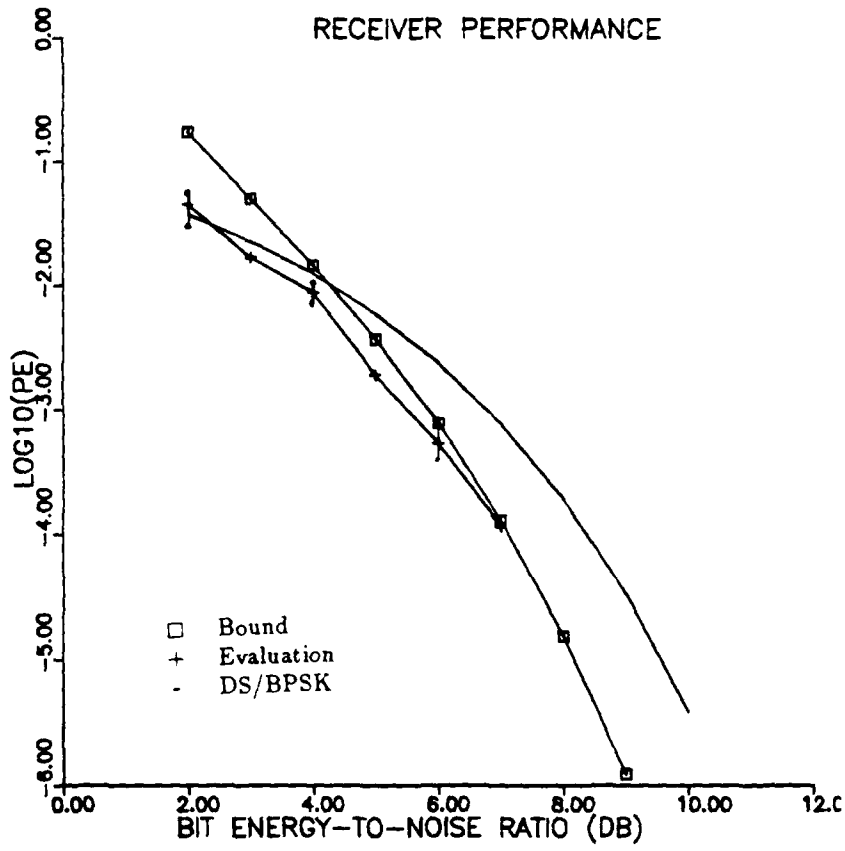


Figure 8.10: Modified $\frac{1}{2}$, $\frac{3}{4}$ SSMH Code; $N_c = 7$ Evaluation

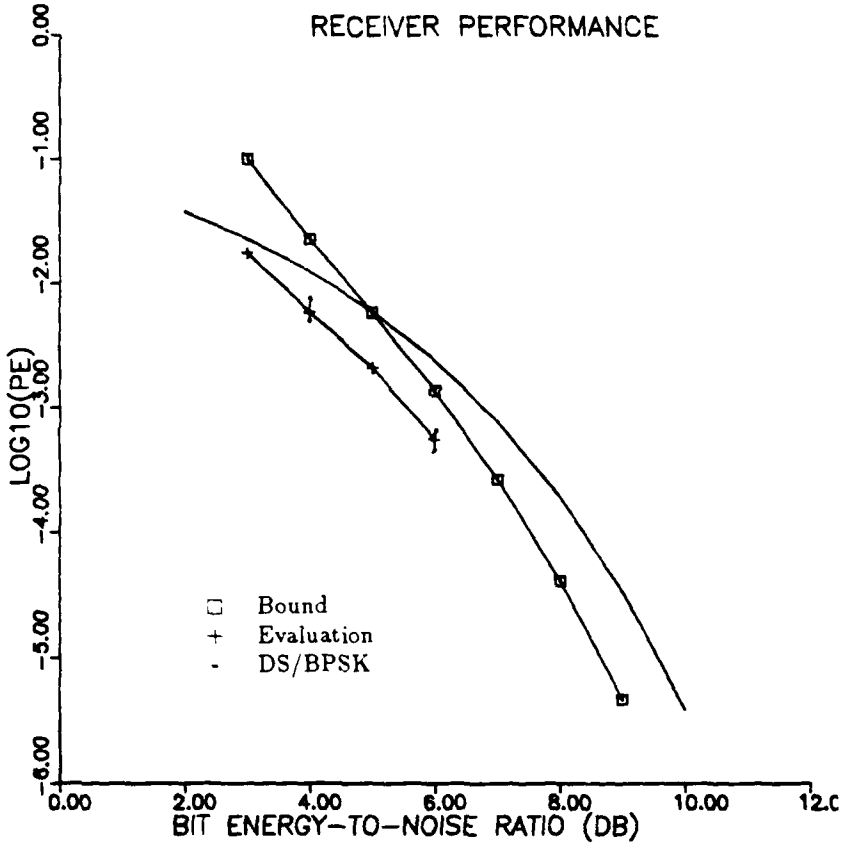


Figure 8.11: Modified $\frac{1}{2}, \frac{5}{8}$ SSMH Code; $N_c = 7$ Evaluation

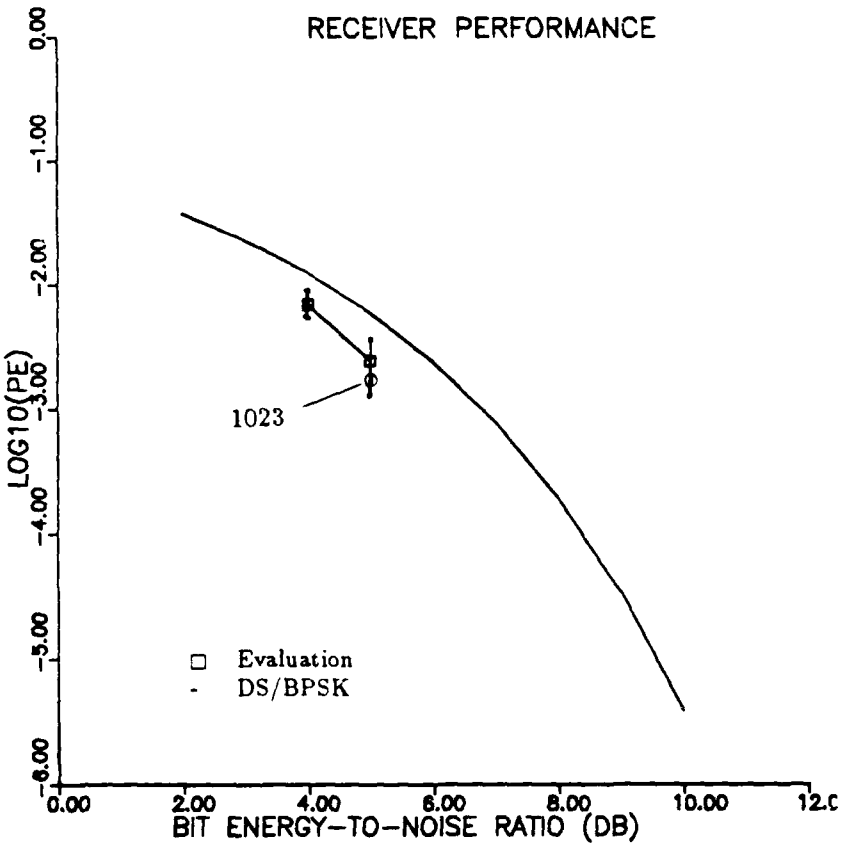


Figure 8.12: Modified $\frac{1}{2}$, $\frac{3}{4}$ SSMH Code; $N_c = 127$ Evaluation

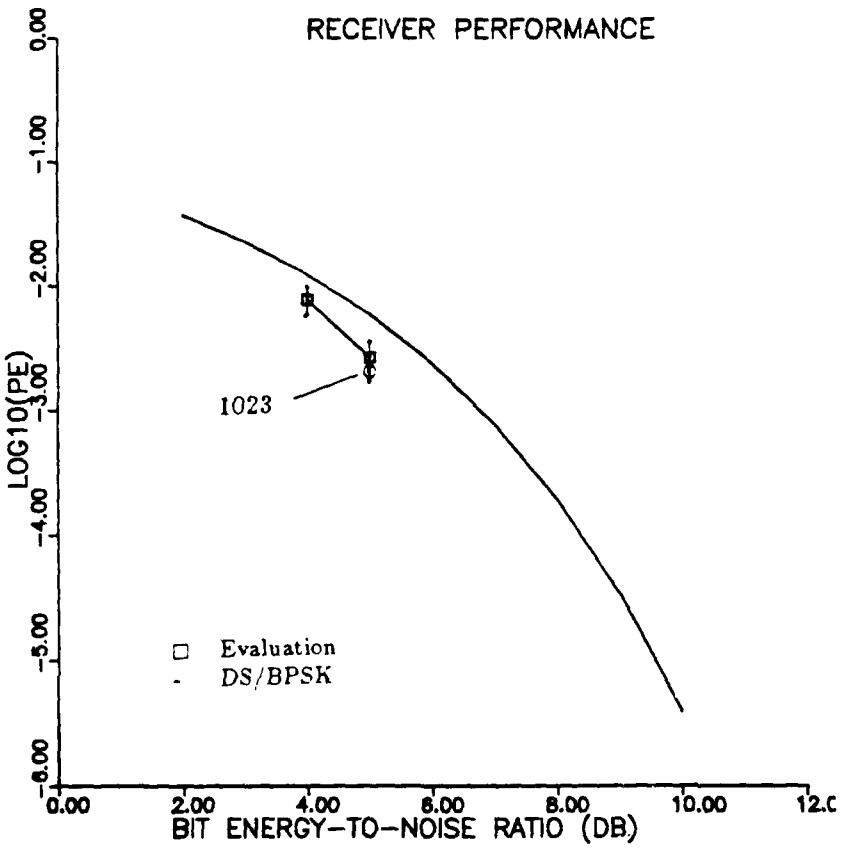


Figure 8.13: Modified $\frac{1}{2}$, $\frac{5}{8}$ SSMH Code; $N_c = 127$ Evaluation

In order to verify the decoding depth for the Viterbi Algorithm obtained from the difference state diagrams in Chapter 7, a modulation code was selected at random from those being discussed in this work and the probability of bit error versus decoding depth for a fixed signal-to-noise ratio was evaluated via the receiver evaluations. Figure 8.14 shows that in fact the minimum distance bound depth as reflected in Table 7.3 is a valid optimal decoding delay. The difference state diagrams for the .5, .75 modified modulation scheme indicated a minimum distance of 3 bits. The evaluations verify that performance does begin to degrade for a decision delay less than three bits.

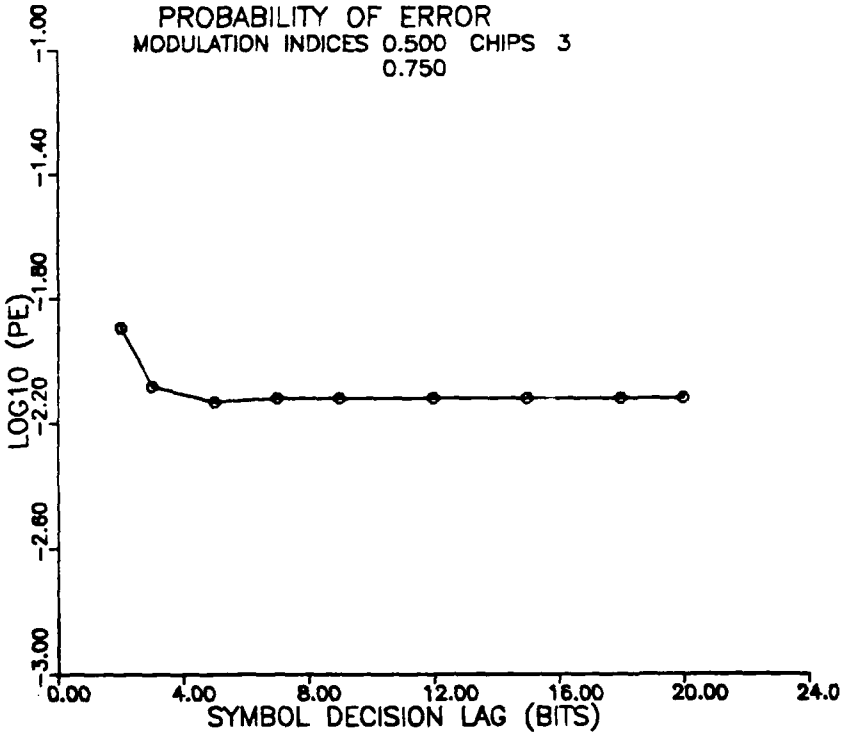


Figure 8.14: Conventional $\frac{1}{2}$, $\frac{3}{4}$ SSMH Error Performance Versus Decoding Delay

Up to this point, this work has defined SSMH signals, derived the transmitted spectrum, and investigated the receiver designed to receive and decode the information sequence. In the next chapter, we turn to examination of the purpose behind the signaling

scheme; that is, the detectability by intended and unintended receivers will be investigated.

# CHAPTER 9

# SSMH Signal Detectability

The previous chapters have considered the issues of signal definition and transmission characteristics, as well as detection by an intended receiver under nearly ideal conditions. Since the purpose of the signaling scheme was to create a signal structure with a low probability of intercept, it is appropriate to address the issue of detectability by an unintended as well as intended receiver. In order to perform this analysis, the 'best possible' assumptions will be made for an unintended receiver leading to upper bounds on reception capabilities. The Neyman-Pearson generalized likelihood ratio test will be used to derive probability of detection and probability of false alarm expressions leading to delineation of receiver operating characteristics. It is shown that even under the best possible conditions, an unintended receiver could not attain sufficient detection reliability to make positive detection possible.

## 9.1 Receiver Operating Characteristics

The detectability of SSMH signals in an AWGN environment is considered in this section where the unintended receiver must make a signal/no signal detection decision based on two hypothesis

$$H1: \quad r(t) = s(t) + n(t), \tag{9.1}$$

$$H0: \quad r(t) = n(t). \tag{9.2}$$

It should be apparent that the longer the observation interval the better the detectability would be; however, so that comparisons can be made with DS/BPSK, it will

be assumed that the observation interval is exactly a bit interval.

In addition, the following assumptions will be made concerning the unintended receiver. In order to obtain 'best possible' capability, it will be assumed that the receiver knows everything about the transmitted signal except the information bits and the spreading code sequence. This implies complete knowledge of

- Modulation index code and timing
- Pulse shaping function
- Bit and chip interval timing
- Carrier frequency and phase

These factors are in increasing order of likelihood that the receiver has complete knowledge. Assuming that the unintended party is willing to commit unlimited resources, it is reasonable to assume that the carrier and chip and bit timing could be obtained by spectral analysis (See Chapter 5). On the other hand, it is extremely unlikely that the receiver will have knowledge of the modulation parameters, but for this analysis every benefit is given so that an upper bound is attained.

For the signals in AWGN, the generalized likelihood decision statistic becomes [49,67]

$$\Lambda = \frac{\frac{1}{\sqrt{\pi N_0}} \exp\{-\frac{1}{N_0}\int_0^{T_b}(r(t)-s(t))^2 dt\}}{\frac{1}{\sqrt{\pi N_0}} \exp\{-\frac{1}{N_0}\int_0^{T_b} r^2(t) dt\}} \underset{<}{\overset{>}{}} \eta. \tag{9.3}$$

Expressing the integrals over a bit interval in terms of the summation of chip intervals, and assuming minimum probability of error detection costs, yields

$$\Lambda = \frac{\exp\{\sum_{j=0}^{N_c-1} -\frac{1}{N_0}\int_0^{T_c}[r^2(t-jT_c) - 2r(t-jT_c)s(t-jT_c) + s^2(t-jT_c)]dt\}}{\exp\{\sum_{j=0}^{N_c-1} -\frac{1}{N_0}\int_0^{T_c} r^2(t-jT_c)dt\}} \underset{<}{\overset{>}{}} 1, \tag{9.4}$$

which reduces to

$$\exp\{\sum_{j=0}^{N_c-1}\frac{1}{N_0}\int_0^{T_c}[2r(t-jT_c)s(t-jT_c) - s^2(t-jT_c)]dt\} \underset{<}{\overset{>}{}} 1. \tag{9.5}$$

Converting the exponential of a sum to the product of exponentials and replacing the bit energy term yields

$$\prod_{j=0}^{N_c-1}\exp\{\frac{2}{N_0}\int_0^{T_c} r(t-jT_c)s(t-jT_c)dt\} \underset{<}{\overset{>}{}} \exp\{\frac{E_b}{N_0}\}. \tag{9.6}$$

At this point, it is assumed that the receiver has complete signal knowledge except for the information bits and the spreading sequence, such that

$$s(t - jT_c) = \sqrt{\frac{2E_c}{T_c}} \cos(2\pi f_0(t - jT_c) + \frac{\pi h_{ij}\alpha_i c_{ij}(t - jT_c)}{T_c}). \tag{9.7}$$

The receiver must also assume a spread spectrum signal and binary signaling such that the distribution for the product of $\alpha_i c_{ij}$ is as before, $f_{\alpha c} = \frac{1}{2}\delta(\alpha c - 1) + \frac{1}{2}\delta(\alpha c + 1)$. As a result, the expected value of the likelihood ratio becomes

$$\mathcal{E}_{\alpha c}\Lambda = \mathcal{E}_{\alpha c}\{\prod_{j=0}^{N_c-1} e^{\frac{2}{N_0}\sqrt{\frac{2E_c}{T_c}}\int_0^{T_c} r(t-jT_c)\cos(2\pi f_0(t-jT_c)+\frac{\pi h_{ij}\alpha_i c_{ij}(t-jT_c)}{T_c})dt}\} \gtrless e^{\frac{E_b}{N_0}}. \tag{9.8}$$

After applying the expectation, expanding the trigonometric functions, and combining terms

$$\mathcal{E}\Lambda = \prod_{j=0}^{N_c-1} \frac{1}{2}e^{L_{cj}+L_{sj}} + \frac{1}{2}e^{L_{cj}-L_{sj}} \gtrless e^{\frac{E_b}{N_0}}, \tag{9.9}$$

where over a given bit and chip interval

$$\begin{aligned} L_{cj} &= \frac{2}{N_0}\sqrt{\frac{2E_c}{T_c}}\int_0^{T_c} r(t)\cos(2\pi f_0 t)\cos(\frac{\pi h_j t}{T_c})dt, \\ L_{sj} &= \frac{2}{N_0}\sqrt{\frac{2E_c}{T_c}}\int_0^{T_c} r(t)\sin(2\pi f_0 t)\sin(\frac{\pi h_j t}{T_c})dt, \end{aligned} \tag{9.10}$$

and therefore,

$$\mathcal{E}\Lambda = \prod_{j=0}^{N_c-1} e^{L_{cj}}\cosh(L_{sj}) \gtrless e^{\frac{E_b}{N_0}}. \tag{9.11}$$

After taking the logarithm, the log-likelihood ratio becomes

$$\ln\Lambda = \sum_{j=0}^{N_c-1} L_{cj} + \ln[\cosh(L_{sj})] \gtrless \frac{E_b}{N_0}. \tag{9.12}$$

If $N_c$ is large, which is typically the case, the probability distribution of the left side of equation 9.12 will approach a Gaussian distribution by the Central Limit Theorem. The mean value would be

$$\mu = \sum_{j=1}^{N_c} \mu_j, \tag{9.13}$$

where

$$\mu_j = \mathcal{E}\{L_{cj} + \ln[\cosh(L_{sj})]\}. \tag{9.14}$$

Similarly, the variance would be

$$\sigma^2 = \sum_{j=1}^{N_c} \sigma_j^2, \tag{9.15}$$

where

$$\sigma_j^2 = \mathcal{E}\{(L_{cj} + \ln[\cosh(L_{sj})])^2\} - \mu_j^2. \tag{9.16}$$

With this background, consideration can be given to determining the probability of false alarm and probability of detection.

The probability of false alarm is the probability of selecting hypothesis one, signal present, when in fact no signal is present. Thus

$$P_F = \int_\gamma^\infty g(n)dn, \tag{9.17}$$

where $g(n)$ is the distribution of the decision ratio when no signal is present, and $\gamma$ is the decision threshold, $\gamma = E_b/N_0$. As mentioned above, $g(n)$ will have a Gaussian distribution with statistics

$$\mu_g = N_c \mu_{gj}, \tag{9.18}$$

$$\sigma_g^2 = N_c \sigma_{gj}^2. \tag{9.19}$$

The mean values on the chip intervals are evaluated from equation 9.14 when no signal is present. Under no signal conditions, the expected values of both $L_{cj}$ and $L_{sj}$ are zero, then by definition

$$\mu_{gj} = \mathcal{E}\{\ln[\cosh(L_{sj})]\}, \tag{9.20}$$

$$\mu_{gj} = \int_{-\infty}^{\infty} \ln\cosh(L_{sj}) f_{L_{sj}}(L_{sj}) dL_{sj}, \tag{9.21}$$

where $L_{sj} \sim N(0, \sigma_{L_{sj}}^2)$. Since $\mathcal{E}\{L_{sj}\} = 0$, the value of $\sigma_{L_{sj}}^2$ can be determined from the second order statistic of $L_{sj}$ (no signal case) with the results

$$\mathcal{E}\{L_{sj}^2\} = \frac{E_c}{N_0}\left(1 - \frac{\sin(2\pi h_j)}{2\pi h_j}\right), \tag{9.22}$$

$$\sigma_{L_{sj}}^2 = \frac{E_c}{N_0}\left(1 - \frac{\sin(2\pi h_j)}{2\pi h_j}\right). \tag{9.23}$$

Therefore, since $L_{sj}$ is normally distributed, and after a change of variables, the chip interval mean value is found from

$$\mu_{gj} = \frac{2}{\sqrt{2\pi}} \int_0^\infty \ln[\cosh(\sigma_{L_{sj}} y)] e^{-\frac{y^2}{2}} dy. \tag{9.24}$$

In order to find the the variance of $g(n)$, a similar argument is followed after defining $Z = L_{cj} + \ln[\cosh(L_{sj})]$. Then

$$\mathcal{E}\{Z^2\} = \mathcal{E}\{L_{cj}^2\} + \mathcal{E}\{\ln^2[\cosh(L_{sj})]\}, \tag{9.25}$$

where by following a procedure exactly as above

$$\mathcal{E}\{L_{cj}^2\} = \sigma_{L_{cj}}^2 = \frac{E_c}{N_0}(1 + \frac{\sin(2\pi h_j)}{2\pi h_j}). \tag{9.26}$$

Using these values gives the desired results after expansion to be

$$\sigma_{gj}^2 = \mathcal{E}\{Z^2\} - \mu_{gj}^2, \tag{9.27}$$

$$\sigma_{gj}^2 = \frac{E_c}{N_0}(1 + \frac{\sin(2\pi h_j)}{2\pi h_j}) + \frac{2}{\sqrt{2\pi}}\int_0^\infty \ln^2[\cosh(\sigma_{L_{sj}} y)]e^{-\frac{y^2}{2}}dy - \tag{9.28}$$

$$\frac{2}{\pi}[\int_0^\infty \ln[\cosh(\sigma_{L_{sj}} y)]e^{-\frac{y^2}{2}}dy]^2. \tag{9.29}$$

The probability of false alarm can now be obtained from equation 9.17 since $g(n)$ is now known to be Gaussian with mean $\mu_g$ and variance $\sigma_g^2$. To accomplish the sum of chip interval values and account for the changing modulation indices, these expressions become

$$\mu_g = \frac{N_c}{2}\mu_{gj|h_1} + \frac{N_c}{2}\mu_{gj|h_2}, \tag{9.30}$$

$$\sigma_g^2 = \frac{N_c}{2}\sigma_{gj|h_1}^2 + \frac{N_c}{2}\sigma_{gj|h_2}^2, \tag{9.31}$$

and

$$P_F = \int_{\frac{E_b}{N_0}}^\infty \frac{1}{\sqrt{2\pi}\ \sigma_g} e^{-\frac{(n-\mu_g)^2}{2\sigma_g^2}} dn. \tag{9.32}$$

A similar analysis is applied to finding the probability of detection, $P_D$, where now the likelihood ratio is considered under hypothesis $H1$ and there is a signal present. Thus

$$P_D = \int_{\frac{E_b}{N_0}}^\infty N(\mu_s, \sigma_s^2)dn, \tag{9.33}$$

where $\mu_s$ is the mean value sum of $\mu_{sj}$'s, which are calculated from equation 9.10, but now considering the presence of the transmitted signal. Similarly, $\sigma_s^2$ is obtained from the second order statistics with the signal present.

The results of these calculations for both hypothesis are summarized below for information and convenience in determining the receiver operating characteristics. Hence,

$$
\begin{aligned}
\mu_{H0} &= \frac{N_c}{2}\mu_{gj|h_1} + \frac{N_c}{2}\mu_{gj|h_2} \\
\sigma^2_{H0} &= \frac{N_c}{2}\sigma^2_{gj|h_1} + \frac{N_c}{2}\sigma^2_{gj|h_2} \\
\mu_{gj} &= \frac{2}{\sqrt{2\pi}}\int_0^\infty \ln[\cosh(\sigma_{L_{s,j}} y)]e^{-\frac{y^2}{2}}dy \\
\sigma^2_{L_{sj}} &= \frac{E_c}{N_0}(1 - \frac{\sin(2\pi h_j)}{2\pi h_j}) \\
\sigma^2_{L_{cj}} &= \frac{E_c}{N_0}(1 + \frac{\sin(2\pi h_j)}{2\pi h_j}) \\
\sigma^2_{gj} &= \frac{E_c}{N_0}(1 + \frac{\sin(2\pi h_j)}{2\pi h_j}) + \frac{2}{\sqrt{2\pi}}\int_0^\infty \ln^2[\cosh(\sigma_{L_{s,j}} y)]e^{-\frac{y^2}{2}}dy - \\
&\quad \frac{2}{\pi}[\int_0^\infty \ln[\cosh(\sigma_{L_{s,j}} y)]e^{-\frac{y^2}{2}}dy]^2
\end{aligned}
\tag{9.34}
$$

and

$$
\begin{aligned}
\mu_{H1} &= \frac{N_c}{2}\mu_{sj|h_1} + \frac{N_c}{2}\mu_{sj|h_2} \\
\sigma^2_{H1} &= \frac{N_c}{2}\sigma^2_{sj|h_1} + \frac{N_c}{2}\sigma^2_{sj|h_2} \\
\mu_{sj} &= \frac{E_c}{N_0}(1 + \frac{\sin(2\pi h_j)}{2\pi h_j}) + \frac{2}{\sqrt{2\pi}}\int_0^\infty \ln[\cosh(\sigma_{L_{s,j}} y)]e^{-\frac{y^2}{2}}dy \\
\sigma^2_{sj} &= \frac{E_c}{N_0}(1 + \frac{\sin(2\pi h_j)}{2\pi h_j}) + \frac{2}{\sqrt{2\pi}}\int_0^\infty \ln^2[\cosh(\sigma_{L_{s,j}} y)]e^{-\frac{y^2}{2}}dy - \\
&\quad \frac{2}{\pi}[\int_0^\infty \ln[\cosh(\sigma_{L_{s,j}} y)]e^{-\frac{y^2}{2}}dy]^2.
\end{aligned}
\tag{9.35}
$$

As indicated above, these expressions form the foundation for calculation of probability of detection and probability of false alarm. However, as shown by Polydoros [67], the two probabilities are interrelated and a simpler expression can be formed to determine the probability of detection for a given false alarm rate. Polydoros and Weber [48,67] showed that

$$
P_D = Q\left[\frac{\sigma_{H0}Q^{-1}(P_{FA}) + \mu_{H0} - \mu_{H1}}{\sigma_{H1}}\right]. \tag{9.36}
$$

This equation can now be used along with the means and variances from equation 9.34 to determine the probability of detection for any given value of false alarm. At the same time the receiver operating characteristics, or the expression of probability of detection versus probability of false alarm, can be shown. The following section shows the results of this investigation.

## 9.2 Detectability Results

Equations 9.36 and 9.34 were implemented numerically in FORTRAN code to determine the probabilities of detection and false alarm for selected SSMH signaling schemes. The probability of detection was calculated for the selected modulation coding and for various values of false alarm rate. This netted the probability of detection curves that follow. At the same time, the receiver operating characteristics can be shown as the plots of $P_D$ versus $P_{FA}$. Table 9.1 below lists the results for the probability of detection and Table 9.2 lists the results for the receiver operating characteristics with the chip energy-to-noise ratios equal to -20, -30, and -40 decibels. For comparison purposes the probability of detection curves are plotted for a consistent value of $P_F = .01$, and for $N_c = 7$ or 15, 127, 1023. It should also be noted that receiver operating curves for modified SSMH reflect the operation over two bit intervals to account for both modulation indices and $N_c = 1000$ chips per bit.

| *Modulation Scheme* | *Figure* |
|---|---|
| Conventional | |
| .5, .75 | 9.1 |
| .5, .625 | 9.2 |
| Modified | |
| .5, .75 | 9.3 |
| .5, .625 | 9.4 |

Table 9.1: Detection Probability Curves

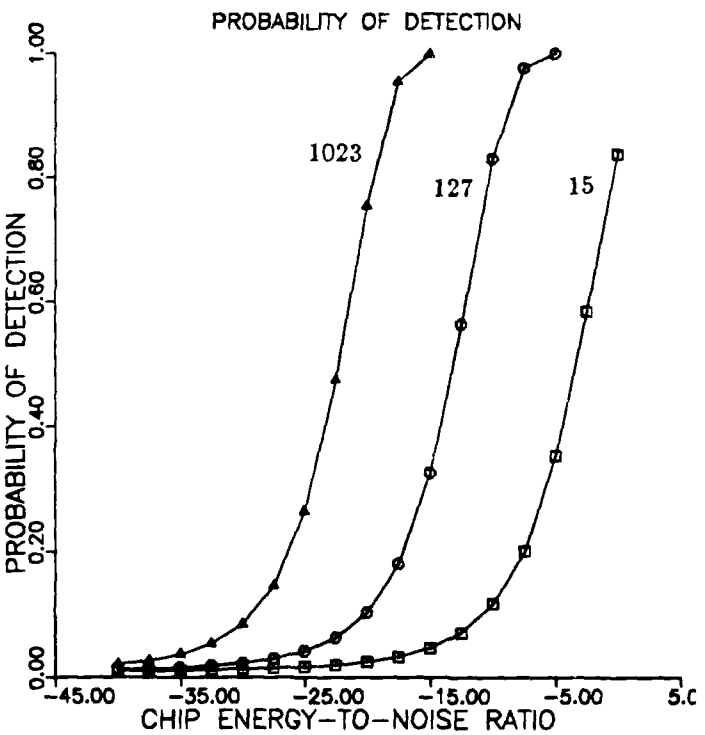


Figure 9.1: Conventional $\frac{1}{2}$, $\frac{3}{4}$ Code SSMH Detectability

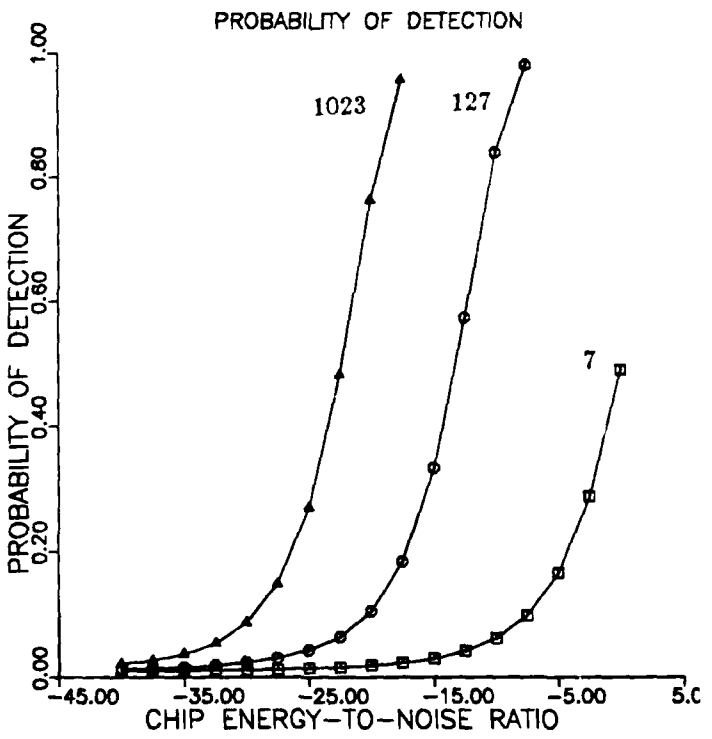


Figure 9.2: Conventional $\frac{1}{2}$, $\frac{5}{8}$ Code SSMH Detectability

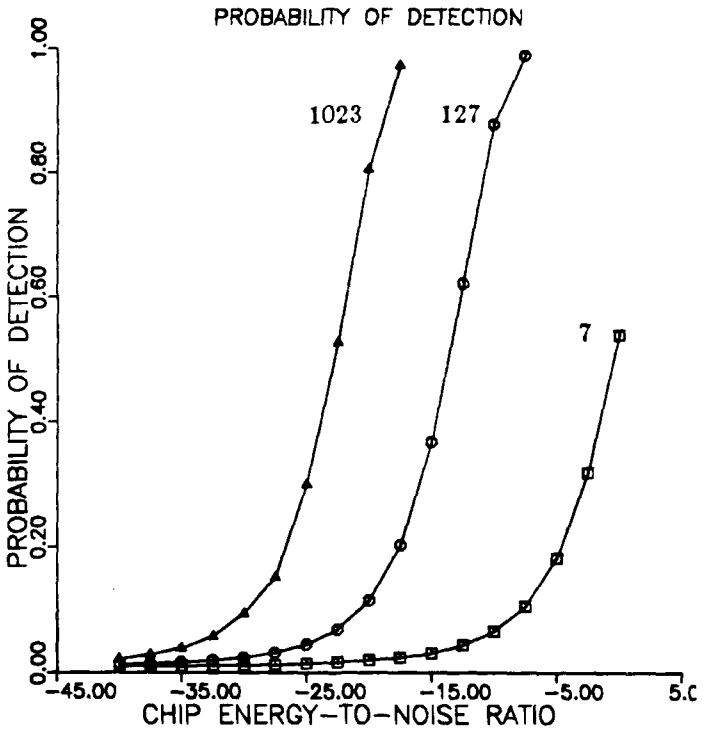


Figure 9.3: Modified $\frac{1}{2}$, $\frac{3}{4}$ Code SSMH Detectability

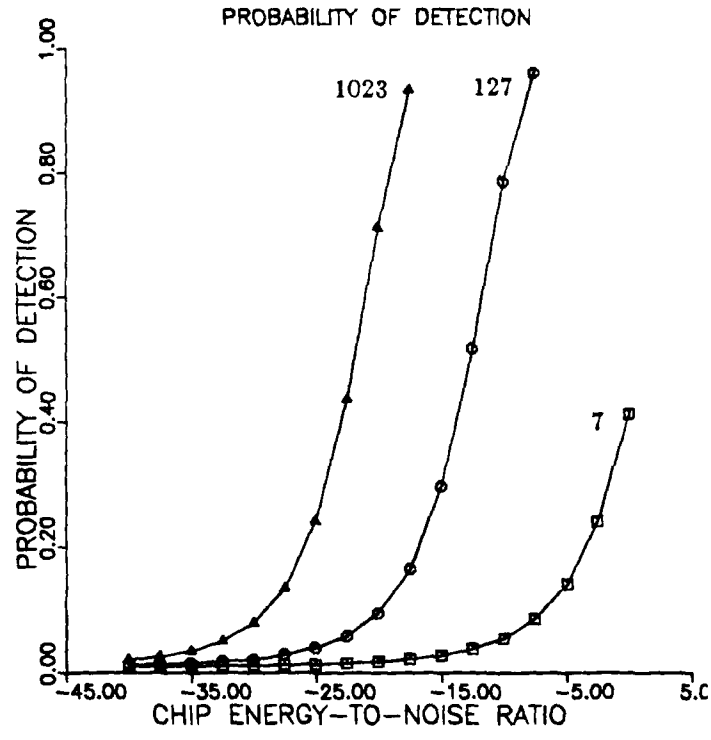


Figure 9.4: Modified $\frac{1}{2}$, $\frac{5}{8}$ Code SSMH Detectability

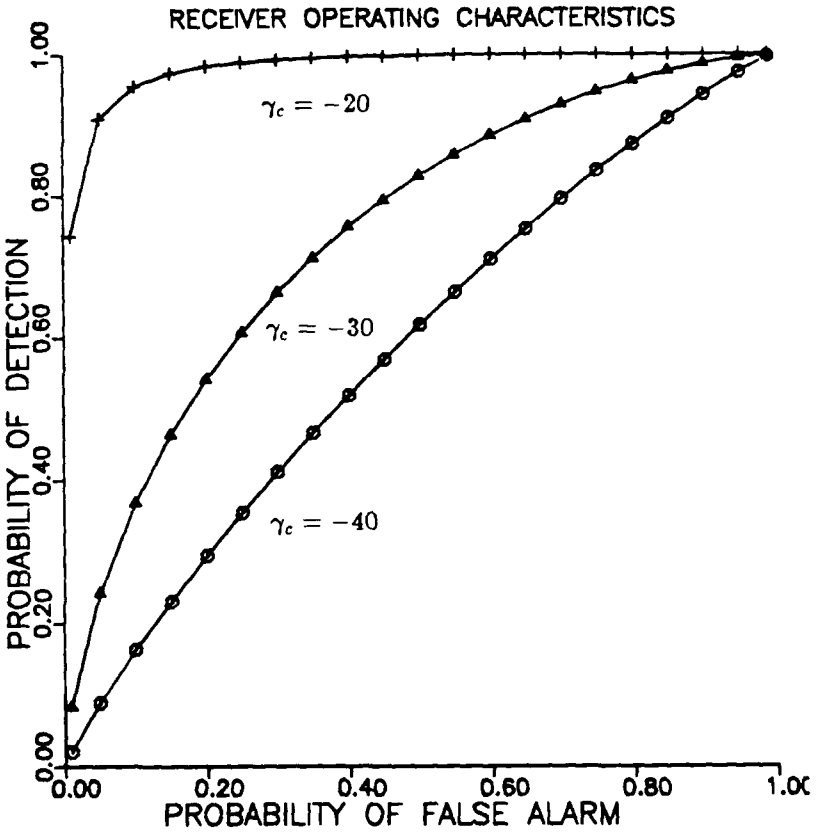


Figure 9.5: Conventional $\frac{1}{2}$, $\frac{3}{4}$ Code SSMH Receiver Operating Characteristics

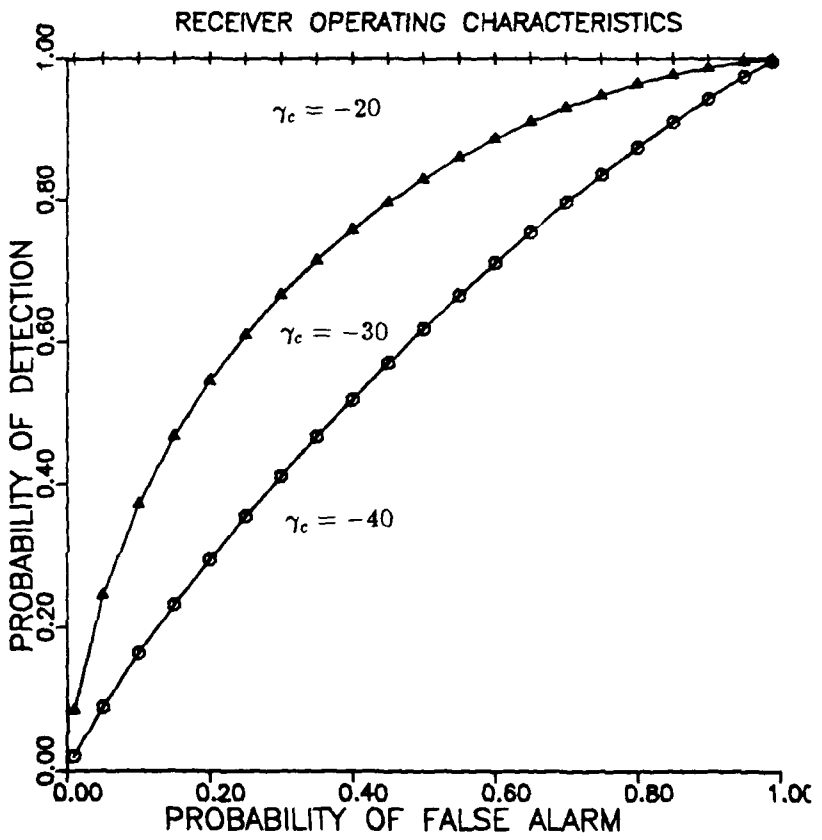


Figure 9.6: Conventional $\frac{1}{2}$, $\frac{5}{8}$ Code SSMH Receiver Operating Characteristics

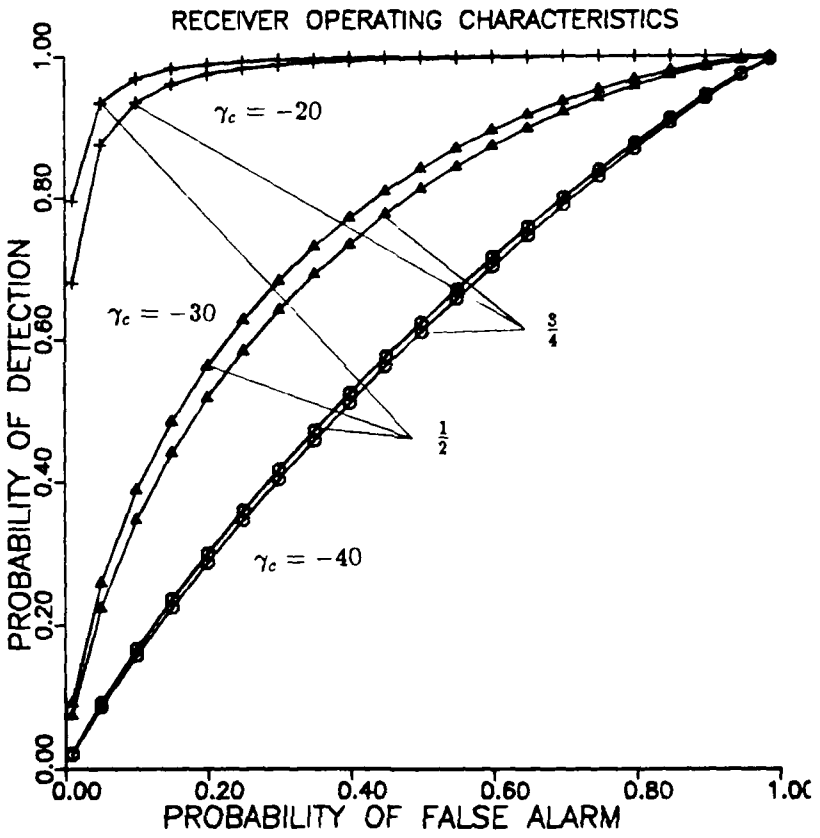


Figure 9.7: Modified $\frac{1}{2}$, $\frac{3}{4}$ Code SSMH Receiver Operating Characteristics

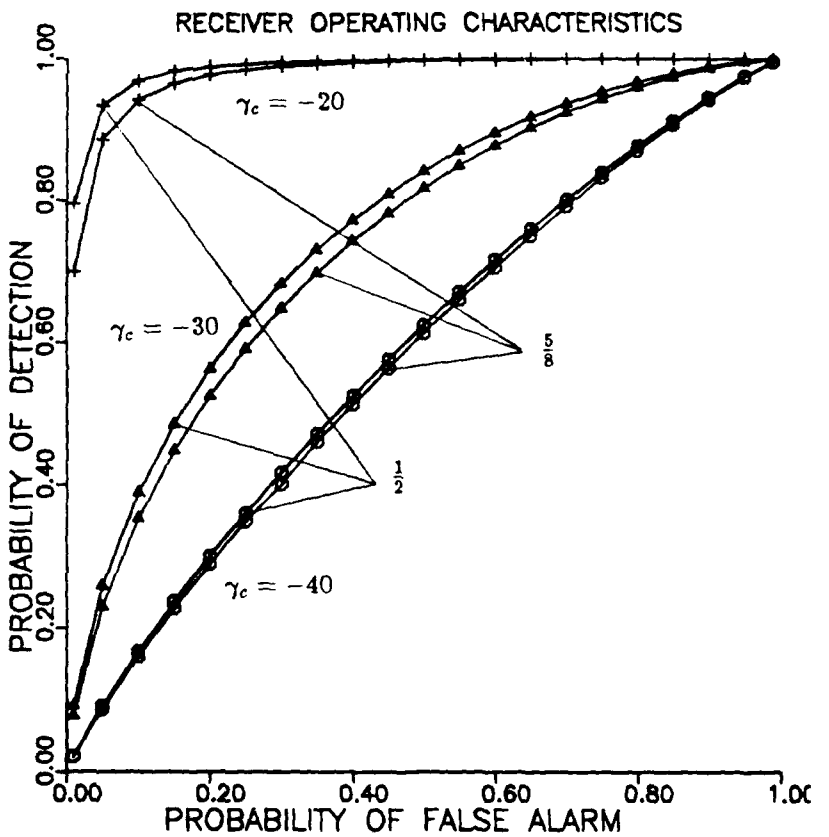


Figure 9.8: Modified $\frac{1}{2}$, $\frac{5}{8}$ Code SSMH Receiver Operating Characteristics

| *Modulation Scheme* | *Figure* |
|---|---|
| Conventional | |
| .5, .75 | 9.5 |
| .5, .625 | 9.6 |
| Modified | |
| .5, .75 | 9.7 |
| .5, .625 | 9.8 |

Table 9.2: Receiver Operating Characteristic Curves

# CHAPTER 10

# Results and Conclusions

Previous chapters have defined the signals which were called spread spectrum multi-$h$ signals and characterized the signaling structure in terms of the transmitted power spectral density, performance bounds, and signal detectability. Additionally, transmitter and receiver structures were derived to transmit and to optimally detect the signals in a white noise environment. The probability of error bounds were compared with the results of a numerically simulated receiver. With this foundation, this chapter summarizes the results from the current work by first comparing the results with existing spread spectrum systems exemplified by direct sequence binary phase shift keying systems. Secondly, the conclusions reached by this work are summarized, and finally, recommendations for future work are presented. It is shown that SSMH is a viable LPI signaling waveform.

## 10.1 Comparisons with DS/BPSK systems

In Chapter 5, the spectra for SSMH signals were analytically derived and simulated. It was shown that the spectra were spread replicas of the spectra of the parent multi-$h$ schemes. Thus significant control over the spectra is gained through the modulation index selection in terms of the amount of spread, the relative flatness of the mainlobe, and the sidelobe rolloff. It was also shown that there would be no distinguishing features to the spectra, such as nulls or discrete components. Conversely, it was shown that the spectra for DS/BPSK signals, by necessity through the $\text{sinc}^2(x)$ nature of the spectrum, would have nulls at the chip rate. It was also shown that simple square law detection would reveal many parameters of a DS/BPSK signals (carrier frequency and chip rate), while no

information is readily apparent on SSMH signals until the signal is raised to the power of the denominator of the modulation indices. This comparison indicates that SSMH signals allow much more control over the transmitted spectral shape and the spectra will be much less susceptible to parameterization than DS/BPSK signals.

Turning to performance comparisons, the performance bounds of Chapter 7 are evoked. As a recapitulation, the exponential bounds for SSMH signals with three chips per bit and with seven chips per bit are shown in Figures 10.1 and 10.2 below.

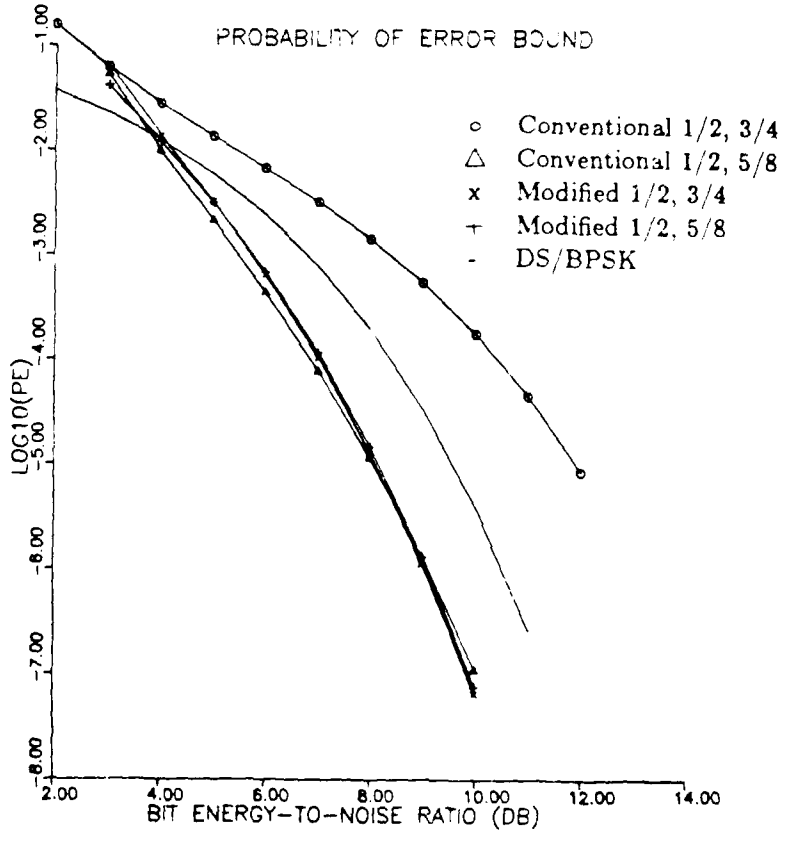


Figure 10.1: SSMH Bit Error Bounds with $N_c = 3$

Additionally, Figure 10.3 below, reproduced from *Spread Spectrum Communications*

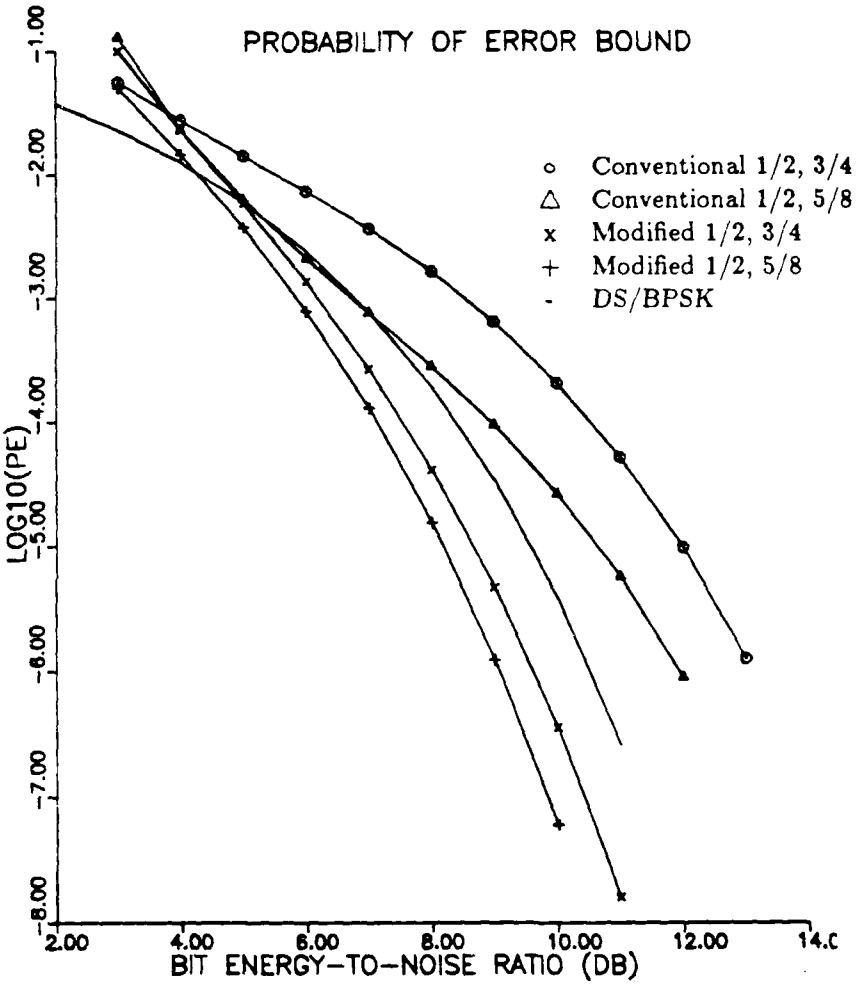


Figure 10.2: SSMH Bit Error Bounds with $N_c = 7$

by Simon, Omura, Scholtz, and Levitt, shows the corresponding uncoded bit error probability bounds for Direct Sequence BPSK.

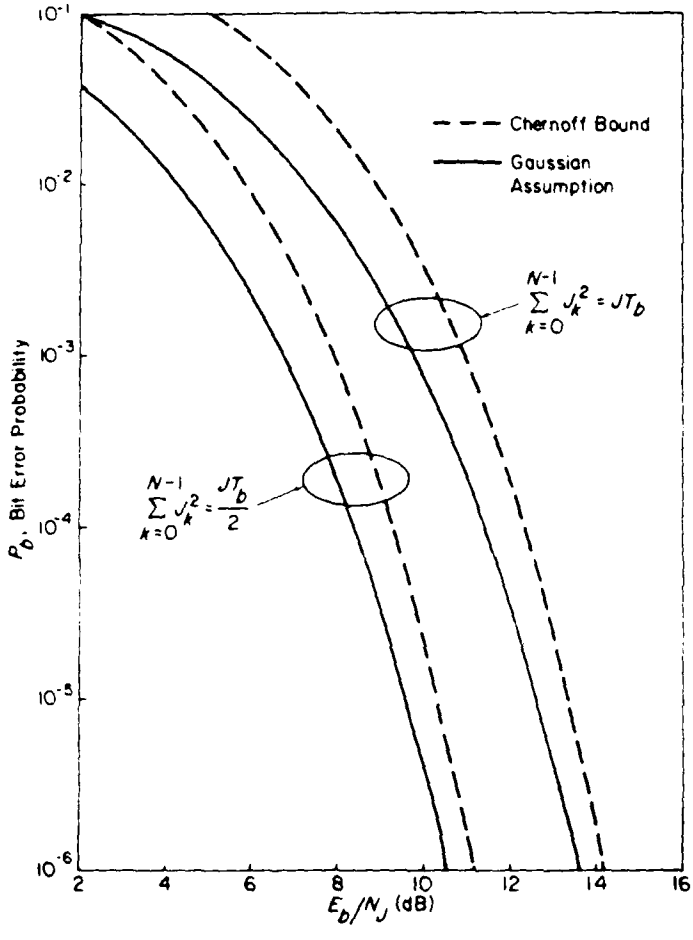


Figure 10.3: Uncoded DS/BPSK Error Bounds

It can be seen as an example that at an error rate of $10^{-5}$, SSMH signals are upper bounded at approximately eight decibels, while DS/BPSK are bounded at approximately 10-12 decibels. From this comparison, it appears that SSMH can perform more reliably than DS/BPSK for a given signal-to-noise ratio. It should be noted though, that at very low signal-to-noise ratios the discrepancy in performance decreases. For example, at four decibels of signal-to-noise ratio the bit error rates are essentially the same Thus in the range 2-4 decibels, DS/BPSK may perform better, but above four decibels SSMH would

be a wiser choice.

With these bounds in mind, the detectability of these signals can be considered. From Chapter 9, the detectability curves for $\frac{1}{2}$, $\frac{5}{8}$ conventional and modified signaling are reproduced in Figures 10.4 and 10.5. It should be remembered that these measures of detectability were based on an unintended receiver having almost complete knowledge of the transmitted signal.

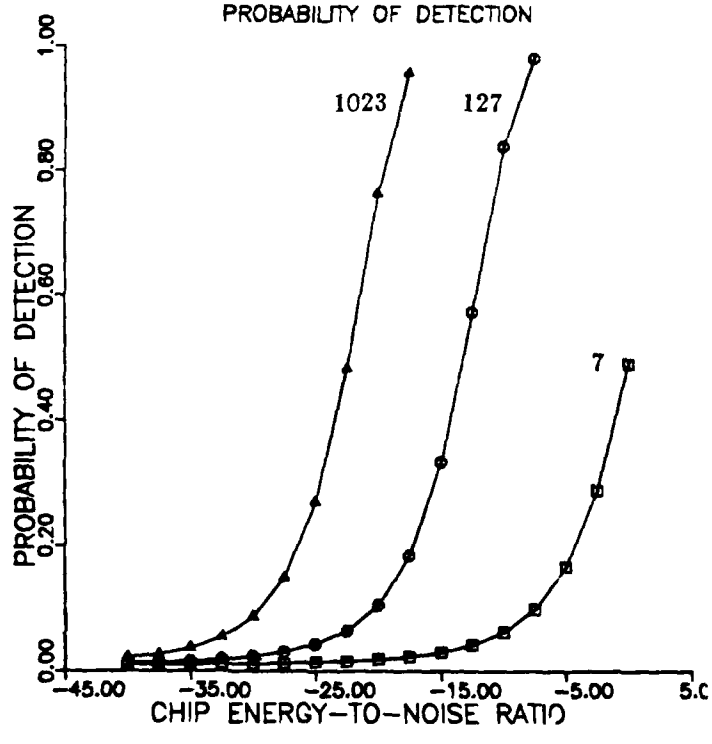


Figure 10.4: Conventional $\frac{1}{2}$, $\frac{5}{8}$ Code SSMH Detectability

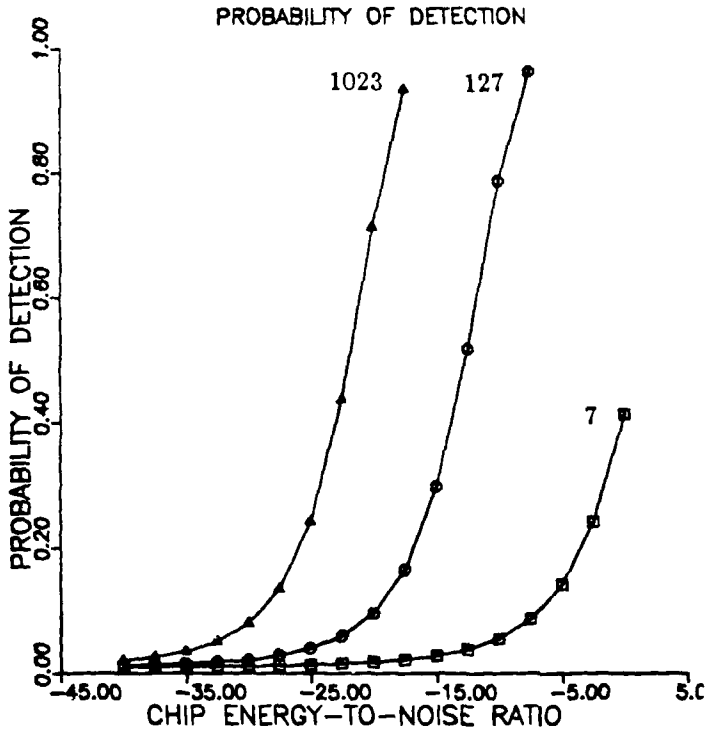


Figure 10.5: Modified $\frac{1}{2}$, $\frac{5}{8}$ Code SSMH Detectability

Additionally, the detectability curves for DS/BPSK are reproduced from the Axiomatix Corporation study on LPI waveforms by Polydoros and Weber [48,49] in Figure 10.6.

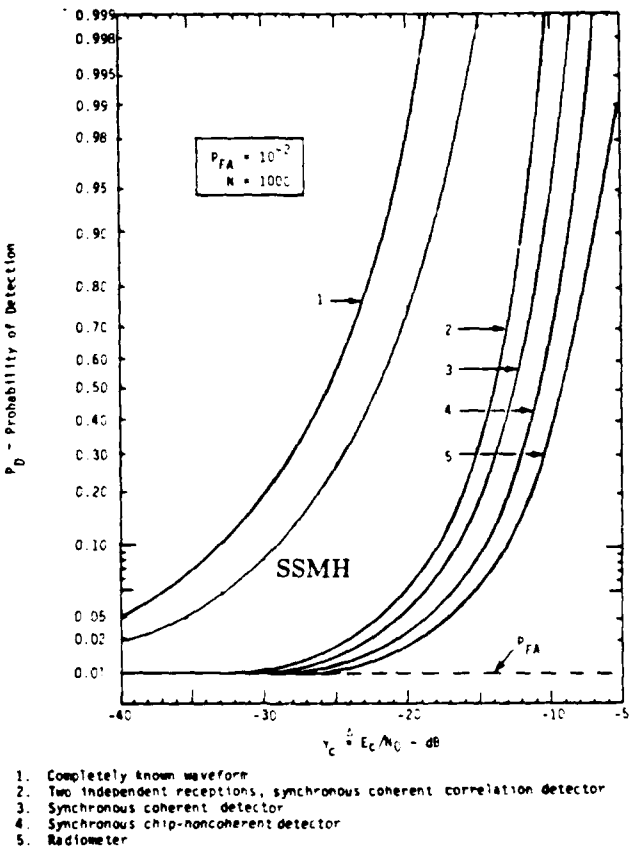


Figure 10.6: DS/BPSK Detectability

Lastly, the probability of detection curves for an equivalent parameter, $N_c = 1000$, $P_F = 10^{-2}$, conventional and modified $\frac{1}{2}$, $\frac{5}{8}$ code SSMH system are shown in Figure 10.7.

One of the key questions of this study can now be answered from these curves. Recalling that the original purpose of the design of SSMH waveforms was to create a signaling waveform that had a low probability of intercept, the performance capabilities can now be reconciled with the signal detectability. The performance curves (Figures 10.4 and 10.5) show that for an intended receiver operating at a received signal-to-noise ratio of seven decibels, the probability of error performance is bounded at approximately $10^{-4}$.

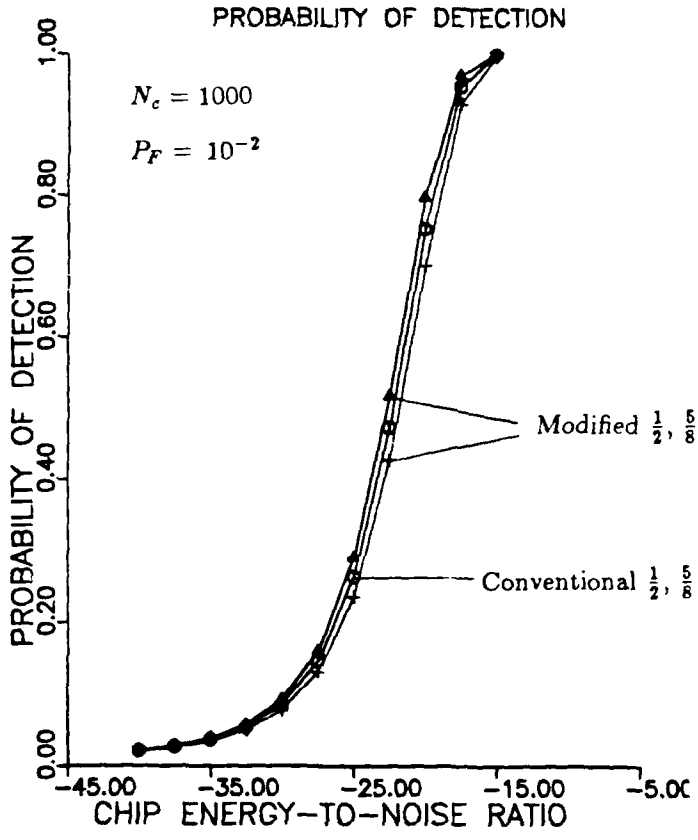


Figure 10.7: Conventional and Modified $\frac{1}{2}$, $\frac{5}{8}$ Code SSMH Detectability

After conversion of this bit energy-to-noise ratio to chip energy-to-noise ratio (-23 decibels at 1000 chips per bit), it is clear from Figure 10.7 and Figures 10.4 and 10.5, that even with knowledge of the signal and the high false alarm rate, the unintended receiver would have unacceptably low probabilities of detection of less than one half. A comparison can also be made to show that as the chip rate increases, the probability of detection decreases.

It should be noted that comparison of the detectability results for SSMH with the detectability of DS/BPSK as shown in Figure 10.6, reveals that a completely known (except for information sequence and spreading sequence) SSMH signal is less detectable than the corresponding completely known DS/BPSK signal. This is a new and significant result showing the potential for this class of continuous phase and spread spectrum signals.

Having shown that SSMH is a viable LPI signaling technique, the following section summarizes the results of this study and recommends further areas of research.

## 10.2 Results and Conclusions

The previous chapters of this study have outlined the definition and characterized the signals that were collectively called spread spectrum multi-$h$ signals. During the course of this study the following results and conclusions have been reached.

- Both *conventional* and *modified* spread spectrum multi-$h$ signals have been defined and parameterized for the first time.
- This class of signals was shown to maintain the Markov state nature and trellis phase state structure of multi-$h$ signals.
- Application of the modulation index over a complete bit interval as opposed to changing during each chip interval was considered for the first time and was found to provide enhanced performance vis-a-vis conventional modulation techniques.
- Analytical expressions for the power density spectrum of SSMH signals have been defined and numerically evaluated for the first time.
- The power density spectrum of a SSMH signal is the spread replica of its multi-$h$ parent indicating that the spectral shape is dependent on the selected modulation

indices.

- The power density spectrum of *conventional* and *modified* SSMH signals is relatively unaffected by the method of application of the modulation indices. This is a novel conclusion regarding the modulation methodology.
- The transmitted spectrum of SSMH signals can be shaped to provide a wide flat mainlobe and rapid sidelobe rolloff and transmitted at relatively low signal-to-noise ratios to create an LPI signature.
- SSMH signal spectra do not present readily identifiable characteristics such as nulls or discrete components.
- A coherent receiver structure can be implemented via the Viterbi Algorithm with bit branch metrics derived from correlation filtering of noise corrupted received signals.
- Maximum likelihood bit metrics for the Viterbi Algorithm result from the sum of correlation filter derived chip metrics.
- Minimum distance criteria were derived and shown to result from the sum of chip distances.
- Performance bounds were derived and verified by numerical evauluation to show that the signaling technique and receiver structure could be used to successfully detect transmitted signals at low signal-to-noise ratios.
- For the first time, it was shown that the spreading sequence had a significant effect on the performance of this spread spectrum system.
- At low spreading rates the modulation index code affects the performance, but at higher rates the modulation index coding effects diminish due to the tendency of the distances to converge. This reflects a novel interpretation of the modulation indices and spread spectrum systems.
- Based on Figures 7.9 and 7.10, application of the modulation indices on a bit basis rather than on a chip basis yields slightly better performance characteristics. This is a novel and significant finding for continuous phase modulated systems.

- The necessary decoding depth of the Viterbi Algorithm is consistent with the minimum distance bounds of the coding scheme.
- Even under known signal parameter conditions, an unintended receiver would encounter difficulties in satisfactorily detecting the signals. This final result is crucial to the ultimate purpose of this novel signaling technique; that is to create a signaling technique that is immune to unintended intercept.

In summary, this work has introduced a new method of spread spectrum signaling known as spread spectrum multi-$h$ modulation. It has been shown this technique is a viable alternative for low probability of intercept communications.

As a prelude to suggesting areas of future study, it is worthwhile to mention the performance of SSMH in a stressed environment. This study has assumed complete coherency and synchronization, and has not considered the effects of jamming, interference, or multipath fading. A few comments in this regard are appropriate. It must be remembered that continuous phase modulated systems rely on the fact that the information is contained in the memory of the phase transitions. As a result, complete coherency is not absolutely required. The implication in this statement is that noncoherent systems may perform with little degradation compared to coherent systems. For the same reason, the loss of individual chips or strings of chips due to fading or interference will not have the deleterious effect that a similar loss would have on DS/BPSK systems. All of these factors and effects are fertile areas of potential research. A few more are considered in the following section.

## 10.3 Recommendations for Future Study

While these results contribute significantly to understanding this new category of signals, many new and unanswered questions arise. As a result, the following suggestions for future research are submitted.

- What are the effects of partial response signaling on the overall signaling structure and performance?

- What are the effects of $M$-ary signaling on the overall signaling structure and performance?
- What are the effects of periodic spreading sequences on overall signal structure?
- Can other methods of spectral definition satisfactorily characterize high spreading rate SSMH signals?
- Can other spectrum feature extraction techniques such as correlation, transform, or edge detection be readily used to detect the signal?
- What are the effects of imperfect synchronization and timing on the coherent reception of these signals?
- What are the effects of transmitter and receiver filtering on the system performance?
- Can noncoherent reception perform as well on this signal structure as on other continuous phase systems?
- Since the distance characteristics are spreading code dependent, can the spreading sequence be optimized?
- What are the effects of interference and fading on the LPI performance?
- Can the modulation index code be optimized in terms of either the optimal number of indices or the selection of specific coding schemes?
- Can coding of the modulation indices on a conventional CPFSK system enhance performance and spectral characteristics?

# Bibliography

[1] J. Anderson. Simulated Error Performance of Multi-$h$ Phase Codes. *IEEE Transactions on Information Theory*, IT-27(3):357–362, May 1981.

[2] J. Anderson and R. deBuda. Better Phase-Modulation Error Performance Using Trellis Phase Codes. *Electronics Letters*, 12(22):587–588, October 1976.

[3] J. Anderson and et al. A Class of Trellis Phase Modulation Codes for Coding Without Bandwidth Expansion. In *Proceedings International Communications Conference*, pages 50.3.1–50.3.5, 1978.

[4] J. Anderson and D. Taylor. A Bandwidth-Efficient Class of Signal-Space Codes. *IEEE Transactions on Information Theory*, IT-24(6):703–712, November 1978.

[5] J. Anderson and D. Taylor. Trellis Phase Modulation Coding: Minimum Distance and Spectral Results. In *Proceedings Electronics and Aerospace Conference*, pages 29.1A–29.1G, 1977.

[6] John B. Anderson and et al. *Digital Phase Modulation*. Plenum Press, New York, 1986.

[7] T. Aulin and et al. Continuous Phase Modulation-Part II: Partial Response Signaling. *IEEE Transactions on Communications*, Com-29(3):210–225, March 1981.

[8] T. Aulin and et al. *Minimum Distance and Spectra of M-ary Constant Envelope Digital FM Signals*. Technical Report 129, University of Lund, Lund, Sweden, May 1979.

[9] T. Aulin and C. Sundberg. Calculating Digital FM Spectra by Means of Autocorrelation. *IEEE Transactions on Communications*, Com-30(5):1199–1208, May 1982.

[10] T. Aulin and C. Sundberg. Continuous Phase Modulation-Part I:Full Response Signaling. *IEEE Transactions on Communications*, Com-29(3):196–209, March 1981.

[11] T. Aulin and C. Sundberg. An Easy Way to Calculate Power Spectra for Digital FM. *IEE Proceedings, Part F*, 130(6):519–526, October 1983.

[12] T. Aulin and C. Sundberg. Exact Asymptotic Behavior of Digital FM Spectra. *IEEE Transactions on Communications*, Com-30(11):2438–2449, November 1982.

[13] T. Aulin and C. Sundberg. Minimum Euclidean Distance and Power Spectra for a Class of Smoothed Phase Modulation Codes with Constant Envelope. *IEEE Transactions on Communications*, Com-30(7):1721–1729, July 1982.

[14] T. Aulin and C. Sundberg. Numerical Calculation of Spectra for Digital FM Signals. In *Proceedings National Telecommunications Conference*, pages D8.3.1–D8.3.7, 1981.

[15] T. Aulin and C. Sundberg. On the Minimum Euclidean Distance for a Class of Signal Space Codes. *IEEE Transactions on Information Theory*, IT-28(1):43–55, January 1982.

[16] T. Baker. Asymptotic Behaviour of Digital FM Spectra. *IEEE Transactions on Communications*, Com-22(10):1585–1595, October 1974.

[17] W. Bennett and S. Rice. Spectral Density and Autocorrelation Functions Associated with Binary Frequency-Shift Keying. *Bell System Technical Journal*, 42:2355–2385, September 1963.

[18] S. Bernstein. *Optimal Detectors of Pseudonoise Waveforms*. Technical Note 1974-37, Massachusetts Institute of Technology, June 1974.

[19] V.K. Bhargava and et al. *Digital Communications by Satellite*. Wiley and Sons, New York, 1981.

[20] C. Cahn. Phase Tracking and Demodulation with Delay. *IEEE Transactions on Information Theory*, IT-20(1):50–58, January 1974.

[21] R. deBuda. Coherent Demodulation of Frequency-Shift Keying with Low Deviation Ratio. *IEEE Transactions on Communications*, 429–435, June 1972.

[22] R. deBuda. Fast FSK Signals and Their Demodulation. *Canadian Electrical Engineering Journal*, 1(1):28–34, January 1976.

[23] R. Dillard. Detectability of Spread Spectrum Systems. *IEEE Transactions on Aerospace and Electronic Systems*, AES-15(4):526–537, July 1979.

[24] R. Dixon. *Spread Spectrum Systems*. Wiley and Sons, New York, 2nd edition, 1984.

[25] G. Forney. The Viterbi Algorithm. *Proceedings of the IEEE*, 61(3):268–278, March 1973.

[26] G. Garrison. A Power Spectral Analysis for Digital FM. *IEEE Transactions on Communications*, Com-23(11):1228–1243, November 1975.

[27] Paul K.M. Ho and Peter J. McLane. Power Spectral Density of Digital Continuous Phase Modulation with Correlated Data Symbols. *IEE Proceedings, Part F*, 133(1):95–114, February 1986.

[28] J. Holmes. *Coherent Spread Spectrum Systems*. Wiley, New York, 1982.

[29] L.S. Howeth. *History of Communications-Electronics in the United States Navy*. U.S. Printing Office, Washington, D.C., 1963.

[30] Chung-Dyi Hsu. *Multi-h Phase Coding-Its Theory and Design*. PhD thesis, University of Virginia, 1981.

[31] David E. Jackson. *Bandwidth Efficient Communication and Coding*. PhD thesis, University of California, Los Angeles, 1980.

[32] N. Krasner. Optimal Detection of Digitally Modulated Signals. *IEEE Transactions on Communications*, Com-30(5):885–895, May 1982.

[33] A. Lereim. *Spectral Properties of Multi-h Phase Codes*. Communications Research Laboratory Report CRL-57, McMaster University, Hamilton, Ontario, Canada, July 1978.

[34] John M. Liebetreu. Joint Carrier Phase Estimation and Data Detection Algorithms for Multi-*h* CPM Data Transmission. *IEEE Transactions on Communications*, Com-34(9):873–881, September 1986.

[35] John M. Liebetreu and Mark A. Wickert. Computer Aided Performance Analysis of Multi-$h$ CPM Data Transmission Systems in Practical Environments. In *Proceedings IEEE Milcom*, pages 36.4.1–36.4.7, 1986.

[36] L. Lind and A. deAlbuquerque. Spectral Calculation of Partial Response Multi-$h$ Phase Codes. *Electronics Letters*, 17(19):711–713, September 1981.

[37] O. Macchi and L. Scharf. A Dynamic Programming Algorithm for Phase Estimation and Data Decoding on Random Phase Channels. *IEEE Transactions on Information Theory*, IT-27(5):581–595, September 1981.

[38] T. Maseng. The Autocorrelation Function for Multi-$h$ Coded Signals. *IEEE Transactions on Communications*, Com-33(5):481–484, May 1985.

[39] T. Maseng. The Spectrum of Digitally Phase and Frequency Modulated Signals. In *Proceedings Globecom 1984*, pages 32.7.1–32.7.5, 1984.

[40] B. Mazur and D. Taylor. Demodulation and Carrier Synchronization of Multi-$h$ Phase Codes. *IEEE Transactions on Communications*, Com-29(3):257–266, March 1981.

[41] Brian M. Mazur. *The Self Synchronization of Multi-h Phase Codes.* Communications Research Laboratory Report CRL-75, McMaster University, Hamilton, Ontario, Canada, April 1980.

[42] H. Miyakawa and et al. A New Digital Modulation Scheme-Multi-Mode Binary CPFSK. In *Proceedings Third International Conference on Digital Satellite Communications*, pages 105–112, Kyoto, Japan, November 1975.

[43] David L. Nicholson. *Spread Spectrum Signal Design LPI and AJ Systems.* Computer Science Press, Rockville, Maryland, 1988.

[44] J. Omura and D. Jackson. Cutoff Rates for Channels Using Bandwidth Efficient Modulations. In *Proceedings National Telecommunications Conference*, pages 14.1.1–14.1.11, 1980.

[45] W. Osborne and M. Luntz. Coherent and Noncoherent Detection of CPFSK. *IEEE Transactions on Communications*, 1023–1036, August 1974.

[46] Athanasios Papoulis. *Probability, Random Variables, and Stochastic Processes.* McGraw-Hill Book Company, New York, 2nd edition, 1984.

[47] R. Pickholtz and et al. Theory of Spread Spectrum Communications-A Tutorial. *IEEE Transactions on Communications*, Com-30(5):855–884, May 1982.

[48] A. Polydoros and et al. *Advanced LPI Intercept Detector Research.* Technical Report R8403-1, Axiomatix Corporation, March 1984.

[49] Andreas Polydoros and Charles L. Weber. Detection Performance Considerations for Direct-Sequence and Time-Hopping LPI Waveforms. *IEEE Journal on Selected Areas of Communications*, SAC-3(5):727–744, September 1985.

[50] A. Premji and D. Taylor. A Practical Receiver Structure for Multi-$h$ CPM Signals. *IEEE Transactions on Communications*, Com-35(9):901–908, September 1987.

[51] A. Premji and D. Taylor. Receiver Structures for Multi-$h$ Signaling Formats. *IEEE Transactions on Communications*, Com-35(4):439–451, April 1987.

[52] M. Ristenbatt and J. Daws. Performance Criteria for Spread Spectrum Communications. *IEEE Transactions on Communications*, Com-25(8):756–762, August 1977.

[53] H. Rowe and V. Prabhu. Power Spectrum of a Digital Frequency Modulation Signal. *Bell System Technical Journal*, 54:1095–1125, July-August 1975.

[54] Ramin Sadr. *Receiver Design and Analysis for Generalized Minimum Shift Keying Modulation Techniques.* PhD thesis, University of California, Los Angeles, 1983.

[55] Ramin Sadr and Jim Omura. Generalized Minimum Shift-Keying Modulation Techniques. *IEEE Transactions on Communications*, Com-36(1):32–40, January 1988.

[56] L. Scharf and et al. Modulo-$2\pi$ Phase Estimation. *IEEE Transactions on Information Theory*, IT-26(5):615–620, September 1980.

[57] T. Schonhoff. Symbol Error Probabilities for M-ary CPFSK: Coherent and Noncoherent Detection. *IEEE Transactions on Communications*, 644–652, June 1976.

[58] S. Simmons and P. Wittke. Low Complexity Decoders for Bandwidth Efficient Digital Phase Modulations. In *Proceedings Globecom 1982*, pages 1126–1130, 1982.

[59] M. Simon and et al. *Spread Spectrum Communications.* Computer Science Press, Rockville, MD, 1985.

[60] Bernard Sklar. A Structured Overview of Digital Communications- a Tutorial Review: Parts I and II. *IEEE Communications Magazine*, 4–17,6–21, August, October 1983.

[61] Henry Stark and John M. Woods. *Probability, Random Processes, and Estimation Theory for Engineers.* Prentice-Hall, Englewood Cliffs, New Jersey, 1986.

[62] D. Taylor and H. Chan. A Simulation Study of Two Bandwidth-Efficient Modulation Techniques. *IEEE Transactions on Communications*, Com-29(3):267–275, March 1981.

[63] R. Titsworth and L. Welch. *Power Spectra of Signals Modulated by Random and Pseudorandom Sequences.* Technical Report 32-140, Jet Propulsion Laboratory, California Institute of Technology, Pasadena, CA, October 1961.

[64] D. Torrieri. *Principles of Secure Communication Systems.* Artech, Dedham, MA, 1985.

[65] G. Ungerboeck. New Application for the Viterbi Algorithm: Carrier-Phase Tracking in Synchronous Data-Transmission Systems. In *Proceedings National Telecommunications Conference*, pages 734–738, 1974.

[66] H. Urkowitz. Energy Detection of Unknown Deterministic Signals. *Proceedings of IEEE*, 55(4):523–531, April 1967.

[67] Harry L. VanTrees. *Detection, Estimation, and Modulation Theory: Part I, Detection, Estimation, and Linear Modulation Theory.* John Wiley and Sons, New York, 1968.

[68] A. Viterbi. Error Bounds for Convolutional Codes and an Asymptotically Optimum Decoding Algorithm. *IEEE Transactions on Information Theory*, IT-13:260–269, April 1967.

[69] Andrew J. Viterbi and Jim K. Omura. *Digital Communication and Coding*. McGraw-Hill Book Company, New York, 1979.

[70] Mark A. Wickert. *The Performance of Full Response Multi-h Modems in Practical Environments*. PhD thesis, University of Missouri-Rolla, 1983.

[71] Mark A. Wickert and Rodger E. Ziemer. Performance Degradations Due to Channel Impairments in Multi-*h* Continuous-Phase Modulation Systems. In *Proceedings Globecom 1983*, pages 30.3.1–30.3.5, 1983.

[72] S. Wilson and R. Gaus. Power Spectra of Multi-*h* Phase Codes. *IEEE Transactions on Communications*, Com-29(3):250–256, March 1981.

[73] S. Wilson, J. Highfill, and C. Hsu. Error Bounds for Multi-*h* Phase Codes. *IEEE Transactions on Information Theory*, IT-28(4):660–665, July 1982.

[74] S. Wilson and C. Hsu. Joint MAP Data/Phase Sequence Estimation for Trellis Phase Codes. In *Proceedings International Communications Conference*, pages 26.1.1–26.1.5, 1980.

[75] John M. Wozencraft and Irwin M. Jacobs. *Principles of Communication Engineering*. John Wiley and Sons, New York, 1965.

[76] Ephraim Zehavi and Jack K. Wolf. On the Performance Evaluation of Trellis Codes. *IEEE Transactions on Information Theory*, IT-33(2):196–202, March 1987.

[77] Rodger E. Ziemer and R. Peterson. *Digital Communications and Spread Spectrum Systems*. MacMillan Publishing Co., New York, 1985.

# VITA

William DeWitt Lane was born [redacted]

He was raised in Littleton, Colorado and graduated from Arapahoe High School in 1966. Following graduation in 1970 from the United States Military Academy at West Point with a Bachelor of Science Degree, he was commissioned as a Second Lieutenant in the United States Army. Following assignments in Germany, Turkey, and Korea, he attended Georgia Institute of Technology and received the Master of Science in Electrical Engineering Degree in 1978. While assigned to the Department of Electrical Engineering at West Point, he received the Master of Business Administration Degree from the C.W. Post campus of Long Island University in 1981. After assignments with the Joint Special Operations Support Element and the Defense Communications Agency Field Office in Turkey, he returned to the Georgia Institute of Technology in 1985 to continue graduate studies.

He is currently a Lieutenant Colonel in the United States Army and a Professional Engineer in the state of Virginia.